SEP 13 1947

JOURNAL OF CHEMICAL PHYSICS

VOLUME 15 NUMBER 8

AUGUST, 1947

Published by the

AMERICAN INSTITUTE OF PHYSICS

...ICAL ...

...ICS

...Editor

Volume ... Number 11, 1959

K. J. McCALLUM
A. L. PATTERSON
HERBERT SCOBER
GEORGE ...
BRUNO ...

...

...ments. The solidus (/) should be used wherever ...sible for fractions.

All illustrations should ... any manuscript and should always be referred to in the text. Line drawings must be made with India ink on plain white paper or on tracing cloth. Coordinate paper is not desirable, but if used must be blue-lined with all coordinates to be reproduced drawn with India ink. Lettering should be of ...ficient size to be legible after reduction.

... and all correspondence concerning papers in the process of publication should be addressed to the Publications Manager, American Institute of Physics, 57 East ... Street, New York 22, New York.

Subscription Rates

The United States and Possessions, Canada and Mexico..... $10.00
Foreign..... 11.00

Back Numbers

Complete set: Vol. 1, 1933—Vol. 14, 1946 (except Vol. 1, No. 1)..... $140.00
Yearly rate: $11.00.
Single copies: $1.00 each.

Subscriptions and orders for ... copies should be addressed to Prince and Lemon Streets, Lancaster, Pennsylvania, or to the American Institute of Physics, 57 East ... Street, New York 22, New York.

Changes of address should be ... the Business Manager, American Institute of ...

... and Lemon Streets, Lancaster, Pennsylvania.

... Lancaster, Pa., under the Act of ... 1912. Acceptance for ... 1925, embodied in paragraph 4, Sec... P. L. & R.: authorized ...

THE JOURNAL
OF
CHEMICAL PHYSICS

VOLUME 15, NUMBER 8 AUGUST, 1947

Photo-Conductivity in Photographic Systems

I. Dye-Sensitization of Photo-Conductivity*,†

W. WEST AND B. H. CARROLL
Kodak Research Laboratories, Rochester, New York

(Received December 19, 1946)

Gelatino-silver halide photographic films increase in electrical conductivity on exposure to light at intensities corresponding to exposures within the normal photographic range, and above. The spectral distribution of this change in conductivity in films containing, respectively, photographic sensitizing dyes, and no dye, is found to be parallel with the spectral distribution of photographic sensitivity—the wave-lengths of maximum and minimum sensitivity in the two effects are identical and coincide with absorption maxima and minima, and there is a general parallelism in the efficiency of a dye in sensitizing the two effects to light not absorbed by the silver halide. The conclusion is drawn that the observed changes in conductivity represent a photo-conductivity originating in the photo-liberation of electrons within the silver halide, the primary act of the photographic process.

The photo-currents are proportional to the applied field up to strengths of at least 140 volts per millimeter, and at intensities of illumination within the normal photographic range and somewhat above, are proportional to the intensity. At still higher light intensities, the photo-currents verge towards a dependence on the square root of the intensity. The change in the intensity relation is interpreted as representing the passage from a situation, at low intensities, in which most of the electrons are captured by foreign traps to that, at high intensities, in which recombination with bromine atoms predominates.

It is shown that a sensitizing dye acts by causing the liberation of an electron within the conduction band of the silver halide under the stimulus of light absorbed by the dye but whether the process involves direct electron-transfer or energy-transfer is left open.

MODERN ideas of the photographic latent image spring from studies, on the one hand, of the conditions for sensitivity in photographic emulsions, and on the other, of the electrical and structural characteristics of silver halide crystals. On the photographic side, an important step was the formulation by Sheppard, Trivelli, and Loveland[1,2] of the "concentration speck theory," according to which high photographic sensitivity is associated with the presence of submicroscopic particles of silver sulfide on the surface of the grains, which act as condensation nuclei for silver produced by exposure to light. On the physical side, the silver halides were recognized to exhibit electrolytic and photoelectronic conductivity.[3] A description of the primary process of photo-excitation in silver halides in terms of quantum-mechanical views of crystal behavior was made by Webb,[4] and in 1938 Gurney and Mott[5] effected a synthesis of

* Communication No. 1111 from the Kodak Research Laboratories.

† Presented in part before the Division of Physical and Inorganic Chemistry at the 109th Meeting of the American Chemical Society, Atlantic City, New Jersey, April 10, 1946.

[1] S. E. Sheppard, Phot. J. **65**, 380 (1925).

[2] S. E. Sheppard, A. P. H. Trivelli, and R. P. Loveland, J. Frank. Inst. **200**, 51 (1925).

[3] R. Hilsch and R. W. Pohl, Trans. Faraday Soc. **54**, 883 (1938); C. Wagner, *ibid.* 851.

[4] J. H. Webb, J. Opt. Soc. Am. **26**, 367 (1936).

[5] R. W. Gurney and N. F. Mott, Proc. Roy. Soc. **A164**, 151 (1938).

all these elements into a detailed description of latent-image formation which forms the starting point of most current discussions of the subject.

Briefly, the hypothesis is that absorption of radiation by silver halides liberates electrons from the bromide ions. The electrons become free to move through the lattice until they are captured by traps; the photo-conduction of silver halide crystals is the manifestation of this process. The lattice also contains mobile interstitial silver ions, whose existence is shown by the electrolytic conductivity of the silver halides. The traps, negatively charged by capture of electrons, attract silver ions, which, after neutralization, are deposited as silver atoms. The experimental facts on the sensitivity of photographic emulsions force the assumption that the most efficient traps are particles of silver sulfide, the "concentration specks" of Sheppard, Trivelli, and Loveland, and the accretion of silver atoms on these specks by the processes just described forms the photographic latent image. The existence of a latent-image particle in a halide grain leads to the complete reduction of the grain to metallic silver on immersion in a developer. The bromine atom left in the crystal after the expulsion of the electron, is assumed to wander by electronic displacement to the surface of the grain and to be rendered harmless with respect to recombination processes by being fixed by the gelatin.

Whatever may be the fate of this hypothesis as it is subjected to the ordeal of experimental test, it seems unlikely that the first step in the mechanism, the photo-liberation of electrons within the halide, will require fundamental alteration. There is, however, much to be learned concerning the details of this primary process, and the manner in which it is influenced by photographically significant treatments in the processes of emulsion making. Hitherto, photo-conduction has been observed only in massive crystals or in fused films of the silver halides. The observations of Pohl and his co-workers are confined to relatively large single crystals of "pure" material. Similarly, the experiments of Toy and Harrison,[6] which led these authors to identify the primary step in the formation of the latent image with the photo-conductive liberation of electrons in the silver salt, were carried out on thin films of previously fused "pure" silver bromide, and more recent experiments of Kameyama[7] and collaborators have also been concerned with the photo-conductance of fused films. It is a main purpose of the program, part of whose results are contained in the present communication, to extend our knowledge of photo-conduction to normal photographic emulsions, and to show how such studies may assist in the understanding of details of the primary photographic process. Unpublished observations by J. H. Webb and C. H. Evans, of the Kodak Research Laboratories, made before the present investigation was begun, showed that photo-currents could probably be detected in normal gelatino-silver bromide emulsions, and that by the addition to the emulsion of sensitizing dyes this internal photoelectric effect could be extended to spectral regions unabsorbed by the halide, in a manner analogous to photographic sensitization by these dyes. In the course of the present investigation it has been demonstrated unequivocally that photo-currents are developed in normal photographic films, and far-reaching parallelisms have been observed between the spectral distribution of photo-conductive and photographic activity.

Sheppard, Vanselow, and co-workers[8] also furnished important clues to the mechanism of the photo-changes in silver halides by studies of the photo-voltaic effect of silver-silver bromide electrodes in conducting solutions. They concluded that the primary action of the light was the liberation of electrons from the bromide ion, which then had a period of free existence before eventual union with silver ions to form silver atoms. These authors also showed that photographic sensitizing dyes extended the sensitivity of the photo-voltaic effect in silver-silver bromide electrodes to longer wave-lengths than exhibited by the undyed salt.[9]

[6] F. C. Toy and G. B. Harrison, Proc. Roy. Soc. **A127**, 613 (1930).

[7] N. Kameyama and T. Fukamoto, J. Soc. Chem. Ind. Japan **42**, 244B (1939); N. Kameyama and K. Mizuta, *ibid.* **42**, 426B (1939).

[8] W. Vanselow and S. E. Sheppard, J. Phys. Chem. **33**, 331 (1929); S. E. Sheppard, W. Vanselow, and V. C. Hall, *ibid.* **33**, 1403 (1929).

[9] S. E. Sheppard, W. Vanselow, and G. Happ, J. Phys. Chem. **44**, 411 (1940).

MEASUREMENT OF PHOTO-CONDUCTIVITY IN PHOTOGRAPHIC FILMS

(a) General Principles

The principle of the measurements in this report is the same as that employed by Toy and Harrison.[6] A piece of film is suitably mounted between electrodes, between which a potential difference is imposed by means of a battery. Part of the film-battery circuit consists of a high resistance of 10^8 to 10^{10} ohms which acts as the input resistance of a direct-current amplifier. The effect of the electrolytic dark current is eliminated by applying a counter potential to the grid, in which condition the amplifier is balanced and the corresponding reading of a galvanometer in the output circuit forms the zero for the measurements. Exposure of the film to light is accompanied by a diminution of resistance and an increase in current in the film-battery circuit, translated in the usual way by the amplifier to a proportional change in the output current. The corresponding deflections of the galvanometer from zero are measured as "photo-currents." Calibration in terms of the current in the input circuit is effected by noting the effect of a small known potential drop applied across the known input resistance.

The electrical system represented by the photographic film, consisting as it does of a suspension of minute photo-conducting crystals, usually 1μ or less in diameter, imbedded in a gelatin matrix of low, presumably electrolytic conductivity, is admittedly more complicated than that represented by the fused film of silver halide, and still more so than the single crystal. Difficulties of interpretation, absent in the simpler systems, might well be anticipated to arise. Moreover, the background of "dark current" against which the photo-currents are observed, exceeds them by some 50-fold at the highest intensities of illumination used and by several thousandfold at lower intensities. In the latter experiments, the photo-currents were of the order of 10^{-12} and 10^{-13} amperes. Although the method of measurement depends only on the change of current produced by exposure to light, it is very necessary to guard against confusion of photo-currents with changes in the dark current produced by spurious incidental effects of the radiation, such as heating. Low luminous intensities, quick-acting recorders and short exposures facilitate in this discrimination.

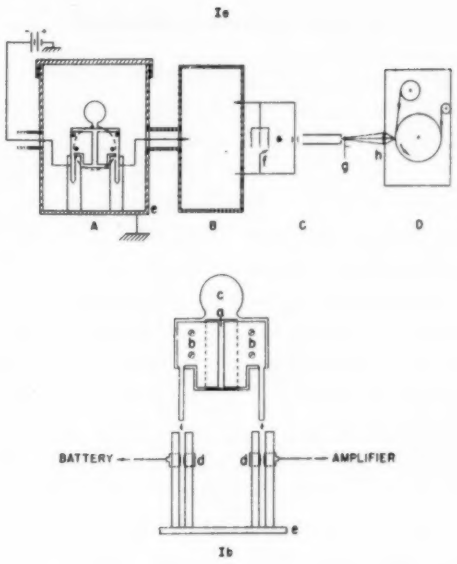

FIG. 1. Apparatus for measuring photo-conductivity of photographic film.

The photographic film, however, in spite of some unfavorable electrical characteristics, offers certain important advantages in the search for clear-cut correlations between photographic and photo-electric properties. In the first place, many features of photographic sensitivity depend on the presence of adsorbed layers on the halide grains; one of these is optical sensitization, which has been our principal interest in this study. Without the high ratio of surface to volume characteristic of the emulsion, enough dye for adequate absorption of radiation cannot be adsorbed. Moreover, in apparently simpler systems like single crystals and fused films of the pure salt, it is difficult to evaluate photographic sensitivity as distinct from direct photolysis to visible silver, and conclusions concerning the photographic process from observations on photolytic systems involve extrapolations that are always uncertain and often unreliable. In attempting to correlate photographic sensitivity with other physical properties of the silver halides it is, in general, a wise principle to make the measurements, as far as possible, on the emulsion for which the sensitivity data have been obtained.

(b) Apparatus and Method

Figure 1a is a diagrammatic sketch of the electrical part of the apparatus, consisting of the four parts: *A*, the box containing the sample, *B*, a d.c. amplifier, *C*, a string galvanometer, and *D*, its recorder. The film sample, *a* (Fig. 1b), was mounted, emulsion side outwards, between silver-plated electrodes, *b*, 48 mm long and 1 mm apart, carried by a polystyrene support, *c*. The diagram, *A*, depicts the arrangement of film, holder, and electrodes as it faced the incident light which is supposed to be directed on the film perpendicularly to the plane of the paper. Ready withdrawal and reproducible replacement of the sample were secured by mounting the film holder in the sockets, *d*, by plugs soldered to the electrodes. The metal sockets were carried in stout polystyrene pillars mounted on the floor of the metal box, *e*, serving as shield. One electrode was connected to the input of the d.c. amplifier, *B*, the other to the negative terminal of a dry-cell battery variable up to 135 volts. The output of the amplifier was connected to the string galvanometer, *C*, Type P of the Cambridge Scientific Instrument Company. The string was a gilded quartz fiber of some 2000-ohms resistance. A set of shunts, *f*, permitted variation of the sensitivity from very low values used in preliminary adjustment to the full sensitivity. The deflections of the string were recorded photographically, time and deflection scales being registered by means of a rotating spoked disk, *g*, driven by a Telechron motor, and an engraved scale on the cylindrical lens, *h*, of the camera, *D*. Calibration was effected by applying to the input of the amplifier, by means of the potentiometer used to compensate for the dark current, an accurately known potential of 1.5 millivolts.

A single-stage amplifier containing a General Electric FP-54 electrometer tube in the circuit of DuBridge and Brown[10] was first used; more recently a linear three-stage amplifier with feed back, of considerably higher sensitivity, has been employed. We are indebted to Dr. R. W. Tyler, of these Laboratories, for the design and for supervising the construction of this amplifier. A voltage sensitivity of 5×10^4 divisions of the galvanometer scale per volt change of the input potential was normally used, corresponding to a current of 5×10^{-15} amperes per division at an input resistance of 10^{10} ohms.

Exposure times of 0.3 second were usually given, determined by a vane shutter of 2-inch aperture placed in front of the glass window of the measuring box, although currents were measurable at exposures of 0.02 second. An auxiliary beam was arranged to pass through this shutter without entering the measuring box, *A*, and by appropriate optical contrivances was focused at one side of the strip of photographic paper in the recording camera so as to form a mark on the developed record indicating the beginning and end of the exposure. In this way it has been ascertained that the photo-current begins immediately the shutter is opened and starts to fall immediately it is closed.

The dark resistance of the film was found to depend on the humidity of the circumambient atmosphere, and the ease of measurement of the photo-currents depended on this resistance. Very low humidity was associated with high film resistance and low values of the photo-currents, while high humidity was associated with experimental difficulties originating in large background currents. Films of the size required for the holder depicted in Fig. 1b were conveniently measured at relative humidities of 30 to 40 percent. Measurements were most easily carried out when the general room humidity was in this range; otherwise, the films were preconditioned in a desiccator over a saturated salt solution of appropriate humidity, e.g., saturated $CaCl_2\cdot6H_2O$ (relative humidity, 31 percent at 24.5°C) or saturated $K_2CO_3\cdot2H_2O$ (r.h. = 43 percent at 24.5°), and the measuring box was also provided with the same solutions. At humidities from about 30 to 50 percent, the magnitude of the photo-current was not highly sensitive to the value of the dark resistance, and no other control than those mentioned was necessary to secure reproducible readings on different samples of the same film.

Re-exposure of a sample once exposed usually yielded a smaller photo-current than the initial current, and for this reason a new sample was used for every determination, for instance, in a set of measurements of a given film at different

[10] See J. Strong *et al.*, *Procedures in Experimental Physics* (Prentice-Hall, Inc., New York, 1939), p. 418.

wave-lengths. Pieces were cut from adjacent places in the roll of film, the operations of mounting the sample in the holder and of placing the holder in the measuring box being carried out, of course, in non-actinic light.

The optical arrangement consisted of a 500-watt tungsten-filament projection lamp, focused on the entrance slit of a lens-grating monochromator of aperture $f:2$, from the exit slit of which beams of desired wave-length, covering a band of about 11 mμ, were projected on the sample so as to cover all of the film between the electrodes. Variation of intensity was effected by introducing "neutral filters" into the exit beam from the monochromator. The grating was a replica furnished by Professor R. W. Wood, with a ruled surface 3 inches by 4 inches, and threw a large percentage of the incident light into one order. In some earlier experiments, isolation of the radiation was effected by filters.

Energy measurements of the light incident on the film were made by means of a Moll microthermopile placed in the position of the film. The thermopile was used with a Cambridge D'Arsonval galvanometer of 40-ohm resistance, and the arrangement was calibrated against a standard lamp furnished by the Bureau of Standards. Transmissions of filters were measured by a photronic cell and the same galvanometer. The linearity of response of these energy-measuring instruments with intensity was established experimentally in the intensity ranges of interest.

The range of exposures (intensity×time) in the photo-conductive experiments extended from values within the normal photographic range to values a thousand or more times greater. Fast negative emulsions were used, as normal film coatings. The lowest intensities used were such that, on developing the film after the photo-conductive exposure, the density of developed silver corresponded to a point on the shoulder of the Hurter and Driffield characteristic curve, definitely below the maximum density for the emulsion and not in the region of solarization. The very high exposures were made by increasing both the intensity and the time of illumination and produced visible print-out silver. Certain quantitative differences are to be found in the behavior of the photo-conductance at low and at high intensities, but no fundamental difference exists in the spectral distribution or in the general correlation with the spectral distribution of photographic sensitivity. In particular, wave-lengths at which maxima and minima in photo-conductivity occur are independent of the intensity level.

The absorption spectra of the films used were determined by means of a General Electric automatic recording spectrophotometer. We are indebted to Mr. E. E. Richardson, of these Laboratories, for these measurements. The percentage transmission and reflection were measured directly, and the percentage absorption was computed as 100 (percent transmission+percent reflection).

(c) Some Characteristics of the Photo-Currents in Photographic Films

When a film mounted in this apparatus was exposed to light of appropriate wave-length, the galvanometer index began to deflect simultaneously with the start of the exposure period, but reached a steady value only in a period greater than that of the galvanometer-amplifier system. The period of growth depended on the type of film and on the intensity and wave-length of the exciting light. In fast photographic emulsions, times of the order of 0.2 to 1.0 second were required for the deflection to assume a steady value in the intensity range in which current was proportional to intensity. At high intensity (for example, at 1000 ergs/sq. cm/sec.), a steady terminal current might not be observed within some seconds, constant illumination producing a rapid initial deflection followed by a prolonged slower rate of increase. At the end of the exposure, the deflection began immediately to fall, approximately exponentially with time, to a value representing a dark resistance lower than the initial resistance, from which there was a slow recovery of the initial resistance.

The absence of a nearly instantaneous component in the photo-currents measured at room temperature is in contrast to the situation in single crystals at low temperature in which the presence of an inertialess component is taken as a criterion of the production of primary photo-electric emission. The immeasurably rapid rise

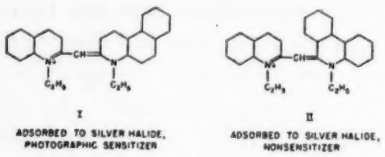

FIG. 2. Dye I, adsorbed to silver halide, photographic sensitizer; dye II, adsorbed to silver halide, non-sensitizer.

and fall of the photo-current at low temperature is probably associated with the permanent trapping of the photoelectrons, the value of the steady current being equivalent to the motion of the electronic charge through a certain distance, the "mean displacement," towards the anode before trapping.[3] At room temperature, however, some of the trapped electrons may be ejected again into the conduction band, making additional contributions to the current, equivalent to an increase in the mean displacement, and the exponential fall of current after the stoppage of the exposure probably represents the decay of thermally ejectable trapped electrons according to a unimolecular law.

The fact, moreover, that the system consists of minute isolated photo-elements, will tend to prolong the time over which photo-current is gaining. In the first instants of exposure, few grains have acquired enough quanta to produce substantial currents, and during exposure the contributions of more and more grains are added to the observed current, which therefore increases at a measurable rate. We have, in fact, found experimentally that the rate of increase of the photo-currents with time becomes greater the larger the grain size. In gelatinless systems composed of grains of silver chloride about 0.1 mm in diameter, 90 percent of the rise to the final steady value is accomplished in a few hundredths of a second.

RESULTS

Variation of Photo-Currents with Voltage

Numerous tests have shown proportionality of the photo-currents in photographic films to the applied field strength, up to the maximum used, 140 volts per mm, at all wave-lengths. No evidence of saturation of these currents has been observed.

TABLE I. Photo-conductivity in dye-sensitized and unsensitized photographic films.

Dye	Relative photo-currents for light of wave-length, in mμ (Hg arc) >620	580	546	(436, 410)	Inertia speeds for light of wave-length, in mμ (tungsten) >590	>500	400–500
—	0	<5*	11	171	0	3	575
I	10	180	85	330	73	1640	406
II	0	8	15	300	0	0	406
III	0	<8*	4	153	0	0	406

Dye-Sensitization of Photo-Conductivity

The first experiments were designed to show whether the currents produced by illumination of photographic films as described in the last section were in fact related to photographic sensitivity or whether they were influenced by heating effects of the radiation on the electrolytic conductivity of the grain or of the gelatin. Measurements were made on films prepared from the same basic bromoiodide emulsion containing, respectively, (a) no dye, (b) the efficient sensitizing cyanine dye, I (Fig. 2), with an absorption maximum and a sensitized photographic maximum at 585 mμ,[11] (c) the non-sensitizing cyanine

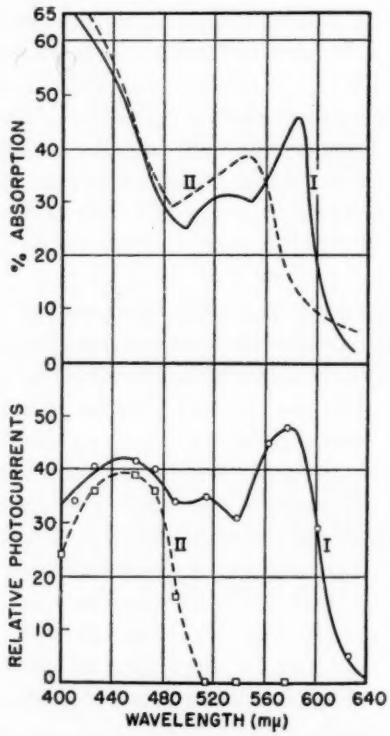

FIG. 3. Percent absorption and photo-conductivity of films containing dyes I and II.

[11] Dye I was brought to a state of maximum photographic efficiency in the emulsion by the addition of a

dye, II, isomeric with I, adsorbed to the halide in the emulsion, with an absorption band in the green comparable in intensity to that of I, and (d) a non-sensitizing dye, III, of the oxonol class, with an intense absorption band in the green, but present in the gelatin and not on the grains. All three dyes absorb light in the same general region of the spectrum; effects caused by any heating of the grains or gelatin by the absorbed energy would, therefore, be expected to be similar, but only dye I is a photographic sensitizer.

A particularly crucial experiment is summarized in Table I. The source was a mercury arc from which different spectral regions were isolated by filters and exposures of two seconds were made. Under these conditions of high intensity and relatively long exposure, any spurious thermal effects of the radiation would be comparatively large. The photographic characteristics of the films are denoted in the right-hand side of the table as inertia speeds[12] with respect to filtered light from a tungsten source; no quantitative comparison can be made between the relative photographic and photo-conductive sensitivities owing to the difference in the nature

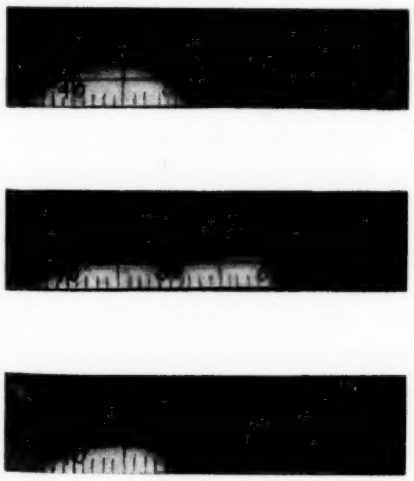

FIG. 4. Spectrograms of emulsion: unsensitized, containing dye I, and containing dye II.

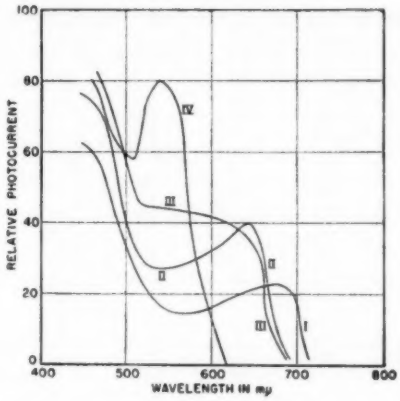

FIG. 5. Photo-conductance in various dye-sensitized photographic films. Dyes: I, a dibenzothiacarbocyanine bromide; II, a thiacarbocyanine iodide; III, a selenacarbocyanine bromide; IV, a merocyanine.

of the sources. The essential fact emerges, however, that only the film showing sensitized photographic activity in the green and yellow exhibited currents on exposure to the green and yellow mercury lines comparable in magnitude and other characteristics to those produced by blue light. The small deflections denoted by the asterisks in the unsensitized films were noticeably more sluggish than correspondingly small deflections produced by blue light, and since later experiments with lower exposures showed no photo-conductivity in unsensitized films exposed to green and yellow light, they probably represent spurious effects. There seems no doubt that the relatively large currents produced by blue light in all four films, and by green and yellow light in the film containing the sensitizing dye are to be ascribed to true photo-conductivity.

The photo-conductivities of the films containing dyes I and II were later determined with the apparatus using the three-stage amplifier at intensities of 14 to 50 ergs per cm² per second and exposure times of 0.3 second to light from a continuous source isolated by the monochromator. Figure 3 shows the spectral absorption and photo-conductivity so determined, while Fig. 4 reproduces the neutral-wedge spectrograms of a tungsten source as recorded by the films containing the dyes and by the undyed film. The photo-conductivity data in Fig. 3 and the sensitometric data in Fig. 4 are both uncorrected to equal incident intensities at the various wave-lengths. Comparison of the figures

small quantity of a "supersensitizer" 1-(*p*-diethylaminostyryl) benzothiazole, itself non-absorbent and photographically inactive when exposed to light in the sensitization band of the dye. (B. H. Carroll and J. A. Leermakers, U. S. Patent 2,313,922 (1943).) See Part II of this series.

[12] C. E. K. Mees, *The Theory of the Photographic Process*, (The Macmillan Company, New York, 1942), p. 204.

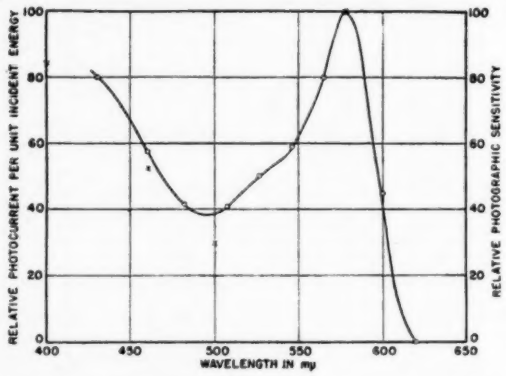

FIG. 6. Spectral distribution of photo-conductance and photographic sensitivity. Dye; 1,1′-diethyl-2,2′-cyanine iodide+supersensitizer. o, photo-currents; x, photographic sensitivity.

shows a very considerable degree of parallelism in the spectral distribution of photo-conductive and photographic sensitivity. From these and many similar experiments, there seems no doubt that the currents discussed in this paper are due to a true photo-conductivity originating in the primary photographic process of the photo-liberation of electrons within the halide grains and that sensitized photo-conduction can be induced by the same dyes as cause sensitized photographic activity, at the same wave-lengths and of relative magnitudes comparable to those shown in photographic sensitization.

The existence of dye-sensitized photo-conductivity in fused films of silver bromide bathed in certain sensitizing dyes was reported by Kameyama and co-workers.[7] No details are given in the notes published by these authors.

We have compared the spectral distribution of photo-conductivity and of photographic sensitivity for emulsions containing a considerable number of dyes of the cyanine, carbocyanine, dicarbocyanine, and merocyanine classes. Figure 5 records some of the results on photo-conductivity. The photographic maxima of the dyes represented by curves I, II, III, and IV are at 680, 640 (550 and 615), and 550 mμ, respectively. Invariably a parallelism in the spectral sensitivity of the two phenomena in dyed photographic films has been found; maxima and minima in the magnitudes of the effects occur at the same wave-length, determined by maxima and minima in the amount of energy absorbed. A good photographic sensitizer gives relatively large sensitized photo-currents and *vice versa*.

While parallelisms in the spectral distribution of photographic and photo-conductive sensitivity have always been found, over the whole intensity range studied, quantitative correspondence between the two effects is closest when they are measured at comparable intensities. The photographic sensitivity is measured by the reciprocal of the incident energy in ergs per cm² required to produce a developed density of 0.5. In Fig. 6, the relative photographic sensitivity so defined and the relative values of the photo-currents for unit incident energy are plotted as functions of the wave-length for a film containing the sensitizer, 1,1′-diethyl-2,2′-cyanine iodide, with a small quantity of a supersensitizer.[11] The photo-currents were measured at exposures corresponding to the shoulder of the characteristic sensitometric curve. There is good quantitative agreement between the spectral distribution of sensitivity in the photographic and photo-conductive effects. On the other hand, when the photo-conductivity is measured at intensities which produce visible silver, the ratio of sensitized photo-conductivity to that produced by absorption by the silver halide tends to be lower than the corresponding ratio of the photographic speeds, which are measured at much lower intensities. Partial destruction of the dye at high intensities may be the explanation.

Variation of the Photo-Currents with Intensity

Within the limits of experimental error, the photo-currents vary with intensity according to the relation $C=kI^{\alpha}$, where C is the photo-current, I the intensity of illumination, k a constant of proportionality, and the exponent α varies from 1 to 0.5 according to the intensity level. Up to intensities of about 150 ergs per cm² per second, the relation of the current to the intensity was usually linear. At higher intensities, the value of α fell, reaching a lower limiting value of 0.5 (Fig. 7). The value of the exponent was the same for unsensitized and dye-sensitized photo-conductivity. The square-root law at high intensities recalls the behavior of systems such as selenium cells, molybdenum crystals, and zinc

sulfide phosphors which show a similar current-intensity relation.[13]

Let us assume that the observed photo-currents in photographic emulsions are determined by the primary liberation of electrons from bromide ions into the conduction band. These electrons move towards the anode, but are brought to rest after traversing a certain mean range by being captured by some kind of trap.[14] Two cases can arise: the electrons, after a period of freedom, may be trapped (a) by "foreign centers," for example, crystal imperfections, traces of impurities, photographic sensitivity specks, self-trapping sites,[15] etc., or (b) by the "positive holes" (essentially bromine atoms) left in the lattice after their expulsion. Schematically, the situations are:

$$\text{(a)}\quad \mathrm{Br}^- + h\nu \rightarrow \mathrm{Br} + \epsilon$$
$$\epsilon + M \rightarrow M^- . \qquad (1)$$

If n is the momentary concentraton of free electrons, m the concentration of foreign traps, M and I the intensity, then

$$dn/dt = k_1 I - k_2 n m .$$

In the steady state, the rate of production equals the rate of trapping of electrons, so that

$$k_1 I = k_2 n m$$
$$n = (k_1/k_2 m) I .$$

Since the steady photo-current is proportional to n, it is, by this mechanism, directly proportional to the intensity, provided m is independent of intensity.

$$\text{(b)}\quad \mathrm{Br}^- + h\nu \rightarrow \mathrm{Br} + \epsilon \qquad (1')$$
$$\mathrm{Br} + \epsilon \rightarrow \mathrm{Br}^- . \qquad (2')$$

In this case, in the steady state,

$$k_1' I = k_2' n[\mathrm{Br}] = k_2' n^2$$
$$n = [(k_1'/k_2') \cdot I]^{\frac{1}{2}} .$$

Here the current is proportional to the square root of the intensity; if both mechanisms are at work, the current is proportional to I^α; $0.5 < \alpha < 1$.

[13] See, for example, D. S. Elliott, Phys. Rev. **5**, 53 (1915); W. W. Coblentz and H. Kahler, Sci. Pap. Bur. Stand. **15**, 121 (1919); H. Gudden and R. Pohl, Zeits. f. Physik **35**, 243 (1925).

[14] R. W. Pohl, "Report of conference on the conduction of electricity in solids," Proc. Phys. Soc. **49**, 16 (1937).

[15] L. Landau, Physik. Zeits. Sowjetunion **3**, 664 (1933).

At sufficiently high intensities, the electronic concentration could be so great as to cause saturation of foreign traps, and recombination with bromine atoms would become the main process terminating the mean range. At low intensities, however, recapture by bromine atoms seems, in the light of the linear intensity photo-current relation, improbable compared with trapping by foreign centers. If this interpretation is correct, loss of primary photoelectrons by bromine-capture is a relatively minor factor in a normal photographic exposure at moderate intensities.

DISCUSSION, AND THE MECHANISM OF PHOTOGRAPHIC SENSITIZATION BY DYES

The results of the present investigation complete the chain of evidence on the photographic function of sensitizing dyes started by the observations of Leermakers, Carroll, and Staud concerning the relation between the absorption of the dye and the photographic sensitivity of dyed emulsions.[16] These workers established the correspondence between the photographic sensitivity and the absorption of the dye as adsorbed on the silver salt; here, we interpret the parallelism between photo-conduction, absorption, and photographic sensitivity to indicate that the function of the light absorbed by the dye is to cause free electrons to appear in the halide, which then participate in the formation of the latent image in the same way as those generated directly by the self-absorption of the silver salt.

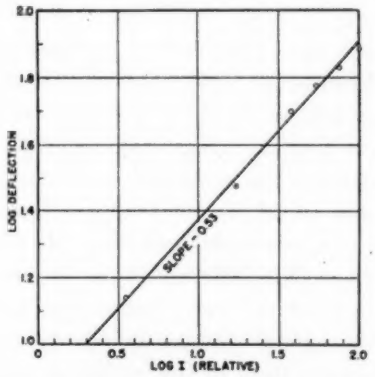

FIG. 7. Intensity photo-current relation at high intensity. $I = 100$ is equivalent to an incident intensity of 2483 ergs/sq. cm/sec. Exposure time = 0.3 sec.

[16] J. A. Leermakers, B. H. Carroll, and C. J. Staud, J. Chem. Phys. **5**, 878 (1937); J. A. Leermakers, *ibid.* **5**, 889 (1937).

The question may be asked: Does the photo-conduction observed in dyed photographic films really originate in the flow of electrons throughout the silver halide grain, or is it confined to the adsorbed layer of dye, a photo-conductivity of the dye? In the first place, the close correlation that exists between the photo-conductivity of dyed films and the photographic sensitivity, particularly the "supersensitizing" effect to be discussed in Part II of this series, is strong presumptive evidence in favor of the essential similarity of the photo-currents produced by the self-absorption of the silver halide and by the absorption of the dye. Moreover, direct experimental evidence indicates that no appreciable photo-conductivity of adsorbed dye layers can be detected under conditions similar to those prevailing in the photographic film, unless in the presence of a light-sensitive substrate. Dyed suspensions of lead chloride crystallites in gelatin were formed into films similar to photographic films. Lead chloride is photographically insensitive to visible light, and no photo-conductivity was observed either in dyed or undyed dry gelatin films of this material. Silver bromide films containing the same dye showed high sensitized photographic and photo-conductive sensitivity. Gelatin films containing sensitizing dye were likewise found photoelectrically insensitive to visible light. We conclude, therefore, that the observed photo-conduction of photographic films exposed to light absorbed by sensitizing dyes is caused by a flow of electrons within the silver halide grain.

Although the characteristics of photo-currents produced in the spectral region of dye-absorption are quite similar to those of the currents produced by silver-salt absorption, there is a difference in detail—the sensitized currents exhibit a rather more rapid rise to their stationary value than the non-sensitized currents. But there are also photographic differences in the behavior of films to light of the two regions; the contrast of the film is usually greater in the dye-sensitized spectral region than in the region of self-absorption. This difference is often attributed to the adsorption of a higher proportion of the dye to the smaller, normally less sensitive grains in the film. The sensitivity of these grains to light absorbed by the dye is therefore increased relative to their sensitivity to light absorbed by the silver salt. If the inertia observed in these photo-currents is partly caused by the relatively gradual "bringing-in" of the contributions of the individual grains, as previously suggested, it seems quite likely that the dye can influence the rate at which the contributions become effective in a manner somewhat analogous to its effect on the photographic contrast.

We are now in a position to discuss the bearing of our observations on the mechanism of photographic sensitization by dyes. Their function is to cause, through their absorption of light, a flow of electrons through the grain. The subsequent fate of these electrons is the same as that of electrons directly produced in the halide.

As to the manner in which the energy primarily absorbed by the dye causes electrons to appear in the silver salt, these measurements do not furnish a definitive answer. The alternative mechanisms are[17] a direct electron transfer from an optically excited adsorbed dye molecule to the conduction band of the halide, or a transfer of excitation energy from the dye in some way which causes a bromide ion of the lattice to expel an electron into the conduction band. There is a certain definiteness about the concept of direct electronic transfer that is lacking in the other mechanism, nor, in view of current notions of the high mobility of the π-electrons in conjugated chains,[18] does such a transfer appear improbable.

As Sheppard, Lambert, and Walker have emphasized, regeneration of the dye molecule may be an important stage in the process of sensitization. In the dye-sensitized production of visible silver in illuminated silver bromide, several silver atoms may be produced for each dye molecule present. Under these conditions, a given dye molecule can evidently participate more than once in the sensitizing act. It therefore seems probable that in the production of the latent image, the dye likewise is not destroyed in the sensitization act, although in that case the amount of dye on the grain is relatively so great compared with the silver produced that it is improbable that any given dye molecule partici-

[17] J. A. Leermakers, J. Chem. Phys. **5**, 889 (1937); S. E. Sheppard, R. H. Lambert, and R. D. Walker, J. Chem. Phys. **7**, 426 (1939).

[18] E. Hückel, Zeits. f. Elektrochemie **43**, 752 (1937).

pates more than once, and sensitization could be realized even if the sensitization act involved the destruction of the dye. If sensitization consists in an energy transfer from the excited dye to an electron in a bromide ion in the lattice, regeneration of the normal dye molecule occurs automatically at the instant of transfer. On the concept of electron transfer, the dye will have, after donating an electron to the halide, a vacant level corresponding to its original ground state, and if an electron can pass from a bromide ion in the lattice to this vacant level, the dye will be regenerated and a bromine atom produced—the whole process of transfer and regeneration leading to material changes in the silver salt exactly the same as those called forth by its self-absorption. At first sight, this regeneration would seem to require considerable energy of activation, particularly in the case of a sensitizer whose absorption band was far displaced from the region of silver halide absorption. Mott and Gurney,[19] however, have argued that, as a result of the excess positive charge on the adsorbed dye left after electronic transfer to the grain, mobile silver ions in the lattice will be repelled, and the electrons in the bromide ions at the grain surface will therefore be in a weaker positive field than before. The energy level of the electrons in these bromide ions is therefore raised nearer the value of the unoccupied dye level, with the result that the activation energy for transfer is lowered or may vanish. In support of this concept may be adduced the observations of Fajans[20] and his co-workers on the effect of adsorbed ions on the light absorption of silver halides. Adsorbed silver ions were found to displace the long wave-length limit of the absorption band of the silver halides to longer wave-lengths, and adsorbed halide ions in the opposite direction, effects consistent with the suggestion of Mott and Gurney of an upward displacement of the electronic levels associated with negative ions by positively charged adsorbed layers. The transition from the displaced level to the conduction band requires less energy, and the absorption limit is shifted towards longer wave-lengths.

It must be emphasized, however, that our present observations on dye-sensitized photo-conductivity do not decide between the mechanisms of electron and energy transfer, but are limited to showing the production of electrons within the halide as a result of energy absorbed by the dye.

[19] N. F. Mott and R. W. Gurney, *Electronic Processes in Ionic Crystals* (Clarendon Press, Oxford, England, 1940), p. 242.

[20] K. Fajans and G. Karagunis, Zeits. f. physik. Chemie **5B**, 385 (1929).

II. Some Applications to the Phenomena of Supersensitization, Desensitization, and the Becquerel Effect*,†

Studies of the photo-conduction of photographic films afford a means of discriminating between photographic effects originating in effects on the primary liberation of electrons and those due to actions effective at later stages in image formation. For example, the photographic action of certain supersensitizers in increasing the sensitizing effect of dyes of the 2,2′-cyanine class has its counterpart in a supersensitized photo-conductivity, showing that the supersensitizer influences the efficiency of the primary transfer of energy (or of an electron) from the sensitizing dye to the halide. On the other hand, photographically desensitizing dyes have only secondary effects on photo-conductivity, showing that their action is not essentially to inhibit the photo-liberation of electrons.

The photographic Becquerel effect—the conferring of sensitivity to light of wave-lengths longer than those absorbed by the silver halide by the presence in the film of photolytic silver—has an analog in photo-conductivity.

Part I described photo-conductivity in photographic emulsions characterized by a marked parallelism in spectral distribution with photographic sensitivity. The photo-currents were concluded to be intimately connected with the primary liberation of photoelectrons in the first step of generation of the latent image. In this communication, observations will be recorded which afford further evidence of the truth of this

* Communication No. 1112 from the Kodak Research Laboratories.

† Presented in part before the Division of Physical and Inorganic Chemistry at the 109th Meeting of the American Chemical Society, Atlantic City, New Jersey, April 10, 1946.

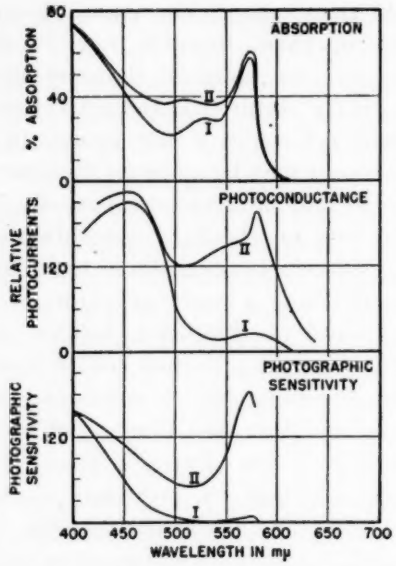

FIG. 1. Supersensitization of photo-conductance and photographic sensitivity. I. 1,1′-diethyl-2,2′-cyanine iodide alone. II. dye+supersensitizer.

conclusion, and also show how the results of studies in photo-conductivity can throw light on certain problems of photographic theory.

It will be recalled that the measurements made in these investigations refer to unsaturated photo-currents produced in the gelatino-silver halide system represented by the normal photographic film. Assuming that the currents are essentially conditioned by the primary liberation of electrons within the grains, it follows that their magnitude will be directly proportional to the rate of liberation of electrons and to the mean range traversed by the free electrons before capture by traps. Other things being equal, an increase in the primary rate of liberation of electrons will increase the photo-currents produced by a given applied field; and other things being equal, an increase in the number of trapping centers or of the efficiency of trapping will decrease the observed currents. In general, therefore, increased photographic sensitivity can be associated with either an increase or a decrease in photo-conductivity, as measured in these experiments. In dye-sensitization, an increase is observed because of the increased rate of liberation of electrons on excitation in spectral regions absorbed by the dye, but increased photographic sensitivity might also be effected by increasing the efficiency of trapping, which would be expected to produce a fall in the magnitude of the photo-currents.

The sensitivity of photographic layers can be greatly influenced by a wide variety of substances added during the preparation of the emulsion or by bathing before exposure. The effect of the addendum may be exerted at any one or more stages in the series of processes elapsing between the primary act of light absorption and the final production of developed silver, and it is not always easy to determine, from observations on the developed image, at what link in the chain the addendum has intervened. If, however, it increases the photo-conductivity, its function is very probably to increase the primary electronic emission. Dye-sensitization is a simple example of such an effect, and certain cases of the phenomenon of supersensitization seem to depend on a similar increase in electron flow within the halide.

SUPERSENSITIZATION[1]

Certain substances, when added to a photographic dye-sensitizer, cause an enhancement of the sensitizing effect, without themselves absorbing light in the sensitized spectral region, or necessarily being themselves sensitizers. A case of this phenomenon was first recorded by Bloch and Renwick.[2] In the course of comprehensive studies, Mees[3] found that the effect, which he termed supersensitization, occurred in most classes of sensitizing dyes, although the cases are by no means common. Other examples are contained in the later patent literature. The effect is somewhat analogous to promotor action in catalysis, and, like that phenomenon, probably has different origins in different cases. The experiments described here are restricted to one type of example, the supersensitization of the dye, 1,1′-diethyl-2,2′-cyanine iodide, and other 2′-cyanines by small quantities of another dye not absorbing in the same spectral region, for example, 1-(*p*-diethylaminostyryl)benzothiazole.[4]

Figure 1 shows the absorption spectrum and

[1] C. E. K. Mees, *The Theory of the Photographic Process* (The Macmillan Company, New York, 1942), pp. 975 and 1070.
[2] O. Bloch and F. F. Renwick, Phot. J. **60**, 145 (1920).
[3] C. E. K. Mees, U. S. Patents 2,075,046-8 (1937).
[4] B. H. Carroll and J. A. Leermakers, U. S. Patent 2,313,922 (1943).

the spectral distribution of photo-conductivity and of photographic sensitivity of photographic films containing the sensitizing dye without and with a supersensitizer. The photo-conductivity curve represents the photo-currents excited by light at various wave-lengths as actually incident on the film from the exit slit of the monochromator, while the photographic sensitivity is expressed in terms of the reciprocal of the incident energy in ergs per square centimeter required to produce a density of 0.5 in the developed image. The maximum in the photo-conductive sensitivity at about 460 mμ is therefore only apparent; when the currents are computed for equal incident energy at different wave-lengths, the curve rises steadily with diminishing wave-length from 500 mμ in a manner parallel with the photographic sensitivity. (See Part I of this series, Fig. 6.) In the experiments summarized in Fig. 1, the photo-conductivity was measured at high intensity (about 2000 ergs per square centimeter per second at 460 mμ and 5000 ergs per square centimeter per second at 575 mμ); later experiments, in which the intensities used in the photoconductivity and photographic determinations were more nearly equal, disclosed more exact quantitative parallelism between the two effects.

It is quite clear that the effects of the supersensitizer on photographic and photo-conductive sensitivity are parallel; and also that the supersensitizer does not function by influencing the absorption spectrum of the sensitizer. It is true that the intensity of absorption of the adsorbed sensitizer at the maximum at 575 mμ is somewhat increased by addition of the supersensitizer, but the increase in absorbed energy is small compared with the increase in photographic and photo-conductive sensitivity. It is not lack of absorbed energy which makes the sensitizer alone inefficient; the inefficiency must lie in the transfer of the absorbed energy (either directly or as a moving electron) to the halide. The increase in photo-conductivity with relatively little increase in absorption demonstrates that the function of the supersensitizer is, in some way, to produce a greater yield of free electrons in the silver halide for every unit of energy absorbed by the dye; these additional electrons then act in the usual way in initiating the growth of the latent image, and the net result is an increase in photographic sensitivity.

It is not our purpose to discuss here in any detail the interesting question of the mechanism of supersensitization in general, but some consideration of the special case just illustrated may be appropriate. It might be suggested that the action of the supersensitizer is to influence the manner of adsorption of the sensitizing dye to the silver halide so as to facilitate transfer. The minor changes produced in the spectral absorption seem, however, to be inconsistent with such an action.

It is possible that the action of the supersensitizer is connected with its disturbing a flow of energy within the adsorbed layer of dye, which otherwise would be retained in the dye and ultimately be dissipated as fluorescence and thermal energy of the dye molecules. When a molecule in a closely packed monolayer of dye absorbs a photon, there will be, with suitable mutual orientation of the dye molecules, a high probability of the propagation of the excited state throughout the layer by resonance interaction between molecule and molecule.[5] Such a layer might well interact inefficiently with the silver halide substrate; only when the excited state happened to reach a dye molecule adjacent to some foreign molecule would the propagation be disturbed, and a transfer to the halide occur. The function of the supersensitizer, which is assumed to be dilutely dispersed as individual molecules throughout the layer of sensitizer, may be to increase the numbers of these loci of disturbance and thus facilitate transfer. The supersensitizing molecule may participate actively in the final transfer, for instance, by first absorbing the energy of excitation in the dye layer and communicating it to the halide layer as a moving electron or as a quantum of energy, as the case

TABLE I. Desensitizer action on photo-conductivity and photographic sensitivity.

	Relative photo-current for illumination at wave-lengths in mμ				Photographic threshold speed for illumination at wave-lengths in mμ		
Dye	>620	>550	500–570	400–500	>590	>500	400–500
—	0	5	11	171	0	3	580
Desensitizer	3	18	9	147	0	0	0

[5] Cf. J. Franck and E. Teller, J. Chem. Phys. 6, 861 (1938).

TABLE II. Photo-conductive Becquerel effect.

Galvanometer response to 578 mμ before exposure to blue	0
Galvanometer response to blue	500
Galvanometer response to 578 mμ after blue exposure	30
Galvanometer response to 578 mμ after a blue exposure 5 times as intense as first	70

may be. To this concept of the action of the supersensitizer, support is furnished by certain observations on fluorescence made in these laboratories. The 2,2′-cyanine dye under discussion, adsorbed to the silver salt in a photographic layer, fluoresces (although the intensity is not sufficient in itself to account for the inefficiency of photographic sensitization), and this fluorescence is readily quenched by dyes such as 1-(*p*-diethylaminostyryl) benzothiazole, that act as supersensitizers, and not by dyes such as 3,3′-diethyloxacarbocyanine iodide which do not supersensitize. The bright fluorescence of the aqueous gel of the chloride of the dye is also very readily quenched by supersensitizers sufficiently soluble in water. These substances are in fact the most efficient and complete quenchers found for this particular fluorescence. Here seems to be evidence of a capacity of the supersensitizer to interrupt the propagation of the excitation energy through the "aggregate" of sensitizer and to use it for its own purpose.

We can also see how, according to this proposed mechanism, the requirements that supersensitizers must fulfill cause examples of the phenomenon to be fairly rare. The supersensitizer must be dilutely dispersed in a state resembling "solid solution" in the two-dimensional crystal represented by the adsorbed sensitizer; it must not segregate on the halide grain apart from the sensitizer. It is therefore likely to be a dye, which must fulfill rather restricted "solubility conditions" in the adsorbed sensitizer and moreover, when in contact with the silver halide grain, it must make no permanent claim on the energy acquired by the sensitizer.

DESENSITIZATION[6]

As is well known, certain dyes, for example, phenosafranin, when incorporated into a photographic emulsion, greatly diminish photographic sensitivity. Desensitizing dyes afford an example of a class of addenda which have profound photographic effects and relatively minor effects on photo-conductivity.

Table I contains data obtained at high intensity of illumination on the action of the desensitizing azacyanine, 3,3′-diethyl-8,9-diazathiacarbocyanine iodide,[7] on photographic and photo-conductive sensitivity. The photographic sensitivity is expressed as inversely proportional to the inertia.[8]

While the addition of the desensitizer practically eliminated photographic sensitivity, photo-conductivity as measured by the steady terminal current was little impaired. Particularly interesting is the small increase in photo-conductivity over that of the undyed film for illumination by orange light, the region of absorption of the adsorbed dye. A slight sensitization for photo-conduction is indicated, and, although in this emulsion no trace of photographic effect was observed in the sensitometric exposure, in other emulsions, a slight optical sensitizing effect of this dye has actually been observed.

The desensitizer does have some effect in slowing the rate of increase of photo-current with time at the start of the exposure and may decrease the final value by some 10 to 15 percent; further studies will be necessary for a complete description of the effect of desensitizers on the photo-conductivity of photographic films. It is clear, however, that the effect of a desensitizer incorporated in a photographic layer is not to inhibit the primary emission of photoelectrons, but must be exerted at a later stage in the sequence of processes concerned in the production of a latent-image speck, for instance, possibly, by acting as a source of alternative electron traps to the sensitivity centers, or by attacking the sensitivity specks or the nascent latent image.

AN ANALOGY TO THE BECQUEREL EFFECT IN PHOTO-CONDUCTIVITY

In 1843 E. Becquerel[9] showed that the photolytic sensitivity of silver chloride papers could be extended into the green, yellow, and red regions

[6] C. E. K. Mees, *The Theory of the Photographic Process* (The Macmillan Company, New York, 1942), pp. 1040 *et. seq.*

[7] Fuchs and Grauaug, *Ber.* **61**, 57 (1928).

[8] See reference 6, p. 712.

[9] E. Becquerel, *Ann. chim. phys.* (3) **9**, 257 (1843).

if a pre-exposure to blue light sufficient to produce some visible photolytic silver was first made. Later studies include those by Eggert and Noddack[10] and by Sheppard.[11]

It is therefore interesting that what appears to be the photo-conductive analog of this photographic effect has been observed. A bromide film, originally inert photo-conductively to light longer than 500 mμ, becomes active to long-wave illumination (in this case 578 mμ) after an exposure to blue light sufficiently strong to produce a slight visible amount of photolytic silver. Table II includes illustrative data. The light source was a mercury arc, General Electric Type H4, the wave-lengths from which were isolated by filters. Further increase in the exposure to blue light caused little increase in sensitivity to yellow. The "sensitized" photo-conduction, like the sensitized photographic effect in the Becquerel phenomenon, is small compared with the effects induced in the region of self-absorption.

A plausible mechanism for the extension of photo-conductivity toward longer wave-lengths by a pre-exposure of the film to blue light is afforded by the discussion of Mott and Gurney[12] on the photoelectric behavior of metals in contact with photo-conducting salts. The "print-out" deposit produced by the blue pre-exposure almost certainly consists of colloidal particles of metallic silver in intimate contact with silver bromide. Although photoelectric emission from metallic silver into a vacuum requires excitation by ultraviolet light, Mott and Gurney point out that silver immersed in silver bromide will be able to emit electrons into the conduction band of the salt under the stimulus of a considerably smaller quantum. Having entered the conduction band, the electron primarily yielded by the silver particle participates in photo-conduction like any other electron raised to that state.

It will be seen that photoelectric emission from "print-out" silver particles followed by the normal fate of electrons ejected into the conduction band of the bromide would lead merely to a redistribution of silver throughout the grain, whereas Eggert and Noddack's observations on the photolytic Becquerel effect point to an increase in silver during the exposure to long wave-lengths, though with low quantum efficiency. It would seem, therefore, that the photolytic Becquerel effect involves something more than the photo-liberations of electrons from silver particles into the conduction band of the salt; this may be the passage of electrons from disturbed sites in the halide lattice adjacent to the silver particle into the metal. On the other hand, there is evidence that the Herschel effect,[13] the regression effected by red and near infra-red light of the photographic image produced by pre-exposure to blue light, is accompanied merely by a redistribution of silver, and it may be that the sensitized photo-conduction produced by print-out silver represents the primary act in this effect. Having lost an electron by absorption of long wave-length light, the colloidal silver particle is likely to lose a silver ion by thermal agitation, which however may be reunited to the electron when the latter is trapped. No change in the total amount of silver is produced by this process, although the original particles may be reduced in size.

[10] J. Eggert and W. Noddack, *Zeits. f. Physik* **31**, 922 (1925).

[11] S. E. Sheppard, J. Frank. Inst. **210**, 587 (1930).

[12] N. E. Mott and R. W. Gurney, *Electronic Processes in Ionic Crystals* (Clarendon Press, Oxford, England 1940), p. 245.

[13] See reference 6, pp. 277 *et. seq.*

Determination of the Ranges of the Fission Fragments Emitting Delayed Neutrons. Chemical Identification of the 4.51-Sec. Delayed Neutron Activity*

NATHAN SUGARMAN
Argonne National Laboratory and Institute for Nuclear Studies, University of Chicago, Chicago, Illinois

(Received April 9, 1947)

The ranges of the fission fragments leading to delayed neutron emission have been determined by absorbing the fragments in Al and counting the penetrating activity. The delayed neutron activities and their corresponding ranges in Al corrected for source thickness are: 4.51 sec., 4.05±0.03 mg Al/cm²; 55.6 sec., 3.98±0.06 mg Al/cm²; 1.52 sec., 3.63±0.12 mg Al/cm²; 22.0 sec., 3.21±0.04 mg Al/cm². Comparing the range of the 4.51-sec. activity with that of the 55.6-sec. Br, one finds that mass assignments possible for the 4.51-sec. activity are 86 to 90. Similarly, the range of the 1.52-sec. activity is compared to that of the 22.0-sec. I, and the possible mass assignments found are 129 to 135.

Chemical separation of Br from irradiated uranyl nitrate resulted in the identification of the 4.51-sec. activity as an isotope of Br.

1. INTRODUCTION

SNELL and co-workers[1] chemically isolated the delayed neutron activities of 55.6-sec. and 22.0-sec. half-lives in Br and I fractions, respectively, leaving three shorter-lived activities unidentified. Bohr and Wheeler[2] postulate that the neutron is emitted following the β^- emission of a fragment if the resultant nucleus is left in a state of excitation above the neutron-binding energy. The neutron emission occurs instantaneously from the excited nucleus, so that the period is determined by the half-life for β^- emission of the precursor. Thus, the 55.6-sec. Br decays to an excited state of Kr which then emits the neutron. Tentative mass assignments of 87 and 137 were given to the 55.6-sec. Br and 22.0-sec. I by Snell *et al.*[1] because of the possible identity of these activities with the 50-sec. Br^{87} and 30-sec. I^{137} found in uranium fission by Strassmann and Hahn.[3]

TABLE I. Half-lives and yields of the delayed neutron emitters.

Half-life	Neutron yield relative to fission neutrons (percent)
55.6 sec.	0.026
22.0 sec.	0.17
4.51 sec.	0.21
1.52 sec.	0.24
0.43 sec.	0.084

A summary of the data of Hughes and co-workers[4] on the half-lives and yields of the prominent delayed neutron emitters in the fission of U^{235} is given in Table I.

The chemical isolation of the delayed neutron emitters remaining to be identified is more difficult because of their relatively short half-lives. Since the task of devising chemical procedures which can be performed in from 10 to 30 seconds for isolation of the delayed neutron periods from among the 30 odd elements in fission appeared to be too laborious, it was decided to use another type of experiment to confine the neutron emitters among fewer elements.

The ranges of the fission fragments in Al have been determined for some of the masses formed in fission by the author and co-workers,[5] and it was found that the range varied with the mass, decreasing as the mass increased. Thus, the mass number of a fission product can be estimated by measuring the range and comparing it with ranges of fission products of known mass numbers. This technique was applied to the 4.51-sec. and 1.52-sec. delayed neutron emitters, with the

* This paper was first issued as an Argonne National Laboratory Report, CP-3622 (September 23, 1946).

[1] J. S. Levinger, E. P. Meiners, M. B. Sampson, A. H. Snell, and R. G. Wilkinson, Report CP-1967 (July 29, 1944); presented at the Chicago meeting, American Physical Society (June 20–22, 1946).

[2] N. Bohr and J. A. Wheeler, Phys. Rev. **56**, 426 (1939).

[3] F. Strassmann and O. Hahn, Naturwiss. **28**, 817 (1940).

[4] A. Cahn, J. Dabbs, and D. J. Hughes, Report CP-3094, (July 30, 1945).

[5] B. Finkle, E. J. Hoagland, S. Katcoff, and N. Sugarman, Report CC-2076 (August 25, 1944); Plutonium Project Record, **9B**, 6.6.2 (1946).

ranges of the 55.6-sec. and 22.0-sec. periods as standards. Once a rough mass assignment was found, it was used as a guide in selecting the chemistry to be used in isolating the activities. After the range of the 4.51-sec. period was found, it was shown that the activity could be separated chemically with the 55.6-sec. Br by extracting Br from irradiated uranyl nitrate solutions. The chemical isolation of the 1.52-sec. period was not attempted.

2. RANGE STUDIES

2.1 Experimental Procedure

The procedure used in the range studies is in outline as follows. A thin extended source of U, enriched in U^{235}, is covered with thin Al absorbers and a recoil catcher and is irradiated with thermal neutrons for a specified time. After irradiation, the catcher is separated from the source and absorbers, and the delayed neutron activity present on the catcher is determined. The delayed neutron curve is analyzed into its components, and the activity of each component is determined. The irradiations are carried out for varying thicknesses of Al absorbers (0, 1.70, 2.59, 3.40 mg Al/cm^2) so that the activity of each component as a function of Al absorption is determined. The technique used in these experiments differed somewhat from the range studies referred to earlier[5] in that the integral activity penetrating a given thickness of Al was determined directly here, whereas in the earlier experiments the Al absorbers themselves were analyzed, and the integral activity was obtained by summing over the individual absorbers. The irradiation times were varied from 5 seconds to 3 minutes for any given absorber in order to accentuate some periods relative to others. From the plot of activity *vs.* thickness of Al absorbers one finds the range of the fragments giving rise to a specific period, and from the range an estimate of the mass number. The thin absorber technique for determining ranges was adapted from that used by Segré and Wiegand[6] in their study of the maximum ranges of the fission fragments in various

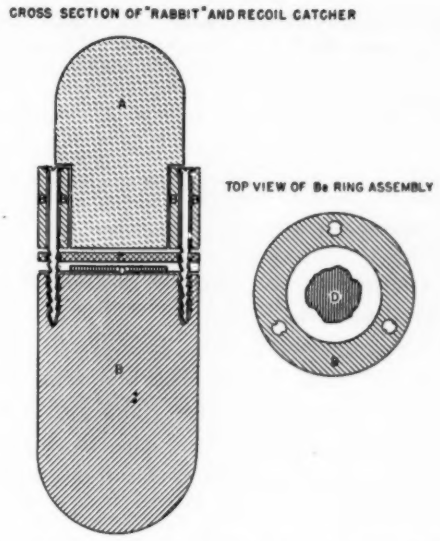

FIG. 1. "Rabbit" and recoil catcher. *A*, Bakelite plastic recoil catcher; *B*, beryllium; *C*, Al absorber; *D*, U^{235} source.

materials. A more detailed description of the apparatus follows:

(a) *"Rabbit" and Recoil Catcher*

The short periods of the neutron emitters make it necessary to use means of introducing and removing the sample rapidly. The pneumatic tube at the heavy water pile of the Argonne Laboratory is well suited for this since samples can be blown in or out of the neutron field in about a second. The sample is contained in a "rabbit," the design of the one used in this experiment is given in Fig. 1. The "rabbit" was made of Be which is strong enough to endure the many shocks suffered in transit through the pneumatic tube. Since Be has a low activation cross section, it may be handled soon after removal from the pile. The source and Al absorbers are held in place by a beryllium ring which is attached to the "rabbit" by three screws. The recoil catcher made of fiber-impregnated Bakelite fits into the beryllium ring rather snugly so that it requires a jar to dislodge it. After irradiation, the "rabbit" is blown out of the pile and strikes a stop in the tube. Since the outer diameter of the recoil catcher is smaller than that of the beryllium "rabbit," the two separate and the former continues to the neutron counter. The activity on the catcher is

[6] E. Segré and C. Wiegand, Report LA-64 (February 29, 1944); recently published in Phys. Rev. **70**, 808 (1946).

TABLE II. Activity of the 55.6-sec. and 22.0-sec. periods on the recoil catcher as a function of Al absorber.

Period \ Al absorber (mg Al/cm²)	0	1.70	2.59	3.40	Range (mg Al/cm²)
55.6 sec.	8700 c/m	4690 c/m	3030 c/m	1120 c/m	3.93±0.06
22.0 sec.	50200 c/m	23900 c/m	8500 c/m	2000 c/m	3.16±0.04

then counted in the absence of the U^{235} source and Al absorbers.

The Al absorbers were 1.70, 2.59, and 3.40 mg Al/cm². The latter absorber was made up of two of the thinner ones. The individual absorbers were weighed, and the thickness used represents an average over the area confined by the "rabbit."

(b) *Neutron-Counting Apparatus*

The neutron counter used here was constructed by Hughes and Hall[7] for their study of the total yield of delayed neutrons from U^{235}. It consisted of a cadmium-covered paraffin block in which there were 8 boron-coated neutron counters arranged cylindrically around a sample slot. Tests with sources of high γ-activity showed that the counters were rather insensitive to γ-radiations. The scaler pulses activating the recorder could be varied by steps of 4, from a scale of 512 to a scale of 2. Since the decay of the samples soon after irradiation was rapid, the scaler pulses were recorded on a moving tape in an electro-cardiograph and later analyzed. After the sample had decayed for about a minute the scaler counts were recorded visually. The counter background was ~40 c/m with the pile operating at full power.

The bombardment and counting procedure is as follows. The "rabbit" is assembled with the source, Al absorber, and recoil catcher in place. It is put into the trap door of the pneumatic tube with the end of the "rabbit" opposite the recoil catcher facing the pile. The scaler is turned on and the electro-cardiograph started. The "in" button of the pneumatic tube is pressed, and the "rabbit" is sucked into the pile. Pressing the "in" button produces a pip on the electro-cardiograph tape. After the desired irradiation time the "out" button is pressed (also producing a pip on the tape which serves as the timing mark for the end of the irradiation), and the rabbit is blown out of the pile. A "stop" in the pneumatic tube, about 8 ft from the neutron counter, separates the "rabbit" from the recoil catcher which continues on toward the neutron counter and is stopped in the sample slot. The time elapsed between pressing the "out" button and the recording of the counting marks on the tape is about 1 second. As the counting rate decreases, the scaler output is varied from a scale of 512 to 8. After a minute has elapsed, the electro-cardiograph is turned off, but the scaler is kept on, and the counting is done by reading the recorder at specified intervals. The electro-cardiogram is developed and read, and the activity is plotted as a function of time. The curve is then ready for analysis into the component neutron activities.

2.2 Results and Discussion

The activities first studied by this technique were the 55.6-sec. Br^{87} and 22.0-sec. I^{137}, since their chemical identities were known and tentative mass assignments had been made. Irradiations were made for 3 minutes, and counting was started 20 seconds after the end of the irradiation. Six irradiations were made for each absorber, and the average decay curve was plotted. The analysis into the 55.6-sec. and 22.0-sec. periods was made by the technique used by Hughes *et al.*[4] of summing up the counts over a time interval (t_1 to t_2) where the 55.6-sec. period alone is present, and equating the sum to $\int_{t_1}^{t_2} A^0 e^{-\lambda t} dt$ from which the value of A^0 (activity at end of

TABLE III. Activity of the 4.51-sec. and 1.52-sec. periods on the recoil catcher as a function of Al absorber.

Period \ Al absorber (mg Al/cm²)	0	1.70	2.59	3.40	Range (mg Al/cm²)
4.51 sec. (15-sec. irradiation)	69000 c/m	41000 c/m	25000 c/m	9300 c/m	4.00±0.04
4.51 sec. (5-sec. irradiation)	38000 c/m	22000 c/m	13500 c/m	3800 c/m*	4.01±0.02
1.52 sec. (5-sec. irradiation)	53500 c/m	30000 c/m	14000 c/m	5000 c/m*	3.58±0.12

* These points were not used in the least-squares analysis because of the difficulty in obtaining reproducible results.

[7] D. J. Hughes and D. Hall, Report CF-3209 (October, 1945).

irradiation) can be calculated. After calculating the value of A^0 for the 55.6-sec. period one subtracts the activity of this period from the total activity and similarly analyzes the residual points for the value of A^0 for the 22.0-sec. period. The results given in Table II were obtained in this way.

The plot of activity *vs.* mg absorber for the recoil geometry used here (~50 percent) should be a straight line represented by the equation:

$$A_t = k(R-t),$$

where A_t is the recoil activity penetrating the absorber thickness t, k is a constant, and R is the range of the recoil fragments. The points establish fairly good straight lines (see Fig. 2), and the ranges found by a least-squares analysis of the points are 3.93±0.06 mg Al/cm² for the 55.6-sec. period and 3.16±0.04 mg Al/cm² for the 22.0-sec. period. The last point was not included in the analysis of the 22.0-sec. period, since it is beyond the range determined by the other points and arises from the straggling of the range of the fragments observed in earlier experiments.[5]

Shorter irradiations of 5 to 15 seconds were used for the 4.51-sec. and 1.52-sec. periods, and the activities of the 22.0-sec. and 55.6-sec. periods present in the sample were calculated from those found in the 3-minute irradiations. Here, again, between 6 and 10 irradiations were averaged for each decay curve. The 0.43-sec. period could not be isolated since the time interval before counting started was ~1 second, and it was difficult to reproduce such short bombardments. The decay curves were analyzed by the standard "peel-off" process using the half-lives given in Table I. The values of A^0 for the 4.51-sec. period for the different absorbers as found in the 15-second and 5-second irradiations, and those for the 1.52-sec. period as found in the 5-second irradiations are given in Table III along with the ranges determined by least-squares analysis.

TABLE IV. Corrected least-squares ranges of the fission fragments leading to delayed neutron emission.

Period	Range (mg Al/cm²)
4.51 sec.	4.05±0.03
55.6 sec.	3.98±0.06
1.52 sec.	3.63±0.12
22.0 sec.	3.21±0.04

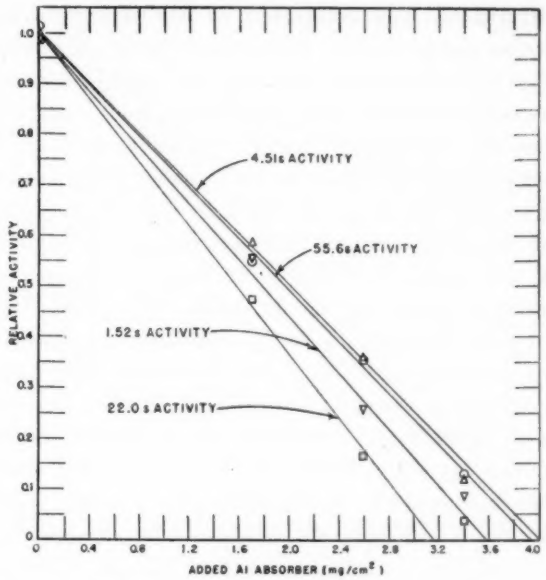

FIG. 2. Aluminum absorption curves of delayed neutron fission fragments.

○ 55.6-sec. period; least-squares range = 3.93 ± 0.06 mgAl/cm².
□ 22.0-sec. period; least-squares range = 3.16 ± 0.04 mgAl/cm².
△ 4.51-sec. period; (av. of 15-sec. and 5-sec. irradiations); least-squares range = 4.00 ± 0.03 mgAl/cm².
▽ 1.52-sec. period; least-squares range = 3.58 ± 0.12 mgAl/cm².

The data of recoil activity *vs.* mg Al absorber are plotted in Fig. 2. A correction resulting from the source thickness needs to be added to the ranges as determined in Al, namely one-half of the equivalent Al thickness of the source, or ~0.05 mg Al/cm². The corrected ranges are given in Table IV.

The ranges of mass numbers 87 and 137, tentatively assigned to the 55.6-sec. Br and 22.0-sec. I, as read off the smooth curve (range in Al *vs.* mass number) of the range experiment referred to earlier,[5] are 3.75 and 2.92 mg Al/cm², respectively. These ranges are about 7 percent lower than the ranges found for the fragments assigned to these mass numbers by the measurement of the delayed neutron activity. The discrepancy is probably due to error in the earlier experiments. In these, the Al absorbers were not weighed individually, but the average weight of the large sheets from which the absorbers were cut was used. Later, the variation in specific mass throughout a single sheet was found to exceed the variation in average weight among large sheets. The probable error in range thus

introduced was estimated at 10 percent. The earlier range results are more reliable on a relative basis, however, and can be used in a comparison of ranges from which the mass numbers may be obtained. A test of the relative comparison may be made by comparing the extremes in ranges of masses 87 and 137 with those found for the 55.6-sec. and 22.0-sec. periods. The ratio of the ranges of mass 87 to mass 137 from the smooth range curve is $3.75/2.92=1.28$. The error in this ratio is rather difficult to estimate but may be taken as about 1 percent. The ratio of the ranges of the 55.6-sec. and 22.0-sec. periods is $(3.98\pm0.06)/(3.21\pm0.04)=1.24\pm0.024$. These values agree as closely as can be expected since the differences in range compared are large, and the mass assignments used may be in error by several mass numbers. A comparison of more nearly similar ranges should yield even better agreement.

An approximate mass may be obtained for the 4.51-sec. period by comparing its range with that of the 55.6-sec. period. The dispersion of the ranges corresponding to the mass numbers in the light group is considerably smaller than in the heavy group; thus there is a larger error in the mass assignment in the light group. The range dispersion in the light group is 0.011 mg Al/cm²/mass number, and in the heavy group, 0.054 mg Al/cm²/mass number. The range of the 4.51-sec. period is 4.05 ± 0.03 mg Al/cm², or 0.07 mg Al/cm² larger than that of the 55.6-sec. period (3.98 mg Al/cm²). The mass number of the 4.51-sec. period is therefore ~6 mass units smaller than that of the 55.6-sec. period, or 81 if a mass number of 87 is assigned to the 55.6-sec. period. The probable error in the mass number, arising from the probable errors in the ranges, is ±7 mass numbers. Many of the possible mass numbers of 81 ± 7 can be eliminated since the fission yield of the 4.51-sec. period of ~0.5 percent** exceeds the radiochemically determined yields of all masses up to mass 84.[8] Masses of 84 and 85 are also excluded, since their fission yields and/or those of the masses which would be formed by delayed neutron emission (83 and 84, respectively) are too small to allow for increments of the order of ~0.5 percent in their fission yields and still lie on the smooth yield *vs.* mass number curve found radiochemically. The remaining possible masses are 86 to 90, if we consider a possible error of 1 to 2 mass numbers in the mass assignment of the 55.6-sec. period. An inspection of the fission chains for these mass numbers indicates that the delayed neutron period should be separated chemically with Se or Br. The results of the chemical identification are given in Section 3.

The range of the 1.52-sec. period is 0.42 mg Al/cm² larger than that of the 22.0-sec. I. This corresponds to a difference of 8 mass numbers since the dispersion in the heavy group is ~0.054 mg Al/cm²/mass number. The probable error in the mass number is ±4 mass numbers, somewhat higher than for the heavy group since the range curve has started to flatten in this mass range. Here, again, one may eliminate some of the possible masses in the range 129 ± 4 because of fission yield considerations. The remaining masses are 129 to 135 if again one considers a possible error of 1 to 2 mass numbers in the mass assignment of the 22.0-sec. period. Possible chemical elements with which the 1.52-sec. delayed neutron period may be separated are In, Sn, and Sb.

3. CHEMICAL ISOLATION OF THE 4.51-SEC DELAYED NEUTRON ACTIVITY

3.1 Se Isolation

Selenium carrier was added as $SeO_3^=$ to 3 g of UO_2Cl_2 in 5 ml of 4*M* HCl solution, and the mixture was irradiated for 5 seconds. After the irradiation, the active solution was mixed with 25 ml of 12*M* HCl, $NaHSO_3$ was added, and Se precipitated. The Se was centrifuged, and the precipitate counted in the neutron counter. The time elapsed between the end of the irradiation and the beginning of the counting was 45 to 50 seconds. The decay curve was that of an unseparated sample. Since the colloidal Se pre-

** For a discussion of the fission yields of the delayed neutron emitters see reference 8. The value of ~0.5 percent was arbitrarily adopted in this article for the fission yields of the 1.52-sec., 4.51-sec., and 22.0 sec. delayed neutron periods. The discussion would not be altered appreciably by fission yield values in the range 0.2 percent to 0.7 percent.

[8] Plutonium Project, "Nuclei formed in fission. Decay characteristics, fission yields, and chain relationships," issued by the J. Am. Chem. Soc. **68**, 2411 (1946); Rev. Mod. Phys. **18**, 513 (1946).

cipitate was removed from the solution by centrifugation and decantation, some of the solution stayed behind and was counted. An inspection of the gross decay curve of delayed neutrons (Fig. 3) shows that the decay of the 4.51-sec. activity would be obscured by the 22.0-sec. and 55.6-sec. activities after 45 to 50 seconds if 5 to 10 percent of the solution remained, even if the 4.51-sec. activity were quantitatively removed by the Se precipitation. Actually, the Se removal was far from complete, and an estimate of the residual solution was the order of 1 to 2 ml, enough to give the observed effect. Efforts to improve the decontamination and speed of the Se removal were not successful. Accordingly, a search for the 4.51-sec. activity in the Br fraction was undertaken.

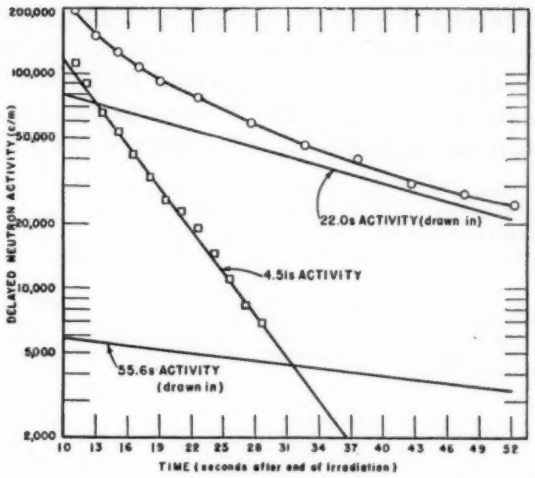

FIG. 3. Decay curve of delayed neutron activity of uranyl nitrate in 2 M Na_2CO_3 solution irradiated for 5 seconds.

○ Total delayed neutron activity.
□ 55.6-sec. and 22.0-sec. activities subtracted from smooth curve of total activity.

3.2 Br Isolation

In the isolation procedure the Br was extracted with CCl_4 after oxidation of I^- to IO_3^-. The method was adapted from that of Glendenin, Metcalf, and Novey[9] for the radiochemical isolation of I. A solution of uranyl nitrate in 2M Na_2CO_3, to which I^- and Br^- carriers are added, is irradiated for 5 seconds. After irradiation, the active solution is mixed with 10 ml of 2M Na_2CO_3 containing Br^- and BrO_3^- carrier and NaOCl in excess of that needed to oxidize the I^- to IO_3^-. The $Br^- - BrO_3^-$ mixture is stable in the basic solution. In separate experiments it was shown that I^- is quickly oxidized to IO_3^- by NaOCl in Na_2CO_3 solution and upon acidification, no I_2 is produced. Br^-, however, when present in the basic NaOCl solution is recoverable as Br_2 when the solution is acidified. Whereas the potential for oxidation of Br^- to BrO_3^- by NaOCl in basic solution is favorable, it was shown that the reaction does not occur during the time of this experiment. In addition, the BrO_3^- initially added as carrier remains as such throughout the procedure.

The solution is then added to a separatory funnel containing 50 ml of CCl_4 and 25 ml of 6N HNO_3. The solution becomes acid, Br_2 is liberated and is extracted in the CCl_4. Since it is present as IO_3^-, very little I is extracted. In the first experiments the solution in the separatory funnel was mixed by a stirring rod connected to a stirring motor, and the CCl_4 layer was siphoned over to a test tube placed in the sample slot of the neutron counter. In a series of six experiments, about 30 seconds elapsed between the end of the irradiation and the initiation of counting. Five to ten seconds of this time were consumed in the transfer of the solution from the separatory funnel to the counter. The radiochemical yields of Br, as determined by the ratio of the 55.6-sec. Br activity in the Br sample to that of an unseparated sample, averaged about 15 percent. Analysis of the neutron-decay curves showed that after 30-seconds decay the activity of the 4.51-sec. period was about that expected for a Br isotope when compared with the activity of the 55.6-sec. Br period, whereas the I activity was repressed by a factor of 2 to 6. The presence of I activity in the CCl_4 layer probably resulted from the suspension of aqueous solution because of the short time (5 to 10 seconds) allowed for the layers to separate. The chemical operations had to be completed in 30 seconds or less since by then the activity of the 4.51-second species had decayed roughly to that of the 55.6-sec. Br and was soon obscured by the latter and any 22.0-sec. I activity present as contaminant.

The Br separation procedure was modified in

[9] L. E. Glendenin, R. P. Metcalf, and T. B. Novey, Report CC-2218, (January 20, 1945); Plutonium Project Record **9B**, 8.21.3 (1946).

later experiments to achieve a higher radiochemical yield and more consistent results. Shaking of the separatory funnel by hand gave better extraction of the Br into the CCl_4 layer than mechanical stirring. Radiochemical yields

TABLE V. Comparison of the activities of the delayed neutron periods in the Br fractions with a chemically untreated sample.

Period \ Activity after 30 seconds decay	Activity (c/m) in Br fractions isolated from uranyl nitrate in Na_2CO_3 irradiated for 5 seconds	Average activity (c/m) from uranyl nitrate in Na_2CO_3 irradiated for 5 seconds	Radiochemical yield (ratio of column II to column III)
4.51 sec.	No. 1: 3700 No. 2: 1900 No. 3: 1700 No. 4: 2500 av.*: 2771	6600	No. 1: 0.56 No. 2: 0.29 No. 3: 0.26 No. 4: 0.38 av.*: 0.42
55.6 sec.	No. 1: 2080 No. 2: 1380 No. 3: 790 No. 4: 2200 av.*: 1484	5250	No. 1: 0.40 No. 2: 0.26 No. 3: 0.15 No. 4: 0.42 av.*: 0.28
22.0 sec.	No. 1: 4200 No. 2: 3450 No. 3: 1880 No. 4: 4800 av.*: 3509	48400	No. 1: 0.087 No. 2: 0.071 No. 3: 0.039 No. 4: 0.099 av.*: 0.072

* The average values were obtained from the arithmetic average decay curve of experiments 1–4 analyzed by a least-squares method.

of the Br samples counted varied from 15 to 42 percent and appeared to be determined by the fraction of the CCl_4 solution withdrawn for counting. The I activity was decontaminated by a factor of 4 with less variation than in the first Br separations. The results of these experiments are given in Table V.

The activities of the three delayed neutron periods in the Br fractions of experiments 1–4, given in Table V, were determined by a graphical analysis of the decay curves by the standard "peel-off" method. The average entry was determined by analyzing the average decay curve by a least-squares method, minimizing relative counting errors, since the time interval of counting was so varied during the decay that the number of counts in each interval was roughly the same. The results of the analysis of the average decay curve by the least-squares method are given in Fig. 4 for the early part of the decay curve where the least-squares curve of the 4.51-sec. activity is compared with the points determined by subtracting the sum of the 22.0-sec. and 55.6-sec. least-squares values from the smooth curve. The least-squares values of the 55.6-sec., 22.0-sec., and 4.51-sec. activities were determined from the complete decay curve extending to 6-minutes decay. The standard values in Table V used for comparison were determined from the average decay curve of an unseparated sample. A typical decay curve of a chemically untreated sample is given in Fig. 3 where the 55.6-sec. and 22.0-sec. activities were determined from the later portion of the decay curve extending to 8-minutes decay.

An examination of the data given in Table V shows that the radiochemical yield of the 22.0-sec. I activity is lowered appreciably relative to that of the 55.6-sec. Br activity as one would expect from the chemical operations performed. The yield of the 4.51-sec. activity, on the other hand, is roughly the same within experimental error as that of the 55.6-sec. Br activity; this demonstrates the chemical identity of the two isotopes. The fact that the average yield of the 4.51-sec. period is somewhat higher than that of the 55.6-sec. period might be indicative of a short-lived Se parent of the 55.6-sec. Br.

The mass assignment of the 4.51-sec. Br depends to some extent on that of the 55.6-sec. Br. In Section 2 it was shown that if the mass assignment of the 55.6-sec. Br is about 87, the mass of the 4.51-sec. period is in the range of 86 to 90. Mass 86 appears unlikely for a Br isotope since the calculation of the maximum β^- decay energy by the Bohr-Wheeler formula shows that the energy is about 1.5 Mev lower than the energy required to boil off a neutron from Kr^{86}. The remaining possible mass assignments of the 4.51-sec. Br are 87 to 90.

3.3 General Discussion

The delayed neutron emitters identified are divided evenly between the two groups of fission products, and their masses are such that they lie on the lighter ends of the mass groups.

The fission-yield *vs.* mass-number curve, determined by radiochemical analysis, appears to be a smooth continuous curve within the limits of experimental error of about 10 percent.[8] True discontinuities, although not observed, should exist because of the delayed neutron emitters. For example, the 4.51-sec. Br activity has a fission yield of ~0.5 percent; thus, the chain of the mass number of Br (87–90) should have its

yield lowered by ~0.5 percent which is about 10 percent of the fission yield of the chain in this region, and the chain of one mass number lower should have its fission yield raised by about 10 percent. Therefore, instead of a slowly rising fission yield at this mass, there should be a sharp discontinuity of about 20 percent. As yet no chemical evidence for this behavior has been found, but this technique may be applied to ascertain the mass numbers of the delayed neutron emitters more exactly. In this respect it should be mentioned that there is some uncertainty about the mass assignment of 137 to the 22.0-sec. I activity. The yield of Xe^{136} should be increased by the delayed neutron yield of ~0.5 percent if the assignment is correct. On the other hand, the relative yield determination, made by Thode and Graham,[10] of the stable noble gases formed in fission shows that the yield of Xe^{136} is about 15 percent lower than that of Xe^{134}, whereas the inverse should be true, first, because of the slow increase of yield with mass number in this region and, second, because of the contribution of the delayed neutron yield. The gas-yield results seem to indicate that the mass assignment of the 22.0-sec. I is 136. If this is true, then the Xe^{135} formed from the 22.0-sec. I should have an independent yield of ~0.5 percent. This is in rough agreement with the independent yield of ~0.3 percent for Xe^{135} determined by Hoagland and the author[11] by measuring the independent Xe^{135} activity directly.

[10] H. G. Thode and R. L. Graham, Report MX 129 (April, 1945); recently published in Can. J. Research **25**, 1 (1947).
[11] E. J. Hoagland and N. Sugarman, Report CC-3007, (April 15, 1945); Plutonium Project Record **9B**, 7.37.3 (1946).

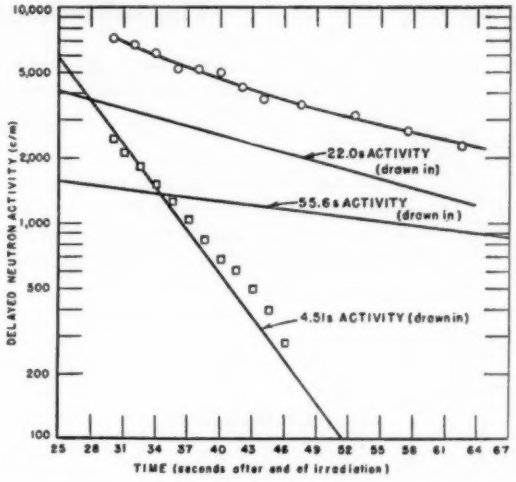

FIG. 4. Decay curve of delayed neutron activity of Br fraction isolated from uranyl nitrate in 2 *M* Na_2CO_3 solution irradiated for 5 seconds (least-squares analysis of average decay curve of 4 irradiations).

○ Total delayed neutron activity.
□ 55.6-sec. and 22.0-sec. activities subtracted from smooth curve of total activity.

This research was performed at the Argonne National Laboratory, Chicago, Illinois, operated by the University of Chicago for the Atomic Energy Commission.

ACKNOWLEDGMENTS

It is a pleasure to acknowledge the assistance given the author in these experiments by Dr. D. J. Hughes and members of his group at the Argonne National Laboratory and by Mr. A. R. Van Dyken of the Institute for Nuclear Studies, University of Chicago.

The Infra-Red Spectrum of Ketene

FREDERICK HALVERSON AND VAN ZANDT WILLIAMS
Stamford Research Laboratories, American Cyanamid Company, Stamford, Connecticut

(Received April 11, 1947)

The infra-red spectrum of gaseous ketene has been studied from 2.5μ to 25μ with a spectrometer using LiF, NaCl, and KBr prisms. A perpendicular band at 3162 cm^{-1} with components relatively free of perturbations has been resolved, and the intensity alternation associated with the twofold axis observed. All fundamental vibrational frequencies have been assigned. A normal coordinate treatment of the general H_2XYZ molecule has been made and reasonable force constants for ketene calculated.

I. INTRODUCTION

FROM chemical evidence and bond theory, ketene is formulated as being a planar molecule with a twofold axis of symmetry, corresponding to the structural formula

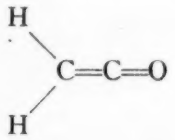

Beach and Stevenson[1] made an electron diffraction study of the molecule and found $r(C-O) = 1.17 \pm 0.02$A, and $r(C-C) = 1.35 \pm 0.02$A. Using these measured dimensions and assuming the given structural formula, one can predict the gross structural features to be expected in the infra-red spectrum of such a molecule.

Making the assumption that $r(C-H) = 1.08$A and $\angle HCH = 120°$, one calculates $I_A \cong 2.9 \times 10^{-40}$ g cm^2 (moment of inertia about the twofold axis) and $I_B \cong I_C \cong 85 \times 10^{-40}$ g cm^2. Consequently, the rotational structure should resemble that of a symmetrical top molecule—vibrations in which the change of electric moment is along the twofold axis giving rise to parallel bands, and the other vibrations giving rise to perpendicular bands. The maxima of the P and R branches of the parallel bands should have a separation of about 25 cm^{-1} at room temperature; the perpendicular bands should consist of rather widely spaced (*ca.* 19 cm^{-1}) Q branches with alternating intensities.

Temporarily neglecting the effect of the hydrogen atoms, one can consider the C=C=O part of the molecule as being analogous to nitrous oxide, $\overset{-}{N}=\overset{+}{N}=O$. The frequencies of the stretching vibrations of this molecule are 1285.0 cm^{-1} and 2223.5 cm^{-1}, and the frequency of the bending vibration is 589 cm^{-1}.[2] The analogous vibrations of ketene minus the hydrogen atoms should have frequencies of approximately the same magnitude—the stretching vibrations giving rise to parallel bands, and the bending vibration giving rise to a perpendicular band. It is probable, however, that the presence of the hydrogen atoms will release the degeneracy of the bending vibration so that two perpendicular bands with nearly the same frequency will appear.

The presence of the hydrogen atoms should also add five fundamental vibrations, three of which are more or less characteristic of the CH_2 group—a symmetric C−H bond stretching and a symmetric CH_2 deformation (parallel bands) and an antisymmetric C−H bond stretching (perpendicular band). The frequencies of these vibrations should be similar to those occurring in ethylene or in the vinyl halides (C−H stretching in the region 2900–3200 cm^{-1}; CH_2 deformation in the region 1300–1500 cm^{-1}). The other two vibrations—out-of-plane and in-plane wagging of the CH_2 group against the rest of the molecule—should give rise to perpendicular bands, and by analogy with ethylene and the vinyl halides should have frequencies in the region 900–1050 cm^{-1}. It is understood, of course, that the true normal vibrations of the complete molecule are superpositions of these postulated modes of

[1] J. Y. Beach and D. P. Stevenson, J. Chem. Phys. 6, 75 (1938).

[2] G. Herzberg, *Infra-red and Raman Spectra of Polyatomic Molecules* (D. Van Nostrand Company, Inc. New York, 1945), p. 278.

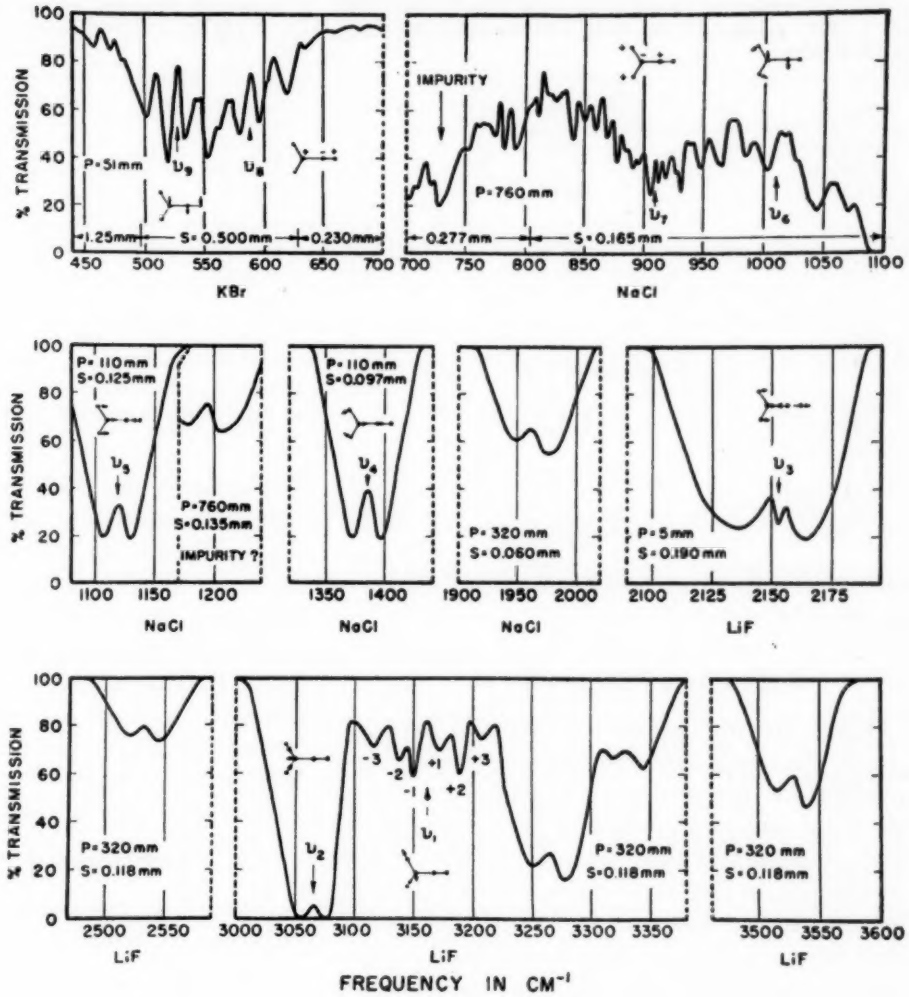

FIG. 1. Infra-red spectrum of ketene.

motion, but it is believed that these simple modes are so chosen that they are almost normal modes.

II. OBSERVED INFRA-RED SPECTRUM[3,4]

The infra-red spectrum of ketene shown in Fig. 1 was obtained using a Perkin-Elmer spectrometer Model 12A with LiF, NaCl, and KBr prisms. With the exception of the very intense band at 2153 cm^{-1}, a 10-cm Pyrex absorption cell with glyptal sealed KBr windows was used in all regions. Ketene pressures were varied from 50 mm to 760 mm of Hg. In order to obtain the structure of the band at 2153 cm^{-1}, a 5-cm cell was used with ketene at a pressure of 10 mm of Hg. The ketene was prepared in these laboratories by Dr. G. L. Simard and Mr. J. F. Steger by pyrolysis of acetone in a quartz column, and purified by low temperature distillation in a vacuum jacketed still.

Some difficulty was experienced in obtaining the spectrum because of the dimerization of ketene, particularly at the higher pressures. By following the changes over a period of several hours, however, it was possible to correct for the presence of diketene.[5] This procedure also per-

[3] H. Gershinowitz and E. B. Wilson, Jr., J. Chem. Phys. 5, 500 (1937). They reported some of these bands in a "Letter to the Editor," but did not give any structure for them and made no assignments.

[4] H. Kopper, Zeits. f. physik. Chemie **B34**, 396 (1936). A report on the Raman spectrum of liquid ketene.

[5] A 10-cm absorption cell was filled with ketene at an initial pressure of one half atmosphere and allowed to stand for several days, with the infra-red spectrum obtained at regular intervals. The diketene absorption bands appeared within two hours, and increased noticeably in intensity for three days. At the end of seven days the ketene pressure was considerably less than 10 mm of Hg; and by the end of the eighth day, even the intense ketene

TABLE I. Observed ketene-absorption bands 3900–2900 cm^{-1} (LiF prism; 10-cm cell; 320-mm pressure; slit = 0.118 mm).

Frequency	Int	Frequency	Int	No.
3538 *R*		3208	*W*	+3
3526 *Av*	*M*			
3515 *P*		3189	*S*	+2
3343 *R*		3173	*W*	+1
3330 *Av*	*W*			
3317 *P*		3151	*S*	−1
3277 *R*		3137	*W*	−2
3264 *Av*	*S*			
3252 *P*		3117	*S*	−3
3079 *R*		⊥ band		
3066 *Av*	*VS*			
3053 *P*				
∥ bands				

mitted identifying certain bands as probably due to other impurities.

Region from 3900 to 2900 cm^{-1}

There are four parallel bands and one perpendicular band in this region. No *Q* branches are resolved for any of these parallel bands, and so the band centers are taken as the mean of the *P* and *R* branches. The perpendicular band is overlapped on the low frequency side by the very intense parallel band at 3066 cm^{-1} and on the high frequency side by the parallel band at 3264 cm^{-1}. Consequently only six components of the perpendicular band are clearly observed. The adjacent components show a fairly regular intensity alternation, and the intensity maximum of the band appears to fall between the components at 3189 cm^{-1} and 3151 cm^{-1}. Since the spacing of the components is a little irregular, the average of the five spacings available, $\langle \Delta\nu \rangle_{Av} = 18.2$ cm^{-1}, is considered the normal spacing. Frequencies for the bands in this region are given in Table I.

Region from 2900 to 1100 cm^{-1}

Several parallel bands are observed in this region, one of them being extremely intense with a *Q* branch at 2153 cm^{-1}. This band shows practically complete absorption if the ketene pressure in a 10-cm cell is 10 mm of Hg or larger. As shown in Fig. 1, the *Q* branch is very weak relative to the *P* and *R* branches. The positions of all the bands in this region are given in Table II. The very weak bands at 1178 cm^{-1} and 1205 cm^{-1} are real and are believed to be due to ketene, but are listed with a question mark since they were found only at the higher pressures where diketene also formed.

TABLE II. Observed ketene absorption bands 2900–1100 cm^{-1} (LiF prism for 2153 cm^{-1} band; NaCl prism for the rest).

Frequency	Int	*P*†	Frequency	Int	*P*†
2540 *R*			1398 *R*		
2533 *Av*	*M*	320 mm	1386 *Av*	*VS*	110 mm
2515 *P*			1375 *P*		
2164 *R*			1205 *R*	?	
2153 *Q*	*VVS*	*	1191 *Av*	*VW*	760 mm
2136 *P*			1178 *P*	?	
1974 *R*			1132 *R*		
1962 *Av*	*M*	320 mm	1120 *Av*	*VS*	110 mm
1949 *P*			1107 *P*		

* A 5-cm cell with 10-mm ketene pressure was used for this band.
† Column headed *P* is pressure in a 10 cm cell.

Region from 1100 to 700 cm^{-1}

This region contains a large number of irregularly spaced bands of varying intensities. There

TABLE III. Observed ketene absorption bands 1100–700 cm^{-1} (NaCl prism; 10-cm cell; 760-mm pressure; slit = 0.160 mm).

Frequency	Int	Frequency	Int
703	*S*	886	*W*
712	*S*	891	*M*
722	*S**	896	*W*
728	*S**	907	*S*
731	*W*	912	*M*
752	*M*	918	*M*
760	*W*	927	*VW*
773	*S*†	932	*S*
783	*S*†	940	?
792	*S*†	948	*S*
807	?	963	?
811	*W*	966	*S*
819	*W*	986	*S*
825	?	1004	*S*
830	*VW*	1018	*VW*
841	*S*	1028	*M*
851	*W*	1044	*MS*
860	*M*	1058	*VVW*
869	*M*	1070	*MS*
878	*M*		

* Definitely due to an impurity.
† Probably due to an impurity.

band at 2153 cm^{-1} did not appear. However, the bands at 722 and 728 cm^{-1} were still present, and so could not be due to ketene. The bands at 773, 783, 792, and 841 cm^{-1} had disappeared, but the rate at which they did made it doubtful that they were ketene bands.

TABLE IV. Observed ketene absorption bands 700–400 cm^{-1} (KBr prism; 10-cm cell; 110 mm of Hg; slit =0.500 mm).

Frequency	Int	Frequency	Int
458	*W*	562	*VW*
472	*W*	571	*W*
482	*VW*	580	*S*
501	*S*	596	*S*
520	*S*	620	*S*
534	*M*	634	*W*
539?	*VW*	658	*W*
546?	*VW*	680	*W*
553	*S*	698	?

appears to be a parallel band at the upper end of the region—*P*, *Q*, and *R* branches at 1044, 1058, and 1070 cm^{-1}, respectively—with the *Q* branch barely resolved. It is in this region that the dimerization gives the most trouble, since the dimer has rather strong bands at 1009, 1000, 950, 910, 890, 877, and 847 cm^{-1}. When a sample of ketene with an initial pressure of one-half atmosphere in a 10 cm cell was allowed to stand two days, most of the bands in the region 750–900 cm^{-1} disappeared with the exception of diketene bands and weak absorption bands at 773, 783, and 792 cm^{-1}. These bands look like *P*, *Q*, and *R* branches, but the spacing is not correct for ketene, and so they are believed to be the result of some impurity. The band structure in the region 900–1100 cm^{-1} was still apparent, however. The observed bands are given in Table III.

Region from 700 to 400 cm^{-1}

This region contains a series of irregularly spaced intense absorption bands extending from 458 cm^{-1} up to 700 cm^{-1} with the greatest intensity between 520 and 620 cm^{-1}. An intensity alternation is apparent, but not nearly so regular as in the 3164 cm^{-1} band. The system has the appearance of two overlapping perpendicular bands, with the components given in Table IV.

TABLE V. Symmetry types and characters for point group C_{2v}.

C_{2v}	I	$C_2(z)$	σxz	σyz
A_1	+1	+1	+1	+1
A_2	+1	+1	−1	−1
B_1	+1	−1	+1	−1
B_2	+1	−1	−1	+1

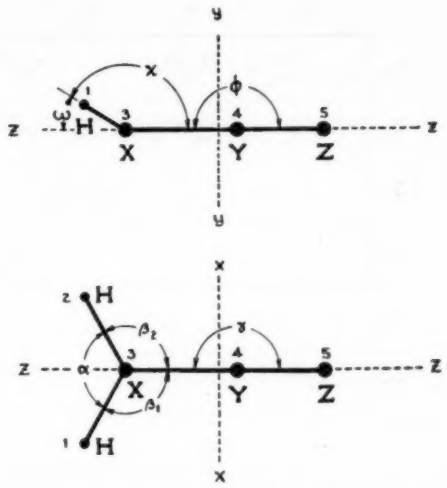

FIG. 2. Structural parameters for H_2XYZ molecule.

III. THEORETICAL CONSIDERATIONS[6]

A molecule H_2XYZ in which the XYZ atoms are collinear, and in which the two H atoms are symmetrically bonded to the X-atom, has nine vibrational degrees of freedom. If the molecule is planar, its symmetry point group is C_{2v} (a two-fold axis with two mutually perpendicular planes through it); if the molecule is non-planar, its symmetry point group is C_s (retaining only the plane of symmetry through the XYZ-atoms which bisects the HXH angle). The representation of the molecular point group which has the vibrational motions as its basis, in the terms of its irreducible components, is $\Gamma_{vib}=4A_1+3B_1+2B_2$ for the C_{2v} molecule, and $\Gamma_{vib}=6A'+3A''$ for the C_s molecule. The symmetry types for point group C_{2v} are given in Table V. We have taken σ_{xz} to be the plane of the molecule. For point group C_s, type A' is symmetric and type A'' is antisymmetric with respect to reflection in the symmetry plane. Ketene is a C_{2v} molecule of this kind, and cyanamide ($H_2N-C\equiv N$) is a corresponding C_s molecule.

The technique of Wilson[7] was used for setting

[6] Since an investigation of cyanamide is also in progress, and since there is considerable similarity between the cyanamide and ketene molecules, the first part of this section is made general for any such a pentatomic molecule. Equations for the frequencies of the totally symmetrical vibrations of ketene have been given before [H. W. Thompson and J. W. Linnett, J. Chem. Soc. 1384 (1937); H. J. Bernstein, J. Chem. Phys. 6, 718 (1938)], but none have been given for the unsymmetrical vibrations or for the non-planar molecule.

[7] E. B. Wilson, Jr., J. Chem. Phys. 7, 1047 (1939); 9, 76 (1941).

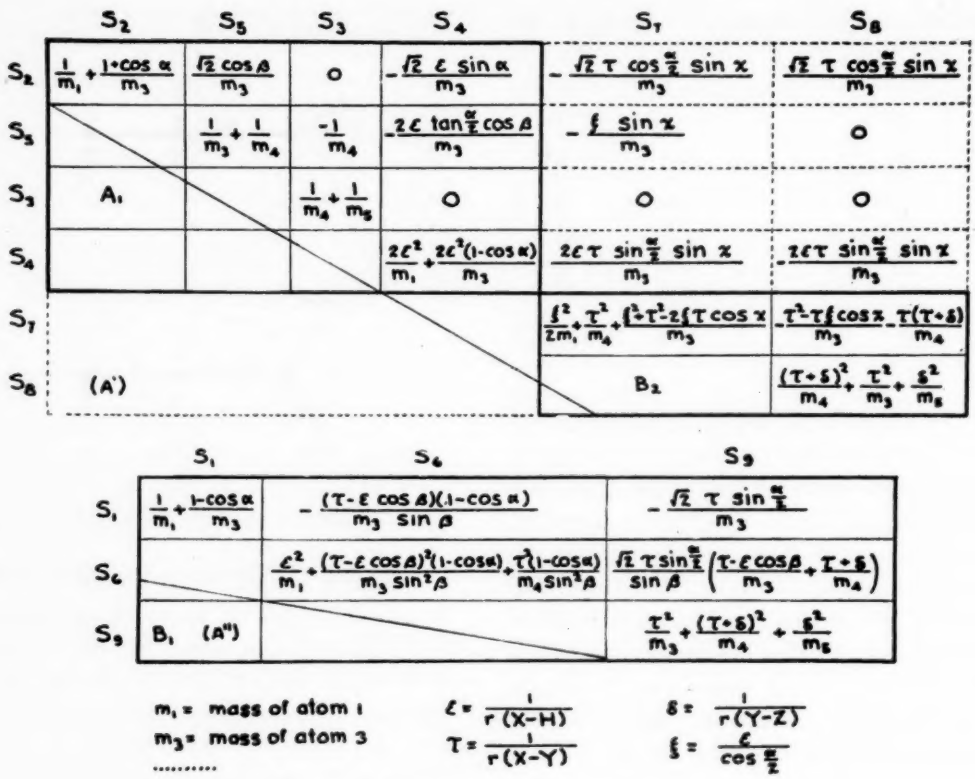
S2 S5 S3 S4 S7 S8
S2 1/m1 + (1+cos α)/m3 √2 cos β/m3 0 −√2 ℓ sin α/m3 −√2 τ cos α/2 sin χ/m3 √2 τ cos α/2 sin χ/m3
S5 1/m3 + 1/m4 −1/m4 −2ℓ tan α/2 cos β/m3 −ξ sin χ/m3 0
S3 A1 1/m4 + 1/m5 0 0 0
S4 2ℓ²/m1 + 2ℓ²(1−cos α)/m3 2ℓτ sin α/2 sin χ/m3 −2ℓτ sin α/2 sin χ/m3
S7 ξ²/2m1 + τ²/m4 + (ξ²+τ²−2ξτ cos χ)/m3 −(τ²−τξ cos χ)/m3 − τ(τ+δ)/m4
S8 (A′) B2 (τ+δ)²/m4 + τ²/m3 + δ²/m5
S1 S6 S9
S1 1/m1 + (1−cos α)/m3 −(τ−ℓ cos β)(1−cos α)/m3 sin β −√2 τ sin α/2/m3
S6 ℓ²/m1 + (τ−ℓ cos β)²(1−cos α)/m3 sin²β + τ²(1−cos α)/m4 sin²β √2 τ sin α/2/sin β ((τ−ℓ cos β)/m3 + (τ+δ)/m4)
S9 B1 (A″) τ²/m3 + (τ+δ)²/m4 + δ²/m5
m1 = mass of atom 1
m3 = mass of atom 3
.....
ℓ = 1/r(X−H)
τ = 1/r(X−Y)
δ = 1/r(Y−Z)
ξ = ℓ/cos α/2

FIG. 3. G matrix for H_2XYZ molecule (symmetrical about diagonal).

up the secular equation, and it was checked by Eliashevich's[8] method. The valence force coordinates (*VFC*) used are indicated in Fig. 2 and Table VI. Factoring of the secular equation is obtained by choosing valence force symmetry coordinates (*VFSC*) which form a basis for irreducible representations of both the C_s and C_{2v} point groups, i.e., are symmetry coordinates for both molecules. In order to do this, the angle χ between the H_2X plane and the XYZ axis is introduced as a structural parameter, and the change in this angle is used as one of the coordinates. For convenience, the *VFSC* are designated by S_1, S_2, $\cdots$, with a corresponding designation ν_1, ν_2, $\cdots$, for the vibration frequencies, meaning that the vibration of frequency ν_1 involves coordinate S_1 primarily, etc. The *VFSC* are given in Table VII.

The G matrix ($2T=\dot{S}'G^{-1}\dot{S}$) for the *VFSC* is given in Fig. 3. It contains the atomic masses, internuclear distances, and functions of the various bond angles. Blocks are outlined to represent the factoring for symmetry point group C_{2v} (ketene); terms outside the blocks enter only for non-planar molecules ($\chi\neq\pi$). Simplifying relationships which exist for a planar molecule are given in Table VIII.

The F matrix[9] ($2V=S'FS$) used with the G matrix in obtaining the secular equation, $|GF-\lambda E|=0$, for the ketene molecule is given in

TABLE VI. Bonds and angles used for *VFC*.

$\angle H_2XY$	$=\chi$
$\angle HXH$	$=\alpha$
$\angle H_1XY$	$=\beta_1$
$\angle H_2XY$	$=\beta_2$
$\angle XYZ$	$=\begin{cases}\varphi\\ \gamma\end{cases}$
$r(H_1-X)$	$=r_1$
$r(H_2-X)$	$=r_2$
$r(X-Y)$	$=r_{34}$
$r(Y-Z)$	$=r_{45}$

[8] M. Eliashevich, J. Phys. Chem. U.S.S.R. **14**, 1381 (1940).

[9] The most general F matrix can be used with the G matrix of Fig. 3. We have limited ours because of the limited amount of experimental information from which to obtain constants.

Fig. 4. In this potential system it is logical to expect F_8 and F_9 to have practically the same value (they would have exactly the same value if the C=C=O axis had had fourfold symmetry). The constants F_1 and F_2 differ only by twice the constant representing interaction between the two $X-H$ bonds ($F_1=K_1+k_{12}$; $F_2=K_1-k_{12}$).

The parallel bands which appear in the infra-red spectrum can arise only from transitions whose over-all vibrational symmetry is of type A_1. Transitions of type A_2 are not allowed to appear in infra-red absorption, and transitions of symmetry species B_1 and B_2 yield perpendicular bands. For transitions of species B_1, the change of electric moment is along the axis of intermediate moment of inertia ("B"-type bands); for transitions of species B_2, the change is along the axis of largest moment of inertia ("C"-type bands). In the case of ketene, however, the "B"- and "C"-type bands are practically identical,[10] since $\rho=I_A/I_B$ is of the order of magnitude of 0.035, and $I_B\cong I_C$. In addition, since ρ has such a small value, the ratio of the intensity of the Q branch of a parallel band to that of the P and R branches must be very small.[11]

IV. ASSIGNMENT OF OBSERVED VIBRATIONAL FREQUENCIES[12]

The strongest parallel band in the 2900–3200 cm^{-1} region is picked as arising from the fundamental vibration ν_2, with a band center near 3066 cm^{-1}. Other parallel bands in this region must be combination bands. The only perpendicular band must be ν_1, and its center is picked at 3162 cm^{-1}. Its components show an intensity alternation which requires the axis of least moment of inertia to be a twofold axis. For Fermi statistics the first component on the low frequency side of the band center must be a strong one ($K'=0\leftarrow K''=1$), and the band center must be between the strongest lines. Consequently the band center is picked half way between the 3151 cm^{-1} and 3173 cm^{-1} components.

The extremely strong parallel band at 2153 cm^{-1} is assigned to ν_3. The other stretching vibration of the C=C=O part of the molecule is assigned the frequency $\nu_5=1120$ cm^{-1}. ν_4 must be assigned to the strong parallel band at 1386 cm^{-1}. Thus all of the totally symmetrical fundamentals are assigned.

The frequencies ν_8 and ν_9 are expected in the region 500–600 cm^{-1} by analogy with N_2O. In this region there is a set of irregularly spaced bands whose structure is qualitatively in agreement with that discussed by Nielsen[13] for the rotational bands of slightly anisotropic oscillators. The alternation in intensities for the rotational bands is not nearly so marked as in the perpen-

F	S_2	S_5	S_3	S_4	S_7	S_8	S_1	S_6	S_9
A_1 S_2	F_2	0	0	0					
A_1 S_5	0	F_5	f_{35}	0					
A_1 S_3	0	f_{35}	F_3	0					
A_1 S_4	0	0	0	F_4					
B_2 S_7					F_7	f_{78}			
B_2 S_8					f_{78}	F_8			
B_1 S_1							F_1	0	0
B_1 S_6							0	F_6	f_{69}
B_1 S_9							0	f_{69}	F_9

FIG. 4. Assumed F matrix for ketene molecule.

TABLE VII. *VFSC* with symmetry designation.

VFSC	C_{2v}	C_s
$S_2=1/\sqrt{2}(\Delta r_1+\Delta r_2)$ $S_3=\Delta r_{45}$ $S_4=\Delta\alpha$ $S_5=\Delta r_{34}$	A_1	A'
$S_7=\Delta\chi$ $S_8=\Delta\varphi$	B_2	
$S_1=1/\sqrt{2}(\Delta r_1-\Delta r_2)$ $S_6=1/\sqrt{2}(\Delta\beta_1-\Delta\beta_2)$ $S_9=\Delta\gamma$	B_1	A''

TABLE VIII. Relationships for a planar molecule.

$$\sin\tfrac{1}{2}\alpha=\sin\beta$$
$$(1-\cos\alpha)/\sin\beta=2\sin\tfrac{1}{2}\alpha$$
$$(1-\cos\alpha)/\sin^2\beta=2$$

[10] Reference 2, p. 480.
[11] Reference 2, p. 421.
[12] Thompson and Linnett (see reference 6) assigned the frequencies of the totally symmetrical vibrations on the basis of Kopper's Raman data. T. Y. Wu [*Vibrational Spectra and Structure of Polyatomic Molecules* (J. W. Edwards, Ann Arbor, Michigan 1946), p. 251.] made a partial assignment using Gershinowitz's and Wilson's (see reference 3) and Kopper's (see reference 4) data. His assignment is given in Table IX.
[13] H. H. Nielsen, J. Chem. Phys. **5**, 818 (1937).

dicular band at 3162 cm^{-1}. Again, however, the first component on the low frequency side of the band center should be strong, and so one center must be very close to 529 cm^{-1}. The other center in this region must be close to 570, 588, or 610 cm^{-1}, and we choose 588 cm^{-1} as being the most plausible. This also can account for the overtone at 1190 cm^{-1} if there is interaction between the overtone and ν_5. (It must be remembered, however, that the 1190 cm^{-1} band may be caused by an impurity.) ν_9 is assigned as 529 cm^{-1} and ν_8 as 588 cm^{-1}. The choice made in this case is dependent on the assignment of ν_6 and ν_7, since best agreement among force constants is obtained if the higher frequency of this pair arises from a vibration of the same symmetry type as the lower frequency of the similar pair near 900–1050 cm^{-1}.[14]

TABLE IX. Observations and assignments of vibrations of ketene.

	Infra-red—Gas H and W*			G and W**	Raman—Liquid K††	Wu†
$\nu_9(B_1)$C=C=O bend	529	⊥	*VS*		501 (1*b*)	ν_8
$\nu_8(B_2)$C=C=O bend	588	⊥	*VS*		599 (1/2*b*)	ν_9
					715 (1/2*b*)	
					801 (1/2*b*)	
$\nu_7(B_2)H_2-C=C$ bend	909	⊥	*W*	890 S		ν_7
$\nu_6(B_1)H_2-C=C$ bend	1011	⊥	*W*		998 (1)	ν_6
$2\nu_9(A_1)$	1058	∥	*W*			
$\nu_5(A_1)$C=C=O S	1120	∥	*VS*	1110 *S*	1130 (6*b*)	ν_5
$2\nu_8(A_1)$	1190	∥	*VW*?	1185 *W*	1198 (1)	
				1325 *W*		
				1350	1344 (2)	ν_4
$\nu_4(A_1)H_2C$ def.	1386	∥	*VS*	1400 *S*	1386 (1*b*)	
$2\nu_6(A_1)$	1962	∥	*M*	1935 *S*	1895 (1/2)	
$\nu_3(A_1)$C=C=O S	2153	∥	*VVS*	2160 *S*	2049 (1/2*b*)	ν_3
$\nu_4+2\nu_8(A_1)$	2533	∥	*M*			
				2915 *W*		
$\nu_2(A_1)$C−H S	3066	∥	*S*	3058 *S*	2952 (5)	ν_2
$\nu_1(B_1)$C−H S	3162	⊥	*W*	3165 *W*	3015 (4*b*)	ν_1
$\nu_3+\nu_5(A_1)$	3264	∥	*S*			
$\nu_3+2\nu_8(A_1)$	3330	∥	*W*			
$\nu_3+\nu_4(A_1)$	3526	∥	*M*			

* Present paper.
† Wu's[13] numbering system has been changed to correspond to this paper.
** See reference 3.
†† See reference 4.

By analogy with ethylene and the vinyl halides, ν_6 and ν_7 should fall in the region 900–1050 cm^{-1}. There are a number of absorption bands in this region, which appear to start at 810 cm^{-1} and continue up into the strong parallel band at 1120 cm^{-1}. Irregular spacings and intensities make it difficult to pick band centers, however. The parallel band appearing at 1962 cm^{-1} gives some aid, since it must be a first overtone of either ν_6 or ν_7 (parallel bands arising only from transitions of over-all A_1 symmetry). Thus the fundamental frequency corresponding to this overtone cannot be less than 981 cm^{-1}, and could hardly be greater than 1030 cm^{-1} and still give rise to the overtone at 1962 cm^{-1}. Apparently, the interaction between the overtone and ν_3 is appreciable in liquid ketene since the Raman spectrum[4] shows the overtone with an intensity comparable to that of ν_3 and presumably displaced in position. If a similar interaction exists in the vapor phase, the fundamental probably lies nearer 1030 cm^{-1} than 981 cm^{-1}. Possible band centers in this region are near 995 cm^{-1} and 1011 cm^{-1}, and we choose 1011 cm^{-1} as the more probable (midway between a strong component at 1004 cm^{-1} and a weak one at 1018 cm^{-1}) and assign it to ν_6 by analogy with formaldehyde.[15] ν_7 is chosen at 909 cm^{-1}, since the over-all absorption seems strongest here and since it places the band center between a strong 907 cm^{-1} component and a weaker 912 cm^{-1} component. This is a little lower than some of the assignments in the vinyl halides,[16] but is higher than others.[17] There is an absorption overlapping the strong 1120 cm^{-1} parallel band, which appears to be a weak parallel band with a Q branch at 1058 cm^{-1} and P and R branches at 1044 cm^{-1} and 1070 cm^{-1}, respectively. This band we assign to $2\nu_9$. Some of the weak bands in the region 750–850 cm^{-1} may be the result of the difference bands $\nu_4-\nu_8$ and $\nu_4-\nu_9$, and some of them may be the result of impurities.

The assignment of frequencies, together with a comparison with other observations on ketene, is given in Table IX. Only band centers are listed, and the uncertain bands in the 750–850 cm^{-1} region are omitted.

V. FORCE CONSTANTS

Using the assignments given in Table IX it is possible to evaluate a number of the force constants appearing in Fig. 4. Since the number of frequencies available for determining the force constants is nine, and we have listed twelve constants as being of probable importance, some

[14] See section *V* of this paper—"Force Constants."

[15] E. S. Ebers and H. H. Nielsen, J. Chem. Phys. **5**, 822 (1937). (Also, it is in agreement with similar vibrations in ethylene.)

[16] K. S. Pitzer and N. K. Freeman, J. Chem. Phys. **14**, 586 (1946).

[17] P. Torkington and H. W. Thompson, Trans. Faraday Soc. **51**, 236 (1945).

of the constants must be fixed by analogy with related molecules. For the geometrical parameters in Fig. 3, we have taken $r(C=C)=1.35A$[1], $r(C=O)=1.17A$[1], $r(C-H)=1.08A$ and $\angle HCH=120°$.

The value of F_4 can be fixed in the range 0.46 to 0.52×10^{-11} erg/radian^2 by estimating extreme values of the ratio F_5/F_3 and solving the resulting cubic equation in F_4. We expect F_3 to have a rather large value since r (C=O) = 1.17A is considerably shorter than the normal double bond distance. A force constant almost as large as the value 15.5×10^5 dynes per cm for CO_2[18] would be very plausible. The C=C distance is only very slightly larger than the normal distance, and so F_5 should be close to 9.8×10^5 dynes per cm. A plausible set of constants which reproduce the observed frequencies of the A_1 vibrations within one and one-half percent is: $F_2=5.23$, $F_3=15.5$, $F_5=9.8$, $f_{35}=1.5$($\times10^5$ dynes per cm) and $F_4=0.494$($\times10^{-11}$ erg per radian^2).

The constants determining the frequencies of B_1 and B_2 vibrations are perhaps best considered together. We have assumed that F_8 and F_9 should have values rather close together and of the order of magnitude of the bending constant in N_2O, 0.69×10^{-11} erg per radian^2.[19] One would not expect the bending constant to be as high as in carbon dioxide, 0.78×10^{-11} erg per radian^2,[20] since the effect of resonance in this case is to give some single bond—triple bond character ($H_2\bar{C}-C\equiv\overset{+}{O}$).[1] By analogy with the calculations of Pitzer and Freeman,[16] the constant F_7 should have a value around 0.23×10^{-11} erg per radian.[2] Keeping the interaction constants small ($|f|\leqslant0.04\times10^{-11}$), and assigning $\nu_6=1011$ cm^{-1} and $\nu_7=909$ cm^{-1} by analogy with formaldehyde,[13] it is necessary to assign $\nu_8=588$ cm^{-1} and $\nu_9=529$ cm^{-1} in order to obtain values for F_8 and F_9 reasonably close together. The constants obtained by this procedure are ($\times10^{-11}$ erg per radian^2): $F_6=0.49$, $F_9=0.68$, $f_{69}=-0.03$, $F_7=0.21$, $F_8=0.75$, and $f_{78}=+0.04$. These constants reproduce the frequencies within 0.5 percent. If the reverse assignment is made for ν_8 and ν_9, the closest values of F_8 and F_9 are 0.70 $\times10^{-11}$ and 0.87×10^{-11} erg per radian.[2] The value chosen for F_1 is 5.23×10^5 dynes per cm. A plausible set of force constants for the ketene molecule is given in Table X.

TABLE X. Force constants for ketene.

$F_1=5.23$	$F_4=0.494$
$F_2=5.23$	$F_6=0.49$
$F_3=15.5$	$F_7=0.21$
$F_5=9.8$	$F_8=0.75$
$f_{35}=1.45$	$F_9=0.68$
	$f_{78}=+0.04$
$\times10^5$ dynes/cm	$f_{69}=-0.03$
	$\times10^{-11}$ erg/radian^2

VI. MOLECULAR DIMENSIONS

The rotational bands in the ketene spectrum exhibit the same irregularities observed in the formaldehyde spectrum.[15] Unlike formaldehyde, however, ketene shows no discrete bands in the ultraviolet spectrum[21–23] from which to obtain the rotational constants. Thus we shall use the average spacing of the components in the 3162 cm^{-1} band to obtain the moment of inertia around the twofold axis. This yields a value of $I_A=2.96\pm0.50\times10^{-40}$ g cm^2 which is compatible with $r(C-H)=1.08A$, and $\angle HCH=120°$.

[13] Reference 2, p. 187.
[19] Reference 2, p. 174.
[20] Reference 12, p. 147.

[21] Lardy, J. chim. phys. **21**, 353 (1924).
[22] R. G. W. Norrish, H. G. Crone, and O. Saltmarsh, J. Chem. Soc. 1533 (1933); J. Am. Chem. Soc. **56**, 1644 (1934).
[23] W. F. Ross and G. B. Kistiakowsky, J. Am. Chem. Soc. **56**, 1112 (1934).

On a Method of Correcting for Incomplete Thermal Isolation in Measurements of Small Heat Capacities

J. G. Aston and G. J. Szasz[1]
School of Chemistry and Physics of The Pennsylvania State College, State College, Pennsylvania

(Received April 7, 1947)

The treatment originally given by Keesom and Kok is simplified in such a manner as to make it applicable to heat-capacity measurements in which the temperature of the system is known only before and after heating.

In the usual determination of heat capacities in an isothermal calorimeter, the temperature drift of the calorimeter is established in the periods before and after heating and the drifts extrapolated linearly to the mid-time of the heating period. However, at temperatures below 20°K, where the heat capacity of the shield and calorimeter with contents drop to a very small value, this procedure is not generally applicable. Keesom and Kok[2a,b] have treated this problem and derived expressions for the corrected or true mid-time of the heat capacity, i.e., the time to which the fore and after drifts should be extrapolated.

The method and conclusions of Keesom and Kok can be summarized as follows:

ASSUMPTIONS MADE

(1) heat capacity of block (shield) and calorimeter constant during the period considered;
(2) the temperature (T) of block and calorimeter are uniform;
(3) heat exchange is proportional to temperature difference (i.e., Newton's Law is applicable);
(4) the heat production during the heating period is constant;
(5) the temperature of the surrounding bath is some regular function of time.

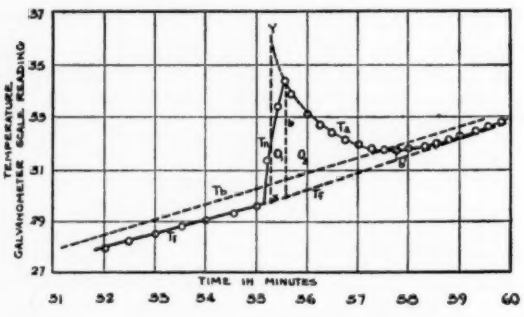

FIG. 1. Time-temperature curve.

MEANING OF SYMBOLS

T_h = real temperature during heating period;
T_f = temperature of block (shield);
T_a = real temperature in the after period;
k = heat exchange between calorimeter and shield in cal. per degree temperature difference per second;
l = heat production during heating period in cal. per second;
c = true heat capacity of system studied;
t = time (variable);
t_1 = end of heating period.

Figure 1 reproduces one of the figures given by Keesom and Kok and shows the time temperature curve during one of their measurements.

From these definitions and Fig. 1, the following equations are deduced by Keesom and Kok:

$$T_h - T_f = \frac{l}{k}\left[1 - \exp\left(-\frac{k}{c}t\right)\right], \tag{1}$$

$$T_a - T_f = b \exp\left[-\frac{k}{c}(t - t_1)\right], \tag{2}$$

$$b = \frac{l}{k}\left[1 - \exp\left(-\frac{k}{c}t_1\right)\right], \tag{3}$$

$$kO_1 = k\int_0^{t_1}(T_h - T_f)dt = lt_1 - bc, \tag{4}$$

$$kO_2 = k\int_{t_1}^{\infty}(T_a - T_f)dt = bc, \tag{5}$$

$$kO = k(O_1 + O_2) = lt_1. \tag{6}$$

If the heat exchange is (relatively) small, the curves in Fig. 1 can be extrapolated by means of

[1] Phillips Petroleum Fellow, 1945–47.
[2a] Keesom and Kok, Comm. Phys. Lab., University of Leyden, No. 219c (1932).
[2b] Keesom and Kok, Proc. Acad. Amsterdam **35**, 294 (1932).

their tangents at $t=t_1$ to a time t^* which corresponds to half the time of heating in the usual correction (when the fore and after drifts are constant), and then

$$t^*=t_1-O_1/b. \tag{7}$$

The use of these equations as given by Keesom and Kok depends on a knowledge of the temperature of the calorimeter at all times. However, in the cases frequently encountered, where the same electrical circuits are used for the temperature measurements on the resistance thermometer and for the current and potential measurements of the heat input, these data are not available. For such cases the following procedure was developed several years ago and used in this laboratory.

Starting with Eqs. (4) and (7), we obtain by simple transformations

$$t^*=\frac{t_1}{2}+\left[\frac{t_1}{2}-\left(\frac{O_1}{b}\right)\right] \tag{7'}$$

$$\frac{O_1}{b}=\frac{kt_1}{kb}-\frac{c}{k}, \tag{4'}$$

and substituting from (3)

$$\frac{O_1}{b}=\frac{t_1}{1-\exp[-(k/c)t_1]}-c/k$$

$$=-c/k\left[\frac{-(k/c)t_1}{1-\exp[-(k/c)t_1]}\right]-c/k. \tag{8}$$

Let

$$Z=-(k/c)t_1,$$

then

$$-\frac{-(k/c)t_1}{1-\exp[-(k/c)t_1]}=-\frac{Z}{1-\exp Z}$$

$$=+\frac{Z}{\exp Z-1}. \tag{9}$$

Upon expanding we get

$$\frac{Z}{\exp Z-1}=1-\frac{Z}{2}+\frac{1}{6}\frac{Z^2}{2!}-\frac{1}{30}\frac{Z^4}{4!}$$

$$+\frac{1}{42}\frac{Z^6}{6!}-\frac{1}{30}\frac{Z^8}{8!}+\frac{5}{66}\frac{Z^{10}}{10!}, \tag{10}$$

where the numbers 2, 6, 30, 42, etc. are the Bernouilli numbers. This converges for $|Z|<2\pi$. Thus

$$\frac{-(k/c)t_1}{1-\exp[-(k/c)t_1]}=1+\left(\frac{k}{c}\right)\frac{t_1}{2}$$

$$+\frac{1}{2!6}\left(\frac{k}{c}t_1\right)^2-\frac{1}{4!30}\left(\frac{k}{c}t_1\right)^4. \tag{11}$$

Therefore

$$\frac{O_1}{b}=\frac{t_1}{2}+\frac{1}{2!6}\left(\frac{k}{c}\right)t_1^2-\frac{1}{4!30}\left(\frac{k}{c}\right)t_1^4, \tag{12}$$

and combining with (7), we get

$$t^*=t_1-\frac{t_1}{2}-\frac{1}{2!6}\frac{k}{c}t_1^2+\frac{1}{4!30}\left(\frac{k}{c}\right)^3t_1^4. \tag{13}$$

Since $c\gg k$ and t_1 is usually 4 (or less), we neglect all terms after the third and get

$$t^*=(t_1/2)-(k/c)(t_1^2/12), \tag{14}$$

wherein t_1 is the actual time of heating, and t^* is the "true" or "corrected" mid-time of the heating period, as discussed above.

APPENDIX

An example.

Measurement made on Butene-1, in isothermal calorimeter C[3]

Foredrift: +0.0281°/min.,
Afterdrift: +0.0075°/min.,
Total time = 5 min.; Uncorrected temperature rise = 1.698°,
$(k/c)=0.055$ min.$^{-1}$, $t^*=5/2-(0.055)(25/12)=2.385$.

This produces a difference in ΔT of 0.0024°, or 0.14 percent in the uncorrected, net heat capacity of the system. This amounts to about 0.3 percent of the heat-capacity value calculated for the sample.

[3] Aston *et al.*, J. Am. Chem. Soc. **68**, 52 (1946).

Thermal Properties of Cyclopentane and Its Use as a Standard Substance in Low Temperature Thermal Measurements

G. J. Szasz,* J. A. Morrison,** E. L. Pace,*** and J. G. Aston
School of Chemistry and Physics, The Pennsylvania State College, State College, Pennsylvania

(Received April 7, 1947)

The thermal properties of cyclopentane were redetermined in the Penn State isothermal calorimeter and adiabatic calorimeter B' and the results compared with other investigations. It is concluded that the heat capacity results of Penn State adiabatic calorimeter B', those of the National Bureau of Standards, and those of the Bureau of Mines Laboratory at Bartlesville, Oklahoma, are in satisfactory agreement, under normal operating conditions, above 30°K.

IN view of the discrepancies observed between the results of various investigators on the thermal properties of simple hydrocarbons,[1–7] it seemed desirable to test our various calorimeters, using cyclopentane as the "standard" substance. The same sample was used as before.[4] The hitherto unreported measurements were carried out in our gold calorimeter C,[8] by Dr. E. L.

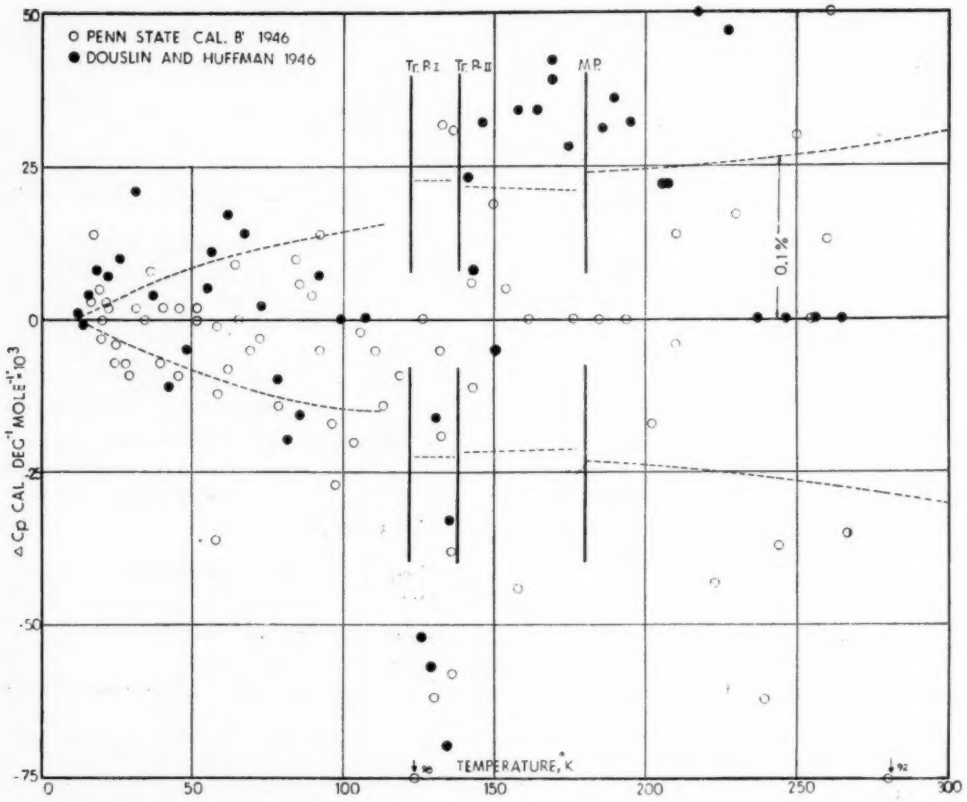

FIG. 1. Comparison plot for cyclopentane. Deviations of experimental points from smooth curve.

* Phillips Petroleum Fellow 1945–47. ** National Research Fellow 1945–46. *** Phillips Petroleum Fellow 1944–46.

[1] Schumann, Aston, and Sagenkahn, J. Am. Chem. Soc. **64**, 1039 (1942).
[2] Guthrie and Huffman, J. Am. Chem. Soc. **65**, 1142 (1943).
[3] Aston, J. Am. Chem. Soc. **65**, 2041 (1943).
[4] Aston, Fink, and Schumann, J. Am. Chem. Soc. **65**, 341 (1943).
[5] Douslin and Huffman, J. Am. Chem. Soc. **68**, 173 (1946).
[6] Aston, Szasz, and Fink, J. Am. Chem. Soc. **65**, 1135 (1943).
[7] Ruehrwein and Huffman, J. Am. Chem. Soc. **65**, 1620 (1943).
[8] Aston and Messerly, J. Am. Chem. Soc. **58**, 2354 (1936); **62**, 886 (1940).

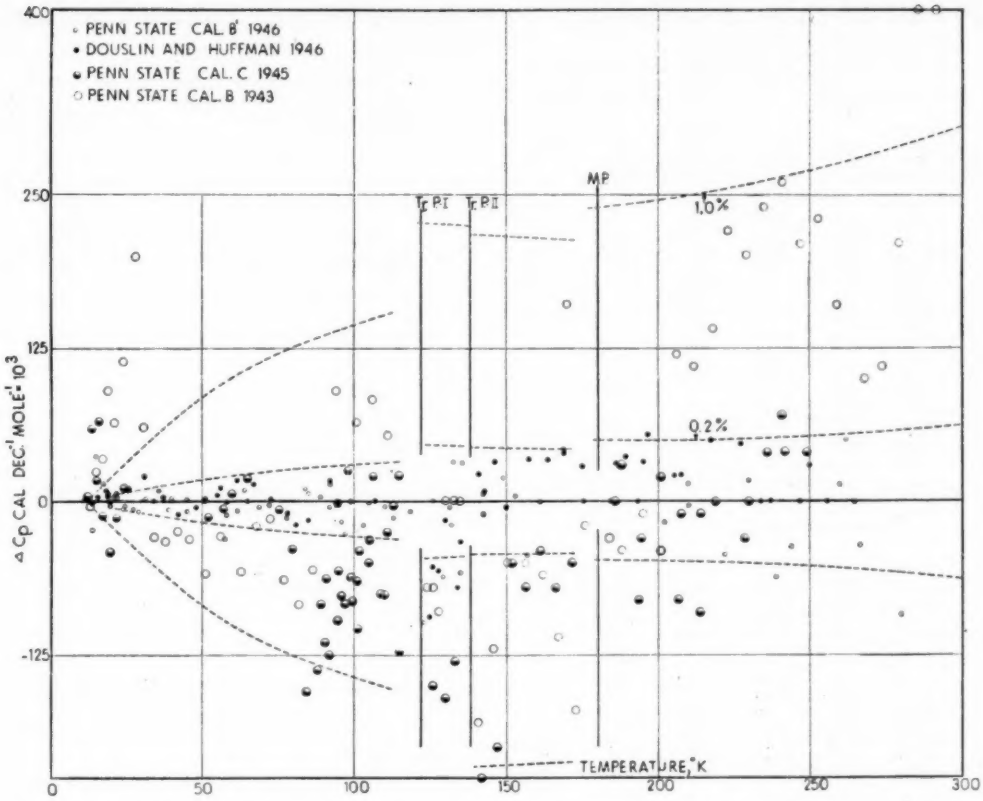

FIG. 2. Comparison plot for cyclopentane. Deviations of experimental points from smooth curve.

Pace,[9] and in our new adiabatic calorimeter B' which is described in detail elsewhere.[10]

The results are summarized in Tables I–III and in Figs. 1 and 2. Table I is a summary of the heat capacity results at rounded temperatures of the various investigators obtained from the best curve through the data in each case, together with the percentage deviations from the "best" curve of calorimeter B'. Figures 1 and 2 show the deviations of the individual points from our smoothed curve. Except for the data on crystals III the results of the heat capacity measurements indicate a satisfactory agreement between the results in our adiabatic calorimeter B' and those of Douslin and Huffman, assuming maximum total errors of 0.10 percent and 0.15 percent, above 30°K, for the Bureau of Mines and our calorimeter, respectively. It should be emphasized that the precision and reproducibility of both calorimeters is better than 0.10 percent at any point. The few deviations in Table I which are larger than 0.25 percent are probably due to the fact that there is a small uncertainty in the smoothing of the experimental data to obtain values at rounded temperatures.

With the exception of the value at 90°K and the data on crystals II and III, the results obtained in our isothermal calorimeter C are in agreement with those in B' within the error expected from the accuracy claimed for calorimeter C (± 0.3 percent above 30°K) and for B' (± 0.15 percent). For crystals II and III the data are difficult to reproduce and equilibrium is slow with all calorimeters, and the large differences may be due to this fact. The heat capacity results obtained in our calorimeter B do show marked deviations, considerably beyond the accuracy originally claimed for it. Since this calorimeter has been dismantled in 1942 (and most of it used in building calorimeter B') there is no way to recheck its performance at this time. However, the main reason for the large errors was the fact that, to increase the speed of measurements, the blocks were set warm and several heat capacities taken successively with the same setting of the blocks. This produced large drifts.

[9] For details see Ph.D. dissertation of E. L. Pace, The Pennsylvania State College (1946).
[10] Aston and Szasz, J. Am. Chem. Soc. (to be published).

TABLE I. The heat capacity of cyclopentane at rounded temperatures.

	C_p, cal. deg^{-1} mole.$^{-1}$				Δ% from PSC Cal. B'		
T°K	PSC Cal. B'	Douslin and Huffman	PSC Cal. B	PSC Cal. C	Douslin and Huffman	PSC Cal. C	PSC Cal. B
			Crystal I				
14	0.717	.72		0.758	0	+5.7	
15	0.878	.88	0.90	0.908	0	+3.5	+2.2
20	1.880	1.89	1.99	1.855	+0.5	−1.3	+6.1
25	3.080	3.08	3.19	3.107	0	+0.9	+3.7
30	4.310	4.33	4.37		+0.5		+1.4
35	5.523	5.53			+0.11		
40	6.660	6.64	6.68		−0.3		+0.3
45	7.663	7.66			0		
50	8.560	8.56	8.54		0		−0.3
55	9.355	9.37		9.385	+0.2	+0.3	
60	10.080	10.11	10.07	10.035	+0.3	−0.5	−0.1
70	11.37	11.37	11.36	11.31	0	−0.5	−0.1
80	12.46	12.45	12.40	12.42	−0.1	−0.3	−0.5
90	13.43	13.44	13.46	13.34	+0.1	−0.7	+0.2
100	14.32	14.32	14.40	14.27	0	−0.3	+0.5
110	15.19	15.20	15.25	15.17	0	−0.1	+0.4
			Crystal II				
125	22.72			22.58		−0.6	
130	22.62	22.58	22.59	22.47	−0.2	−0.7	−0.2
135	22.53			22.42		−0.5	
			Crystal III				
140	21.68	21.72	21.49	21.40	+0.2	−1.3	−0.9
150	21.45	21.56	21.38	21.31	+0.5	−0.6	−0.3
160	21.32	21.46	21.30	21.26	+0.7	−0.3	−0.1
170	21.26	21.35	21.20	21.22	+0.4	−0.2	−0.3
			Liquid				
180	23.85	23.88	23.79	23.87	+0.1	+0.1	−0.2
190	24.10	24.14	24.06	24.09	+0.2	0	−0.2
200	24.42	24.45	24.42	24.39	+0.1	−0.1	0
210	24.81	24.84	24.90	24.75	+0.1	−0.2	+0.4
220	25.25	25.28	25.38	25.21	+0.1	−0.2	+0.5
230	25.74	25.76	25.94	25.74	0	0	+0.8
240	26.28	26.28	26.53	26.28	0	0	+0.9
250	26.85	26.87	27.07	26.91	+0.1	+0.2	+0.8
260	27.51	27.52	27.66		0		+0.6
270	28.19	28.22	28.31		+0.1		+0.4
280	28.90	28.93	29.10		+0.1		+0.7
290	29.68	29.68	30.05		0		+1.2
300	30.46	30.44	30.96		−0.1		+1.7

Table II, which records the transition and melting temperatures, shows a good agreement between the temperature scales used here and at the Bureau of Mines in Bartlesville. Table III shows the results on the heats of transition and fusion. The poor agreement of the heats of fusion is hard to explain as also is the unsatisfactory agreement of the heats of the upper transition. This is true for the comparison between any two sets of data and may be connected with the nature of crystals II and III.

For the low temperature extrapolation to 0°K, the following characteristic Debye Temperatures (θ) were found from the low temperature heat capacities (all assuming six degrees of freedom).

Penn State Calorimeter B'[11]	151.6
Douslin and Huffman[5]	151.6
Penn State Calorimeter B[4]	149.7

It should be noted that the discrepancies mentioned do not seriously affect the entropy

[11] Ph.D. Dissertation of G. J. Szasz, The Pennsylvania State College (1947).

TABLE II. Transition temperatures of cyclopentane.

Lower transition temperature of cyclopentane	
Aston, Fink, and Schumann	122.39 ±0.05°K
Douslin and Huffman	122.39 ±0.05°K
This research	122.36 ±0.005°K
Upper transition temperature of cyclopentane	
Aston, Fink, and Schumann	138.07 ±0.05°K
Douslin and Huffman	138.08 ±0.05°K
Triple point temperature of cyclopentane	
Aston, Fink, and Schumann	179.69 ±0.05°K
Douslin and Huffman	179.71 ±0.05°K

TABLE III. Heats of transition of cyclopentane.

Molal heat of lower transition of cyclopentane	
Aston, Fink, and Schumann	1165.1 ±0.8
Douslin and Huffman	1167.3 ±1.0
This research	1167.4 ±1.0
Molal heat of upper transition of cyclopentane	
Aston, Fink, and Schumann	82.80 ±0.08
Douslin and Huffman	82.32 ±0.19
This research	81.91 ±0.07
Molal heat of fusion of cyclopentane	
Aston, Fink, and Schumann	144.05 ±0.30
Douslin and Huffman	145.54 ±0.34
This research	144.31 ±0.30

results. Aston *et al.*[4] obtained 48.97±0.05 e.u. for $S(l)_{298.16}$, while Douslin and Huffman[5] obtained 48.79 e.u.±0.10.

Figure 2 includes all results and gives a good indication of the relative accuracy of the various measurements. The actual heat capacity values used in constructing this plot can all be found elsewhere.[4, 5, 9, 11]

Other recent comparisons between precise thermodynamic measurements performed in different laboratories are those on ethyl benzene and naphthalene. Ethylbenzene was studied by Guthrie, Spitzer, and Huffman[12], and by Scott and Brickwedde.[13] The agreement in the heat capacities was satisfactory above 60°K, while the heats of fusion differed by 0.19 percent. Naphthalene was studied by Southard and Brickwedde,[14] and by Hicks.[15] The agreement was satisfactory—within the limits of the somewhat less accurate isothermal calorimeter used by Hicks.

ACKNOWLEDGMENT

This work was made possible by financial aid from the Phillips Petroleum Company.

[12] Guthrie, Spitzer, and Huffman, J. Am. Chem. Soc. **66**, 2120 (1944).

[13] Scott and Brickwedde, J. Research Nat. Bur. of Stand. **35**, 501 (1945).

[14] Southard and Brickwedde, J. Am. Chem. Soc. **55**, 4378 (1933).

[15] Hicks, J. Am. Chem. Soc. **60**, 1000 (1938).

The Heat Capacity of Benzene Vapor. The Contribution of Anharmonicity*

D. W. Scott, Guy Waddington, J. C. Smith, and H. M. Huffman
Petroleum Experiment Station, Bureau of Mines, Bartlesville, Oklahoma

(Received May 12, 1947)

The heat capacity of benzene vapor was measured at two or more pressures at each of five temperatures in the range 68° to 198°C; and values of $C_p°$, the heat capacity in the ideal gas state, were obtained. By assuming a moderate degree of anharmonicity of the vibrations, it was possible to obtain excellent agreement between values of $C_p°$ calculated statistically from spectroscopic data, and the observed values. An empirical equation for the second virial coefficient of benzene vapor was obtained from the observed values of $(\partial C_p/\partial P)_T$, and heat of vaporization and vapor pressure data.

INTRODUCTION

THE Petroleum and Natural Gas Division of the U. S. Bureau of Mines is carrying on a research program to study the vapor-heat capacity of petroleum hydrocarbons and related substances. Previous publications from this laboratory[1,2] have described the flow calorimeter currently in use, and have reported experimental results for the vapor-heat capacity of *n*-heptane, 2,2,3-trimethylbutane, *n*-hexane, and 2,2-dimethylbutane. The emphasis in this work has been on obtaining data of high accuracy. The study of the vapor-heat capacity of benzene reported in the present paper, was undertaken because the heat capacity of this substance can be calculated from spectroscopic data to the harmonic-oscillator rigid-rotator approximation. It was felt that a comparison of measured values of the heat capacity with values so calculated would give significant information about the accuracy of results obtained with the flow calorimeter. Actually, because of the inherent inaccuracies of the harmonic-oscillator rigid-rotator treatment, no direct check of the experimental measurements was possible. However, it was found that, by assuming a moderate degree of anharmonicity of the vibrations, excellent agreement between calculated and observed values of the heat capacity of benzene vapor was obtained over the whole temperature range of the experimental measurements.

EXPERIMENTAL

The apparatus and experimental procedures have been described in detail in a recent publication[1] from this laboratory. The sample of benzene used was made available by the Chemistry and Refining Section of this station. It had been prepared for other purposes by distillation in an efficient column followed by several fractional crystallizations. From its melting-point curve,[3] the sample was found to have a purity of 99.93 mole percent, assuming the impurity to be liquid-soluble, solid-insoluble. A bomb sulfur analysis[4] (A.S.T.M. designation: D 129–44) did not indicate any significant amount of sulfur.

The vapor-heat capacity data are given in Table I. The values of $C_p°$ were obtained by linear extrapolation to zero pressure of plots of heat capacity *vs.* pressure. For the two lower temperatures, the heat capacity was measured at three different pressures; on a plot of C_p *vs.*

Table I. Vapor-heat capacity of benzene; cal./deg./mole.

1 cal. = 4.1833 int. joules; mole. wt. = 78.108; 0°C = 273.16°K

T, °K	341.60	371.20	402.30	436.15	471.10
C_p (1 atmos.)		25.60	27.59	29.73	31.81
C_p (404 mm)	23.32	25.33			
C_p (270 mm)	23.18				
C_p (194 mm)	23.10	25.18	27.32	29.55	31.69
$C_p°$	22.90	25.04	27.23	29.49	31.65

* Contribution No. 8 from the Thermodynamics Laboratory of the Petroleum Experiment Station, Bureau of Mines. Published by permission of the Director of the Bureau of Mines, U. S. Dept. of the Interior.

[1] Waddington, Todd, and Huffman, J. Am. Chem. Soc. 69, 22 (1947).

[2] G. Waddington and D. Douslin, "Experimental vapor heat capacities and heats of vaporization of *n*-hexane and 2, 2-dimethylbutane," J. Am. Chem. Soc. (to be published).

[3] Determined by Mr. H. J. Coleman of this station.

[4] Determined by Mr. E. L. Garton and Miss Shirley Nix of this Station.

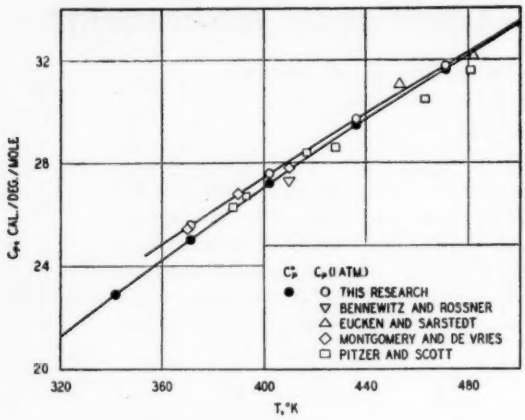

FIG. 1. $C_p°$ and C_p (1 atmos.) of benzene as a function of temperature. The values of C_p (1 atmos.) of this research are compared with the results of other recent measurements of the vapor-heat capacity of benzene.

pressure, the observed values deviated from linearity by less than 0.05 percent. In Fig. 1 the values of $C_p°$ and C_p (1 atmos.) are plotted as a function of temperature, and the latter are compared with the results of other recent measurements of the heat capacity of benzene vapor.[5–8]

The heat of vaporization data for benzene, obtained in the course of flow-calibration experiments with the vapor-heat capacity calorimeter, have already been reported,[2] but for the sake of completeness are repeated here in Table II.

DISCUSSION

In Table III the observed values of $C_p°$ for benzene are compared with those calculated from spectroscopic data to the harmonic-oscillator rigid-rotator approximation, by use of the vibrational assignment of Herzfeld, Ingold, and Poole,[9] and values of the fundamental constants given by Wagman, Kilpatrick, Taylor, Pitzer, and Rossini.[10]

As shown in the fourth column of Table III, there is a significant difference between the values of the heat capacity so calculated and those observed experimentally. It seems improbable that this difference could be entirely accounted for by any error in the vibrational assignment used. Lowering a single vibrational frequency would have the effect of raising the calculated heat capacity by virtually the same amount at each temperature, so that agreement with the observed values could be obtained at any one temperature but not at all five temperatures. Only an improbably drastic change of two or more vibrational frequencies would increase the slope of the calculated heat-capacity curve to agree with that observed experimentally over the entire temperature range.

If it is assumed that the vibrational assignment and the experimentally measured values of the heat capacity are correct, the difference, $C_p°(\text{obs.}) - C_p°(\text{calc.})$, must be attributed to the contribution to the heat capacity of the factors neglected in the harmonic-oscillator rigid-rotator treatment, namely anharmonicity, rotational stretching, and rotational-vibrational coupling. Of these factors, anharmonicity is the only one that would be expected to make a significant contribution to the heat capacity in the temperature range covered by the experimental measurements.

It is impossible at present to make a rigorous calculation of the contribution of anharmonicity to the heat capacity of benzene, as the available spectroscopic data yield only a few of the numerous anharmonicity coefficients required for such a calculation. However, it is possible to show that the difference, $C_p°(\text{obs.}) - C_p°(\text{calc.})$, is consistent, both in magnitude and in temperature dependence, with moderate values of the anharmonicity coefficients.

To show this, it is convenient to use the approximation, suggested by Stockmayer, Kavanagh, and Mickley,[11] that the anharmonicity

TABLE II. Heat of vaporization of benzene.

1 cal. = 4.1833 int. joules; mole. wt. = 78.108

t, °C	No. expts.	ΔH_{vap}, cal./mole.
41.6	2	7868±2[a]
49.9	3	7755±4[a]
60.9	3	7606±2[a]
80.1	3	7349±1[a]

[a] Maximum deviation.

[5] K. Bennewitz and W. Rossner, Zeits. f. physik. Chemie **B29**, 126 (1938).
[6] A. Eucken and B. Sarstedt, *ibid.* **B50**, 143 (1941).
[7] J. B. Montgomery and T. DeVries, J. Am. Chem. Soc. **64**, 2375 (1942).
[8] K. S. Pitzer and D. W. Scott, *ibid.* **65**, 803 (1943).
[9] Herzfeld, Ingold, and Poole, J. Chem. Soc. (London), 316 (1946).
[10] Wagman, Kilpatrick, Taylor, Pitzer, and Rossini, J. Research Nat. Bur. Stand. **34**, 143 (1945).
[11] Stockmayer, Kavanagh, and Mickley, J. Chem. Phys. **12**, 408 (1944).

coefficients are proportional to the sum of the frequencies, i.e., $X_{ij}=a(\nu_i+\nu_j)$, where X_{ij} is an anharmonicity coefficient, a the proportionality constant, and ν_i and ν_j the frequencies of the ith and jth modes of vibration. If the adjustable parameter, a, is given the value 9×10^{-4}, it is found that the calculated contribution of anharmonicity to the heat capacity of benzene is in excellent agreement with the values of $C_p°$(obs.) $-C_p°$(calc.) given in Table III. This is shown in Fig. 2. The maximum deviation of the points representing $C_p°$(obs.) $-C_p°$(calc.) from the calculated curve showing the contribution of anharmonicity to the heat capacity, assuming $X_{ij}=9\times10^{-4}$ $(\nu_i+\nu_j)$, is only 0.04 percent of the total heat capacity. The order of magnitude of the anharmonicity coefficients required to fit the data in this manner (0.7 cm^{-1} for the lowest frequencies to 5.5 cm^{-1} for the carbon-hydrogen stretching frequencies) seems reasonable for a molecule such as benzene.

For calculating the contribution of anharmonicity to the heat capacity, the expansion of the vibrational partition function for a polyatomic molecule given by Stockmayer, Kavanagh, and Mickley[11] was used. In terms of this partition function, the contribution of anharmonicity to the heat capacity, C_p(anh.), becomes

$$C_p(\text{anh.})\cong R(d/dT)T^2(d/dT)\sum_{i\leq j} f_{ij},$$

where $f_{ii}=d_i(d_i+1)X_{ii}hc/kT[\exp(\mu_i)-1]^2$, and $f_{ij}(i<j)=d_id_jX_{ij}hc/kT[\exp(\mu_i)-1][\exp(\mu_j)-1]$. In these expressions, $\mu_i=hc\nu_i/kT$ with ν_i given in cm^{-1}, and d_i is the degeneracy of the ith mode of vibration. The above equation for C_p(anh.) is a satisfactory approximation for the temperature range of interest here but would fail at somewhat higher temperatures.

It is rather improbable that a systematic error in the experimental heat-capacity measurements would have the same temperature dependence as the contribution of anharmonicity to the heat capacity. It seems very likely, therefore, that the values of $C_p°$(obs.) $-C_p°$(calc.) represent the true contribution of anharmonicity to the heat capacity of benzene vapor. To this extent, the results reported here are evidence of a high degree of accuracy in the experimental vapor heat-capacity measurements.

TABLE III.

T, °K	$C_p°$(obs.)	$C_p°$(calc.)[a]	$C_p°$(obs.) $-C_p°$(calc.)
341.60	22.90	22.77	0.13
371.20	25.04	24.87	0.17
402.30	27.23	27.00	0.23
436.15	29.49	29.18	0.31
471.10	31.65	31.29	0.36

[a] Harmonic-oscillator rigid-rotator approximation.

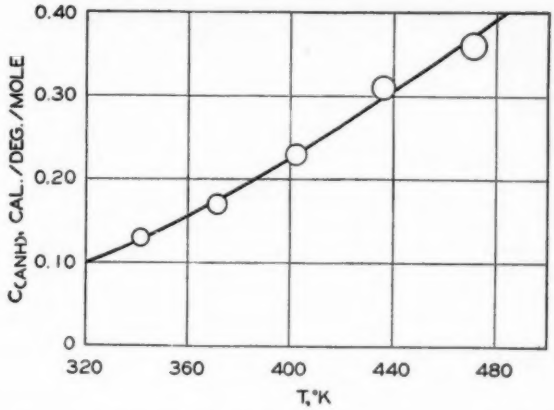

FIG. 2. Contribution of anharmonicity to the heat capacity of benzene vapor. The plotted points are the values of $C_p°$ (obs.) $-C_p°$ (calc.), i.e., the difference between the observed heat capacity and that calculated from spectroscopic data to the harmonic-oscillator rigid-rotator approximation. The radius of each circle is 0.05 percent of the total heat capacity. The curve shows the contribution of anharmonicity to the heat capacity calculated, assuming $X_{ij}=9\times10^{-4}(\nu_i+\nu_j)$.

SECOND VIRIAL COEFFICIENT OF BENZENE

The second virial coefficient, B, in the equation of state $PV=RT+BP$ is related to the variation of the vapor-heat capacity with pressure by the equation $(\partial C_P/\partial P)_T=-T(\partial^2B/\partial T^2)_P$. Also values of the second virial coefficient may be obtained from heat of vaporization and vapor pressure data by use of the relation

$$B=[\Delta H_{\text{vap}}/T(dP/dT)]-RT/P+v_l, \quad (1)$$

obtained by substituting the above equation of state into the exact Clapeyron equation, $\Delta H_{\text{vap}}=T(V-v_l)dP/dT$.

The values of $(\partial C_p/\partial P)_T$ and ΔH_{vap} for benzene found in this work, in conjunction with the Antoine equation for the vapor pressure given in the A.P.I. Tables[12] were used to obtain an em-

[12] American Petroleum Institute Research Project 44 at the National Bureau of Standards. Selected Values of

TABLE IV. Second virial coefficient and $(\partial C_P/\partial P)_T$ for benzene.

t, °C	B, cc: From ΔH_{vap} and vapor pressure	B, cc: Calc., Eq. 3
25.0	−1570	−1496
41.6	−1272	−1296
49.9	−1213	−1214
60.9	−1138	−1121
80.1	− 994	− 989
110.0	− 847	− 840

t, °C	$(\partial C_P/\partial P)_T$ cal./deg./mole./atmos. Obs.	Calc., Eq. 3
68.44	0.78	0.81
98.04	.55	.53
129.14	.37	.35
162.99	.24	.24
197.94	.17	.17

pirical equation for the second virial coefficient, of the form[13]

$$B = b - c\exp(a/T). \qquad (2)$$

On the basis of this empirical equation, the variation of heat capacity with pressure is given by $(\partial C_p/\partial P)_T = c(a^2/T^3 + 2a/T^2)\exp(a/T)$; values of the constants c and a were selected to fit the $(\partial C_p/\partial P)_T$ data. To evaluate the remaining constant, b, values of the second virial coefficient were calculated by means of Eq. (1), using the heat of vaporization data of Table II and the Antoine equation for the vapor pressure. Substituting these values of B, and the previously obtained values of c and a into Eq. (2) gave four closely agreeing values of b, and the mean of these was taken as the final value. The resulting empirical equation for the second virial coefficient is

$$B = -202 - 53.5\exp(950/T) \text{ cc.} \qquad (3)$$

Values of B calculated with this equation are compared in the first part of Table IV with those obtained from heat of vaporization and vapor-pressure data. The value at 25° is calculated from the heat of vaporization determined by Osborne and Ginnings,[14] and that at 110° from the heat of vaporization reported by Fiock, Ginnings, and Holton.[15] At the other four temperatures the heat of vaporization data of Table II were used. Equation (3) may be further compared with the vapor density measurements of Magnus and Schmid,[16] and of Eucken and Meyers.[17] The twelve vapor density determinations reported by Magnus and Schmid, all at approximately 373°K, give values of B ranging from −614 cc to −972 cc, with a mean of −747 cc. For this same temperature, the value of B from Eucken and Meyer's equation, corrected to 1941 atomic weights, is −922 cc. The value given by Eq. (3) is −884 cc at 373°K.

The values of $(\partial C_P/\partial P)_T$ calculated from Eq. (3) are in satisfactory agreement with those found experimentally; this is shown in the second part of Table IV.

Properties of Hydrocarbons. Table No. 5k (Part 1), alkyl benzenes, C_6 to C_8, vapor pressure and boiling points, at 10 to 1500 mm-Hg, dated June 30, 1944.

[13] Hirschfelder, McClure, and Weeks, J. Chem. Phys. **10**, 201 (1942).

[14] N. S. Osborne and D. C. Ginnings, Nat. Bur. Stand., unpublished data.

[15] Fiock, Ginnings, and Holton, J. Research Nat. Bur. Stand. **6**, 881 (1931).

[16] A. Magnus and E. Schmid, Zeits. anorg. allgem. Chemie **120**, 232 (1922).

[17] A. Eucken and L. Meyers, Zeits. physik. Chemie **B5**, 452 (1929).

Heat Flow through Composite Cylinders*

S. S. PENNER** AND S. SHERMAN***
Allegany Ballistics Laboratory, Cumberland, Maryland

(Received April 11, 1947)

The differential equations are solved for the time-dependent flow of heat through a composite cylinder. The composite cylinder is assumed to be thermally insulated at the outer boundary and to consist of a cylindrical core, initially at the uniform temperature U_0, surrounded by a cylindrical shell, initially at temperature zero. Included in this paper are corresponding treatments for composite slabs of finite and infinite widths.

INTRODUCTION

THE present paper is concerned with the flow of heat through a composite cylinder for the special case where the thermal conductivity is independent of temperature. The solution for the differential equations for the flow of heat may be modified so as to apply to the diffusion of a given substance through two different media separated by an immovable boundary.

Problems related to those treated in this paper have been considered in connection with the flow of heat through composite walls.[1,2] Barrer[3] has developed a method for measuring the diffusion coefficient and the thermal conductivity where these quantities depend respectively on concentration and temperature. Approximate formulae which represent solutions for large and small values of the time may be obtained by asymptotic and Heaviside wave expansions.[1,4]

HEAT FLOW THROUGH A COMPOSITE CYLINDER

Consider an infinitely long cylinder of radius b surrounded by a cylindrical shell of thickness $c-b$. The initial temperature of the cylindrical core is U_0, while the cylindrical shell is initially at the temperature zero. The thermal diffusivity in the cylinder is designated as K_1 and the thermal diffusivity in the shell is K_2. The temperatures in the cylinder and in the shell are designated as $u_1(r, t)$ and $u_2(r, t)$, respectively, where r represents the radial distance from the axis of the cylinder and t is the time.

The boundary value problem may be formulated as follows:

$$\partial u_1/\partial t = K_1[(\partial^2 u_1/\partial r^2)+(1/r)(\partial u_1/\partial r)], \quad 0\leqslant r<b, \quad t>0, \tag{1}$$

$$u_1(r, 0) = U_0, \quad 0\leqslant r<b, \tag{2}$$

$$\partial u_2/\partial t = K_2[(\partial^2 u_2/\partial r^2)+(1/r)(\partial u_2/\partial r)], \quad b<r<c, \quad t>0, \tag{3}$$

$$u_2(r, 0) = 0, \quad b<r<c, \tag{4}$$

$$\partial u_2(c-0, t)/\partial r = 0, \quad t>0, \tag{5}$$

$$u_1(b-0, t) = u_2(b+0, t), \quad t>0, \tag{6}$$

$$K_1[\partial u_1(b-0, t)/\partial r] = K_2[\partial u_2(b+0, t)/\partial r], \quad t>0. \tag{7}$$

* This paper is based on OSRD report No. 4963 (PB report No. 50864) on the diffusion of nitroglycerin in wrapped powder grains. The work on this diffusion problem was done in 1944 at the Allegany Ballistics Laboratory, Cumberland, Maryland, operated by the George Washington University under OSRD contract OEMsr-273. The authors are indebted to Dr. J. B. Rosser for helpful suggestions.

** Present address: Jet Propulsion Laboratory, California Institute of Technology, Pasadena, California.
*** Present address: 413 Eckart Hall, University of Chicago, Chicago, Illinois.

[1] R. V. Churchill, Math. Ann. **115**, 720 (1938).
[2] M. V. Griffith and G. K. Horton, Proc. Phys. Soc. London **58**, 481 (1946).
[3] R. M. Barrer, Proc. Phys. Soc. London **58**, 321 (1946).
[4] H. S. Carslaw and J. C. Jaeger, *Operational Methods in Applied Mathematics* (Oxford University Press, New York, 1941).

Condition (5) arises from the fact that no heat flow is assumed to occur across the boundary $r=c$. Equations (6) and (7) are the conditions of continuity at the interface between the two media.

Assuming that

$$u_2(r, t) = R_2(r)T_2(t),$$

Eq. (3) becomes

$$T_2'/K_2T_2 = (1/R_2)(R_2''+R_2'/r) = -\lambda_2^2,$$

and

$$T_2 = \text{constant} \exp[-K_2\lambda_2^2 t], \tag{8}$$

$$R_2(r) = A_2J_0(\lambda_2 r)+B_2N_0(\lambda_2 r). \tag{9}$$

Here A_2 and B_2 are constants, and J_0 and N_0 denote, respectively, Bessel functions of order zero of the first and second kind. From condition (5) it follows that

$$R_2'(c-0) = \lambda_2 A_2 J_0'(\lambda_2 c)+\lambda_2 B_2 N_0'(\lambda_2 c) = 0,$$

or

$$A_2J_1(\lambda_2 c)+B_2N_1(\lambda_2 c) = 0, \quad \lambda_2 \neq 0.^5 \tag{10}$$

A particular solution of Eq. (3) which satisfies condition (5) may be written as

$$u_2(r, t) = \{A_2J_0(\lambda_2 r)+B_2N_0(\lambda_2 r)\} \exp[-K_2\lambda_2^2 t], \quad b<r<c, \quad t>0. \tag{11}$$

In Eq. (1) let

$$u_1(r, t) = R_1(r)T_1(t);$$

then

$$T_1'/K_1T_1 = (1/R_1)(R_1''+R_1'/r) = -\lambda_1^2,$$

and

$$T_1 = \text{constant} \exp[-K_1\lambda_1^2 t], \tag{12}$$

$$R_1 = A_1J_0(\lambda_1 r)+B_1N_0(\lambda_1 r). \tag{13}$$

Since $R_1(0)$ is finite a particular solution of Eq. (1) may be written as

$$u_1(r, t) = A_1J_0(\lambda_1 r) \exp[-K_1\lambda_1^2 t]. \tag{14}$$

From the conditions of continuity it now follows that

$$A_1J_0(\lambda_1 b) \exp[-K_1\lambda_1^2 t] = [A_2J_0(\lambda_2 b)+B_2N_0(\lambda_2 b)] \exp[-K_2\lambda_2^2 t], \tag{15}$$

$$K_1\lambda_1 A_1J_1(\lambda_1 b) \exp[-K_1\lambda_1^2 t] = K_2\lambda_2[A_2J_1(\lambda_2 b)+B_2N_1(\lambda_2 b)] \exp[-K_2\lambda_2^2 t]. \tag{16}$$

Since Eqs. (15) and (16) are to be valid for all values of t, it is evident that

$$K_1\lambda_1^2 = K_2\lambda_2^2, \tag{17}$$

or

$$\lambda_1 = (K_2/K_1)^{\frac{1}{2}}\lambda_2 = \mu\lambda_2 \quad \text{where} \quad \mu = (K_2/K_1)^{\frac{1}{2}}. \tag{18}$$

Hence Eqs. (15) and (16) become

$$A_1J_0(\lambda_1 b) = A_2J_0(\lambda_2 b)+B_2N_0(\lambda_2 b), \tag{19}$$

and

$$A_1J_1(\lambda_1 b) = \mu A_2J_1(\lambda_2 b)+\mu B_2N_1(\lambda_2 b). \tag{20}$$

In order to determine the particular values $\lambda_{2j}=\lambda_{21}, \lambda_{22}, \cdots$ for which Eqs. (10), (19), and (20) are satisfied, it is necessary to solve the equation

$$\begin{vmatrix} J_0(\mu\lambda_{2j}b) & J_0(\lambda_{2j}b) & N_0(\lambda_{2j}b) \\ J_1(\mu\lambda_{2j}b) & \mu J_1(\lambda_{2j}b) & \mu N_1(\lambda_{2j}b) \\ 0 & J_1(\lambda_{2j}c) & N_1(\lambda_{2j}c) \end{vmatrix} = 0. \tag{21}$$

[5] If $\lambda_2=0$ a special investigation is required.

The zeros of Eq. (21) may be found by plotting the values of the determinant as a function of λ_{2j}. The coefficients $A_1=A_{\mu j}$, $A_2=A_j$, and $B_2=B_j$, are easily evaluated for particular values of λ_{2j} by use of relations (10), (19), and (20).[6] Define

$$Z_j(r)=\begin{cases} Z_{1j}(\mu\lambda_{2j}r)=A_1J_0(\lambda_1 r)=A_{\mu j}J_0(\mu\lambda_{2j}r), & 0\leqslant r<b, \\ Z_{2j}(\lambda_{2j}r)=A_2J_0(\lambda_2 r)+B_2N_0(\lambda_2 r)=A_jJ_0(\lambda_{2j}r)+B_jN_0(\lambda_{2j}r), & b<r<c. \end{cases} \tag{22}$$

With the aid of Eq. (22) the general solution of the problem under consideration may be written as[7]

$$u(r,t)=\sum_{j=1}^{\infty} C_jZ_j(r)\exp[-K_2\lambda_{2j}^2t]=\begin{cases} u_1(r,t), & 0\leqslant r<b, \\ u_2(r,t), & b<r<c. \end{cases} \tag{23}$$

The functions $Z_j(r)$ are orthogonal in the interval $0\leqslant r<c$ with respect to the weight function r, as is shown in the Appendix. This corresponds to the result

$$\int_0^{c-} rZ_jZ_k\,dr=0, \quad j\neq k. \tag{24}$$

The given boundary conditions also lead to the relation (see Appendix)

$$\int_0^c rZ_j^2\,dr=(c^2/2)[A_jJ_0(\lambda_{2j}c)+B_jN_0(\lambda_{2j}c)]^2+[b^2(\mu^2-1)/2][A_jJ_1(\lambda_{2j}b)+B_jN_1(\lambda_{2j}b)]^2. \tag{25}$$

For $t=0$ Eq. (23) becomes

$$u(r,0)=\sum_{j=1}^{\infty} C_jZ_j(r). \tag{26}$$

If $\lambda_{21}=0$, then $Z_1(r)=1$, $0\leqslant r<c$, and since $Z_j(r)$, $j=1, 2, \cdots$ form a complete[8] and orthogonal set with respect to the weight function r in the interval $0\leqslant r<c$,

$$C_1=U_0b^2/c^2. \tag{27}$$

For $j>1$

$$C_j=\left[U_0\int_0^b rZ_j(r)\,dr\right]\Big/\left[\int_0^c rZ_j(r)^2\,dr\right]$$

$$=\frac{U_0bJ_1(\mu\lambda_{2j}b)/\mu\lambda_{2j}}{(c^2/2)[A_jJ_0(\lambda_{2j}c)+B_jN_0(\lambda_{2j}c)]^2+[b^2(\mu^2-1)/2\mu^2][J_1(\mu\lambda_{2j}b)]^2},$$

and

$$u(r,t)/U_0=(b^2/c^2)$$

$$+\sum_{j=2}\frac{[bJ_1(\mu\lambda_{2j}b)/\mu\lambda_{2j}]Z_j(r)\exp[-K_2\lambda_{2j}^2t]}{(c^2/2)[A_jJ_0(\lambda_{2j}c)+B_jN_0(\lambda_{2j}c)]^2+[b^2(\mu^2-1)/2\mu^2][J_1(\mu\lambda_{2j}b)]^2}=\begin{cases} u_1(r,t)/U_0, & 0\leqslant r<b, \\ u_2(r,t)/U_0, & b<r<c. \end{cases} \tag{28}$$

[6] For the non-zero eigenvalues λ_{2j} the matrix associated with the determinant of Eq. (21) is of rank two. The rank is less than three because of Eq. (21). In the minor

$$\begin{vmatrix} J_0(\lambda_{2j}b) & N_0(\lambda_{2j}b) \\ \mu J_1(\lambda_{2j}b) & \mu N_1(\lambda_{2j}b) \end{vmatrix}=(-\mu/\lambda_{2j})\begin{vmatrix} J_0(\lambda_{2j}b) & N_0(\lambda_{2j}b) \\ dJ_0(\lambda_{2j}r)/dr|_{r=b} & dN_0(\lambda_{2j}r)/dr|_{r=b} \end{vmatrix}$$

the first factor is non-zero and the last term cannot equal zero since it is the Wronskian for the two independent solutions $J_0(\lambda_{2j}r)$ and $N_0(\lambda_{2j}r)$ of Bessel's equation of order zero evaluated at the non-zero value b. [See E. C. Ince, *Ordinary Differential Equations* (Dover Publications, Inc., New York, 1944), p. 118.] Since the matrix is of rank two for the non-zero solutions λ_{2j} of Eq. (21), the result may be normalized by making $A_{\mu j}=1$ so that A_2 and B_2 are uniquely determined.

[7] For verification of solutions of differential equations see reference 1; also R. V. Churchill, Math. Ann. **114**, 591 (1937).

[8] The completeness of the family of functions has not been proved in this paper.

HEAT FLOW THROUGH COMPOSITE SLABS OF FINITE WIDTH

If $(c-b)\ll b$ then the composite cylinder may be approximated by an infinite slab of width b from which heat flow occurs into an infinite slab of width $(c-b)$. In this case the boundary value problem may be formulated as follows:

$$\left.\begin{aligned} \partial u_1/\partial t &= K_1(\partial^2 u_1/\partial x^2), \quad 0\leqslant x<b, \quad t>0,\\ \partial u_2/\partial t &= K_2(\partial^2 u_2/\partial x^2), \quad b<x<c, \quad t>0,\\ u_1(x,0) &= U_0, \quad 0\leqslant x<b,\\ u_2(x,0) &= 0, \quad b<x<c,\\ u_1(b-0,t) &= u_2(b+0,t), \quad t>0,\\ K_1[\partial u_1(b-0,t)/\partial x] &= K_2[\partial u_2(b+0,t)/\partial x], \quad t>0. \end{aligned}\right\} \tag{29}$$

The solution of (29) is

$$u(x,t)=bU_0/c+\sum_{j=1}^{\infty} C_j Z_j \exp[-K_2\lambda_{2j}^2 t]=\begin{cases} u_1(x,t), & 0\leqslant x<b,\\ u_2(x,t), & b<x<c, \end{cases} \tag{30}$$

where

$$Z_j=\begin{cases} A_{\mu j}\cos\mu\lambda_{2j}x, & 0\leqslant x<b,\\ A_j\cos\lambda_{2j}x+B_j\sin\lambda_{2j}x, & b<x<c,\\ \text{provided } \lambda_{2j}\neq 0, \end{cases} \tag{31}$$

and

$$\begin{vmatrix} \cos\mu\lambda_{2j}b & \cos\lambda_{2j}b & \sin\lambda_{2j}b\\ -\sin\mu\lambda_{2j}b & -\mu\sin\lambda_{2j}b & \mu\cos\lambda_{2j}b\\ 0 & \sin\lambda_{2j}c & -\cos\lambda_{2j}c \end{vmatrix}=0. \tag{32}$$

Equation (32) reduces to

$$\mu\cos\mu\lambda_{2j}b\sin\lambda_{2j}(c-b)+\sin\mu\lambda_{2j}b\cos\lambda_{2j}(c-b)=0,$$

which becomes

$$\mu\tan\lambda_{2j}(c-b)+\tan\mu\lambda_{2j}b=0 \quad \text{if} \quad \cos\mu\lambda_{2j}b\cos\lambda_{2j}(c-b)\neq 0. \tag{33}$$

The coefficients A_j, B_j, and $A_{\mu j}$ are given by the relations leading to (32):

$$\left.\begin{aligned} A_j\sin\lambda_{2j}c-B_j\cos\lambda_{2j}c&=0,\\ A_{\mu j}\cos\mu\lambda_{2j}b&=A_j\cos\lambda_{2j}b+B_j\sin\lambda_{2j}b,\\ A_{\mu j}\sin\mu\lambda_{2j}b&=\mu A_j\sin\lambda_{2j}b-\mu B_j\cos\lambda_{2j}b. \end{aligned}\right\} \tag{34}$$

The coefficients C_j in Eq. (30) are determined by the equation

$$C_j=\frac{[U_0\sin\mu\lambda_{2j}b]/\mu\lambda_{2j}}{(bA_{\mu j}^2/2)+(c-b)(A_j^2+B_j^2)/2}. \tag{35}$$

HEAT FLOW THROUGH COMPOSITE SLABS OF INFINITE EXTENT

Heat flow through a composite cylinder may be further simplified if the circular cylinder is so large that it may be represented, as a first approximation, by a slab of infinite width. The boundary

value problem becomes now

$$\left.\begin{aligned}
\partial u_2(x,t)/\partial t &= K_2\{\partial^2 u_2(x,t)/\partial x^2\}, \quad b \leqslant x < c, \quad t>0,\\
\partial u_1(x,t)/\partial t &= K_1\{\partial^2 u_1(x,t)/\partial x^2\}, \quad x<b, \quad t>0,\\
u_2(x,0) &= 0, \quad b<x<c,\\
u_1(x,0) &= U_0, \quad x<b,\\
\partial u_2(c-0,t)/\partial x &= 0, \quad t>0,\\
u_1(b-0,t) &= u_2(b+0,t), \quad t>0,\\
K_1\{\partial u_1(b-0,t)/\partial x\} &= K_2\{\partial u_2(b+0,t)/\partial x\}, \quad t>0,\\
\lim_{x\to-\infty} u_1(x,t) &= U_0.
\end{aligned}\right\} \tag{36}$$

By some modification of the material in Churchill[9] it is found that

$$\left.\begin{aligned}
u_2(x,t) = [U_0(1-\lambda)/2]\sum_{n=0}^{\infty}\lambda^n[&\operatorname{erfc}\{[(2n+1)(c-b)-(c-x)]/2(K_2t)^{\frac{1}{2}}\}\\
&+\operatorname{erfc}\{[(2n+1)(c-b)+(c-x)]/2(K_2t)^{\frac{1}{2}}\}], \quad b<x<c, \quad t>0,
\end{aligned}\right\} \tag{37}$$

and

$$\left.\begin{aligned}
u_1(x,t) = U_0-[U_0(1+\lambda)/2]\sum_{n=0}^{\infty}\lambda^n[&\operatorname{erfc}\{[2n(c-b)+\mu(b-x)]/2(K_2t)^{\frac{1}{2}}\}\\
&-\operatorname{erfc}\{[(2n+2)(c-b)+\mu(b-x)]/2(K_2t)^{\frac{1}{2}}\}], \quad x<b, \quad t>0,
\end{aligned}\right\} \tag{37}$$

where

$$\operatorname{erfc}x = 1-\operatorname{erf}x = (2/\pi^{\frac{1}{2}})\int_x^{\infty} e^{-y^2}dy,$$

$$\mu = (K_2/K_1)^{\frac{1}{2}},$$

and

$$\lambda = [K_2K_1^{\frac{1}{2}}-K_1K_2^{\frac{1}{2}}]/[K_2K_1^{\frac{1}{2}}+K_1K_2^{\frac{1}{2}}].$$

If the radius of the cylindrical core of the composite cylinder is sufficiently large, and if the cylindrical shell is sufficiently wide, then the following approximate treatment may be made for the flow of heat through a composite cylinder:

$$\left.\begin{aligned}
\partial u_1(x,t)/\partial t &= K_1[\partial^2 u_1(x,t)/\partial x^2], \quad x<b, \quad t>0,\\
\partial u_2(x,t)/\partial t &= K_2[\partial^2 u_2(x,t)/\partial x^2], \quad b<x, \quad t>0,\\
u_1(x,0) &= U_0, \quad x<b,\\
u_2(x,0) &= 0, \quad b<x,\\
u_1(b-0,t) &= u_2(b+0,t), \quad 0<t,\\
K_1[\partial u_1(b-0,t)/\partial x] &= K_2[\partial u_2(b+0,t)/\partial x], \quad 0<t,\\
\lim_{x\to-\infty} u_1(x,t) &= U_0; \quad \lim_{x\to+\infty} u_2(x,t) = 0.
\end{aligned}\right\} \tag{38}$$

By some change of the material in Churchill[10] it may be shown that the solution of Eq. (38) is

$$\left.\begin{aligned}
u_1(x,t) &= [U_0/(1+\mu)][1+\mu\operatorname{erf}\{(b-x)/2(K_1t)^{\frac{1}{2}}\}], \quad x<b\\
u_2(x,t) &= [U_0/(1+\mu)][\operatorname{erfc}\{(x-b)/2(K_2t)^{\frac{1}{2}}\}], \quad x>b.
\end{aligned}\right\} \tag{39}$$

[9] R. V. Churchill, *Modern Operational Mathematics in Engineering* (McGraw-Hill Book Company, New York, 1944), pp. 122–124.

[10] Reference 9, pp. 124–125.

APPENDIX

Evaluation of Integrals

Orthogonality of the functions $Z_j(r)$ in the interval $0 \leqslant r < c$ with respect to the weight function r may be shown as follows: For $k \neq j$,

$$\int_0^{c-} rZ_jZ_k dr = \int_0^{b} rZ_{1j}(\mu\lambda_{2j}r)Z_{1k}(\mu\lambda_{2k}r)dr + \int_b^{c} rZ_{2j}(\lambda_{2j}r)Z_{2k}(\lambda_{2k}r)dr. \tag{A-1}$$

Integration of Eq. (A-1) and utilization of the definitions of Z_{1j} and Z_{2j} leads to the desired results:

$$\int_0^{c-} rZ_jZ_k dr = [1/\mu^2(\lambda_{2j}^2-\lambda_{2k}^2)][rZ_{1j}(\mu\lambda_{2j}r)\{dZ_{1k}(\mu\lambda_{2k}r)/dr\}_{r=0}{}^{r=b-} - rZ_{1k}(\mu\lambda_{2k}r)\{dZ_{1j}(\mu\lambda_{2j}r)/dr\}_{r=0}{}^{r=b-}]$$
$$+(1/[\lambda_{2j}^2-\lambda_{2k}^2])[rZ_{2j}(\lambda_{2j}r)\{dZ_{2k}(\lambda_{2k}r)/dr\}_{r=b+}{}^{r=c-} - rZ_{2k}(\lambda_{2k}r)\{dZ_{2j}(\lambda_{2j}r)/dr\}_{r=b+}{}^{r=c-}]$$
$$=(1/[\lambda_{2j}^2-\lambda_{2k}^2])\{rZ_{2j}(dZ_{2k}/dr) - rZ_{2k}(dZ_{2j}/dr)\}_{r=c-}.$$

Therefore,

$$\int_0^{c-} rZ_jZ_k dr = 0, \quad j \neq k, \tag{24}$$

where use has been made of Eqs. (10), (19), and (20).

Similarly,

$$2\lambda_{2j}^2\int_0^{c-} rZ_j^2 dr = (1/\mu^2)[\{rdZ_{1j}/dr\}^2+\mu^2\lambda_{2j}^2r^2Z_{1j}^2]_{r=0}{}^{r=b-} + [\{r(dZ_{2j}/dr)\}^2+\lambda_{2j}^2r^2Z_{2j}^2]_{r=b+}{}^{r=c-}.$$

Substitution of the limits into the preceding relation leads to the result

$$2\lambda_{2j}^2\int_0^{c-} rZ_j^2 dr = (1/\mu^2)[b^2(dZ_{1j}/dr)_{r=b}{}^2+\mu^2\lambda_{2j}^2b^2Z_{1j}^2(\mu\lambda_{2j}b)]$$
$$+\lambda_{2j}^2c^2Z_{2j}^2(\lambda_{2j}c)+c^2(dZ_{2j}/dr)_{r=c}{}^2-b^2(dZ_{2j}/dr)_{r=b}{}^2-\lambda_{2j}^2b^2Z_{2j}^2(\lambda_{2j}b).$$

From Eq. (10) it can be seen that

$$dZ_{2j}(\lambda_{2j}r)/dr\,|_{r=c}=0.$$

From Eq. (19)

$$Z_{1j}(\mu\lambda_{2j}b)=Z_{2j}(\lambda_{2j}b).$$

Hence,

$$2\lambda_{2j}^2\int_0^{c-} rZ_j^2 dr = \lambda_{2j}^2c^2Z_{2j}^2(\lambda_{2j}c)+(\mu^2-1)b^2[dZ_{2j}(\lambda_{2j}r)/dr]_{r=b}{}^2. \tag{A-2}$$

Equation (25) follows immediately from Eq. (A-2).

THE JOURNAL OF CHEMICAL PHYSICS VOLUME 15, NUMBER 8 AUGUST, 1947

Dynamics of a Square Lattice

I. Frequency Spectrum

ELLIOTT W. MONTROLL
Division of Research in the Natural Sciences, University of Pittsburgh, Pittsburgh 13, Pennsylvania
(Received October 21, 1946)

The distribution of frequencies of normal modes of vibration of a monatomic square lattice is obtained as a function of the force constants of the lattice. Since the forces between pairs of atoms in the lattice are short ranged, interactions between all atoms, other than nearest and next nearest neighbors, are neglected.

Two constants, α and γ, are used to describe the lattice. α is a force constant derived from the interaction of nearest neighbors, and γ is that derived from the interaction of next nearest neighbors.

According to the Debye continuum theory the frequency spectrum, or density of normal modes, should be a linear function of the frequency. In the Born-Karman atomic model used in the present paper it is shown that this is only the case at very low frequencies and that there actually exist two sharp infinities in the frequency spectrum.

We define $g(\nu)$ so that $g(\nu)d\nu$ is the number of normal modes of vibration with frequencies between ν and $\nu+d\nu$. A closed expression involving complete elliptic integrals is obtained for $g(\nu)$ when $\tau=[1+(\alpha/2\gamma)]^{-1}=\frac{1}{3}$. For general values of $\tau<\frac{1}{2}$, $g(\nu)$ is shown to have the following properties:

(a) The largest frequency, ν_L, occurs at

$$\nu_L=[(4\alpha+8\gamma)/4\pi^2M]^{\frac{1}{2}},$$

where M = mass of each atom.

(b) There is an infinity in $g(\nu)$ at $\nu=\nu_L\tau^{\frac{1}{2}}$.

(c) The second infinity is at $\nu=\nu_L(1-\tau)^{\frac{1}{2}}$ if $\tau<\frac{1}{3}$, and $\nu=\nu_L(1+3\tau)/4\tau^{\frac{1}{2}}$ if $\tau>\frac{1}{3}$.

(d) As $\nu/\nu_L\to 0$, $g(\nu)$ is linear in ν.

A. INTRODUCTION

THERMODYNAMIC and optical properties of crystals are closely associated with the dynamics of the crystal lattice and in particular with the nature of the distribution of its frequencies of normal modes of vibration. At the beginning of this century Einstein[1] proposed that by quantizing the harmonic oscillations in a crystalline solid one could explain the observed temperature variations in its specific heat. Two diametrically opposite types of distributions of frequencies of normal modes were suggested for use in the detailed calculations needed in this explanation. Einstein suggested the very simple hypothesis that all atoms in a lattice vibrate independently of each other and with the same frequency about their equilibrium positions. This idea, and its extension by Lindeman and Nernst, states that there exist a small number of different modes of vibration in a crystal. Debye's[2] representation of a solid as an elastic continuum leads to the other type of distribution, namely a *continous* one.

Equations for thermodynamic quantities based on Debye's assumptions reproduce experimental data more accurately than do those derived from Einstein's hypothesis. In spite of this success the continuum model cannot be accepted as final because it is at variance with the proven periodic structure of a crystalline solid. Born and Karman[3] were the first to study the dynamics of lattices of periodically spaced particles. Even in the case of the one-dimensional lattices with which they dealt, it was clear that the continuous nature of the Debye frequency spectrum depended not only on the continuum model of the crystal but also on the large number of degrees of freedom and of the interaction between particles in the system.

In the generalization of the Born-Karman analysis to two- and three-dimensional lattices the frequencies of the normal modes of vibration appear as roots of a set of characteristic determinants (whose number is of the same order as the number of degrees of freedom of the system). Recently two independent procedures have been used for the determination of the frequency spectrum from these determinants. In the first, developed by Blackman,[4] one obtains the roots

[1] A. Einstein, Ann. d. Physik **22**, 180, 800 (1907); **34**, 170, 590 (1911).
[2] P. Debye, Ann. d. Physik **39**, 789 (1912).
[3] M. Born and T. Karman, Physik. Zeits. **13**, 297 (1912).
[4] M. Blackman, Proc. Roy. Soc. **A148**, 384 (1935); **159**, 416 (1937).

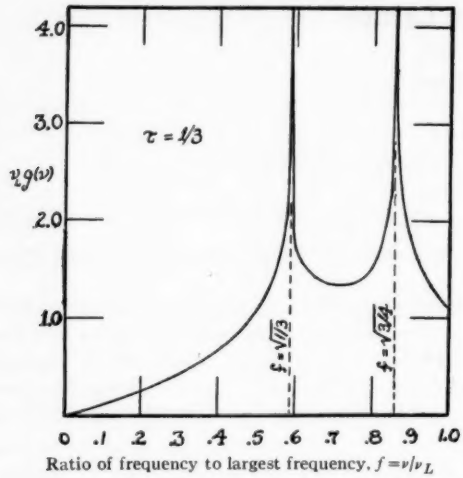

FIG. 1. A typical variation of density of normal modes with frequency in a two-dimensional lattice.

of a large number of the determinants and assumes that the distribution of these roots is representative of the complete frequency spectrum. The accuracy of this procedure depends on the size of the sample of roots, and is therefore limited by the computational efforts one is willing to expend. In the second method, developed by the author,[5] one rigorously obtains a number of moments of the frequency spectrum and finds the distribution function which has these moments. The accuracy of this method is also restricted by the amount of work a computer is willing to do, for it depends on the number of moments computed. The approximate frequency spectra, as obtained by both of these methods, are in good mutual agreement and retain the continuous character of the Debye spectrum. These spectra differ from Debye's by having several maxima.

Although a continuous spectrum is necessary to explain the thermodynamic behavior of a crystal, Raman and his collaborators[6] have condemned it as being inconsistent with optical measurements they have made. For example they feel that the observed fine structure of restrahlen is caused by a spectrum of discrete frequencies of the Einstein-Lindeman type. Born[7] has recently mentioned that the sharp restrahlen lines are due to the maxima in the frequency spectrum, and has promised a detailed discussion of this point in the case of rocksalt.

It is the purpose of the present paper to determine, by use of the Born-Karman model, the nature of the frequency spectrum of a two-dimensional square lattice. Although no real crystals are two dimensional, we feel that the results obtained in this study will lead to a better understanding of crystal dynamics in general. The continuous character of the Debye theory will remain, but at the same time several infinities will appear. These infinities would correspond to a sharp line spectrum (as demanded by the Indian investigators) superimposed on a continuous background.

In particular, we shall show that the density of normal modes, $g(\nu)$, at frequency ν has the following properties: (a) as $\nu \to 0$, $g(\nu) \sim a\nu$, as is also the case in the Debye theory of a two-dimensional crystal; (b) there are logarithmic infinities at frequencies ν_1 and ν_2. As $\nu \to \nu_j$ $(j=1, 2)$, $g(\nu) \sim b_j \log(1-\nu/\nu_j)$. a, b_j, and ν_j are independent of frequency but depend on the force constants between nearest and next nearest neighbors. A typical frequency-spectrum is plotted in Fig. 1.

As will be shown in a later paper, the frequencies ν_1 and ν_2 of infinite density would be optically active in ionic crystals and would, therefore, lead to a restrahlen spectrum of several sharp lines.

B. EQUATIONS OF MOTION

Let us consider a monatomic square lattice containing N lattice points in each direction and, therefore, a total of N^2 atoms. Also, let a be the distance between adjacent lattice points, and M the mass of each atom. A diagram of the lattice is given in Fig. 2. Where lattice points are identified by two parameters (l, m) both of which range over integral values between $-\frac{1}{2}N$ and $\frac{1}{2}N$. Components of the displacement of the atom (l, m) from its equilibrium position are designated by $u_{l,m}$ and $v_{l,m}$ in the directions indicated in the figure.

The kinetic energy of the lattice is

$$T=(M/2)\sum_{l,m=-\frac{1}{2}N}^{\frac{1}{2}N}(\dot{u}_{l,m}{}^2+\dot{v}_{l,m}{}^2). \qquad (1)$$

[5] E. Montroll, J. Chem. Phys. **10**, 219 (1942); E. Montroll and D. Peaslee **12**, 98 (1944).
[6] C. V. Raman, *et al.* 1941, "Symposium on papers on the quantum theory of x-ray reflections," Proc. Ind. Acad. Sci. **A14** (1941); **A15** (1942).
[7] M. Born, Rev. Mod. Phys. **17**, 245 (1945).

Assuming the existence of central forces only, we can write the potential energy function as

$$V(\mathbf{r}_1, \mathbf{r}_2, \cdots) = \sum_{i>j}^{N^2} V_{ij}(\mathbf{r}_i - \mathbf{r}_j). \tag{2}$$

If we restrict ourselves to situations in which the displacements of the atoms from their equilibrium positions are small, and if we choose the zero-point energy as the energy of the atoms in their equilibrium positions, the total potential energy of the system can be written as a quadratic form in the displacements from equilibrium:

$$V(\mathbf{r}_1, \mathbf{r}_2, \cdots) = \sum_{i>j=1}^{N^2} \tfrac{1}{2}(\xi_i - \xi_j)^2 c(a_{ij}). \tag{3}$$

Here ξ_i is the displacement vector of the atom from its equilibrium position, and $c(a_{ij})$ is a function the equilibrium distance between the ith and the jth atoms.

If we assume that the interatomic forces are sufficiently short ranged so that only those between nearest and next nearest neighbors are significant, $V(\mathbf{r}_1, \mathbf{r}_2 \cdots)$ becomes a function of the two parameters α and γ:

$$\alpha = c(a) \quad \text{and} \quad 2\gamma = c(a2^{\frac{1}{2}}). \tag{4}$$

a is the distance between nearest, and $a2^{\frac{1}{2}}$ that between next nearest neighbors. It is well known that the constants α and γ can be expressed in terms of the elastic constants for the lattice. In this notation:

$$V(\mathbf{r}_1, \mathbf{r}_2, \cdots) = \tfrac{1}{2}\alpha \sum_{\text{nearest}} (\xi_i - \xi_j)^2 + \gamma \sum_{\text{next nearest}} (\xi_i - \xi_j)^2.$$

Resolving the displacement vectors into components in the u and v directions (neglecting those components at right angles to the lines connecting pairs of atoms because they lead to higher powers of the displacements than the second) we can write the potential energy as

$$\begin{aligned} V(\mathbf{r}_1, \mathbf{r}_2 \cdots) = {} & \tfrac{1}{2}\alpha \sum_{l,m} \{(u_{l,m} - u_{l+1,m})^2 \\ & + (v_{l,m} - v_{l,m+1})^2\} + \tfrac{1}{2}\gamma \sum_{l,m} \\ & \times \{(u_{l,m} - u_{l+1,m+1} + v_{l,m} - v_{l+1,m+1})^2 \\ & + (u_{l,m} - u_{l+1,m-1} - v_{l,m} + v_{l+1,m-1})^2\}. \end{aligned} \tag{5}$$

Substituting (1) and (5) into Lagrange's equation

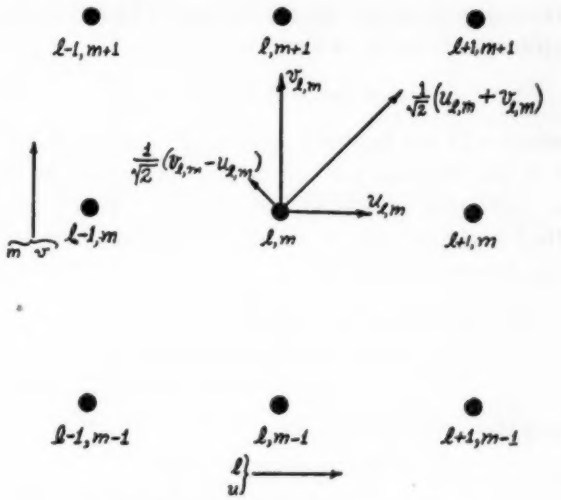

FIG. 2. Designation of lattice points in a two-dimensional lattice.

we obtain the equations of motion

$$\begin{aligned} -M\ddot{u}_{l,m} = {} & \alpha(2u_{l,m} - u_{l+1,m} - u_{l-1,m}) \\ & + \gamma(4u_{l,m} - u_{l+1,m+1} - u_{l+1,m-1} \\ & - u_{l-1,m-1} - u_{l-1,m+1} - v_{l+1,m+1} \\ & + v_{l+1,m-1} - v_{l-1,m-1} + v_{l-1,m+1}), \end{aligned} \tag{6a}$$

and

$$\begin{aligned} -M\frac{d^2 v_{l,m}}{dt^2} = {} & \alpha(2v_{l,m} - v_{l,m+1} - v_{l,m-1}) \\ & + \gamma(4v_{l,m} - v_{l+1,m+1} - v_{l-1,m+1} \\ & - v_{l-1,m-1} - v_{l+1,m-1} - u_{l+1,m+1} \\ & + u_{l-1,m+1} - u_{l-1,m-1} + v_{l+1,m-1}). \end{aligned} \tag{6b}$$

In a very large lattice the nature of the vibrations could be expected to be independent of the conditions imposed on its boundaries. For convenience we use the Born-Karman boundary conditions

$$\begin{aligned} u_{l,N+1} &= u_{l,1}, \quad u_{N+1,m} = u_{1,m}, \\ v_{l,N+1} &= v_{l,1}, \quad v_{N+1,m} = v_{1,m}. \end{aligned} \tag{7}$$

Physically these conditions describe a lattice on a large torus. They have been discussed in great detail elsewhere.[8]

Let us assume the existence of particular periodic solutions of (6a) and (6b):

$$u_{l,m} = u' \exp i(2\pi\nu t + l\varphi_1 + m\varphi_2), \tag{8a}$$

$$v_{l,m} = v' \exp i(2\pi\nu t + l\varphi_1 + m\varphi_2). \tag{8b}$$

[8] M. Born, Proc. London Phys. Soc. **54**, 362 (1942); W. Ledermann, Nature **151**, 197 (1943).

Here φ_1 and φ_2 are phase differences in successive atoms and can be written as

$$\varphi_j=2\pi a_j/N, \quad j=1, 2, \tag{9}$$

where a_j's are integers such that $-\frac{1}{2}N\leq a_j\leq\frac{1}{2}N$. ν is the frequency of vibration corresponding to a particular solution. Substitution of (8) into (6a) and (6b) yields the two equations for the amplitudes u' and v':

$$\begin{aligned}-4M\pi^2\nu^2u'+2\alpha u'(1-\cos\varphi_1)\\ +4\gamma u'(1-\cos\varphi_1\cos\varphi_2)\\ +4\gamma v'\sin\varphi_1\sin\varphi_2=0,\end{aligned} \tag{10a}$$

$$\begin{aligned}-4M\pi^2\nu^2v'+2\alpha v'(1-\cos\varphi_2)\\ +4\gamma v'(1-\cos\varphi_1\cos\varphi_2)\\ +4\gamma u'\sin\varphi_1\sin\varphi_2=0.\end{aligned} \tag{10b}$$

In order for solutions u' and v' to exist for these equations the determinant of the coefficients of u' and v' must vanish:

$$\begin{vmatrix}A(\varphi_1,\varphi_2)-4\pi^2\nu^2M & B(\varphi_1,\varphi_2)\\ B(\varphi_1,\varphi_2) & A(\varphi_2,\varphi_1)-4\pi^2\nu^2M\end{vmatrix}=0, \tag{11}$$

where

$$\begin{aligned}A(\varphi_i,\varphi_j)=2\alpha(1-\cos\varphi_i)\\ +4\gamma(1-\cos\varphi_i\cos\varphi_j),\end{aligned} \tag{11a}$$

$$B(\varphi_1,\varphi_2)=4\gamma\sin\varphi_1\sin\varphi_2. \tag{11b}$$

This equation has been derived previously by Blackman.[4] The possible frequencies of normal modes of vibration of the lattice are the positive roots of the characteristic determinants (11). All roots ν^2 are real because of the symmetry of the matrix of the determinant. Since both φ_1 and φ_2 extend over a set of N possible values there are $2N^2$ possible frequencies, one corresponding to each degree of freedom. Any vibration of the lattice can be expressed as a linear combination of its normal modes.

The largest possible frequency is determined by

$$\partial\nu/\partial\varphi_1=0 \quad \text{and} \quad \partial\nu/\partial\varphi_2=0.$$

It corresponds to the points $(\pi, 0)$, $(0, \pi)$, $(-\pi, 0)$ and $(0, -\pi)$ and has the value

$$\nu_L=[(4\alpha+8\gamma)/4\pi^2M]^{\frac{1}{2}}. \tag{12}$$

A new parameter τ defined by

$$\tau=8\gamma/4\pi^2M\nu_L^2 \tag{13}$$

will appear in the future discussion. Its value is restricted to numbers between 0 and 1. The restriction is clear if τ is written as

$$\tau=8\gamma/(8\gamma+4\alpha)=1/[1+(\alpha/2\gamma)]. \tag{13a}$$

As $\alpha/\gamma\to0$, $\tau\to1$ and as $\alpha/\gamma\to\infty$, $\tau\to0$. In terms of τ

$$4\alpha=4\pi^2M\nu_L^2-8\gamma=4\pi^2M\nu_L^2(1-\tau),$$

and the characteristic determinant becomes

$$\begin{vmatrix}(1-\tau)(1-c_1)+\tau(1-c_1c_2)-2f^2 & \tau s_1s_2\\ \tau s_1s_2 & (1-\tau)(1-c_2)+\tau(1-c_1c_2)-2f^2\end{vmatrix}=0, \tag{14}$$

where the new symbols c_j, s_j, and f are defined by

$$c_j=\cos\varphi_j=\cos(2\pi a_j/N), \tag{14a}$$

$$s_j=\sin\varphi_j=\sin(2\pi a_j/N), \tag{14b}$$

$$f=\nu/\nu_L. \tag{14c}$$

Expanding the determinant, we obtain

$$\begin{aligned}4f^4-2f^2\{2\tau(1-c_1c_2)+(1-\tau)(2-c_1-c_2)\}\\ +(1-\tau)^2(1-c_1)(1-c_2)\\ +\tau(1-\tau)(1-c_1c_2)(2-c_1-c_2)\\ +\tau^2(c_1-c_2)^2=0.\end{aligned} \tag{15}$$

Solving for the square of the frequency

$$\begin{aligned}f^2=(\nu/\nu_L)^2=\tfrac{1}{4}\{2\tau(1-c_1c_2)+(1-\tau)(2-c_1-c_2)\}\\ \pm\tfrac{1}{4}\{4\tau^2(c_2^2-1)(c_1^2-1)\\ +(1-\tau)^2(c_2-c_1)^2\}^{\frac{1}{2}}.\end{aligned} \tag{16}$$

The branch of frequencies which results from the positive choice of the square root term will henceforth be designated as the f_+ branch of the spectrum, and that originating from the negative choice as the f_- branch. For a particular lattice, the parameters α and γ have definite values as do τ and ν_L^2. Therefore, by substituting all N^2 combinations of φ_1 and φ_2 into (16) one can determine one by one all the $2N^2$ frequencies of the normal modes of vibration of the lattice. However, lattices of interest in molecular and atomic problems contain so many lattice points, $0(10^8)$ in each direction, that a direct application of (16) is not feasible. Fortunately in statistical mechanics of lattices there is little interest in particular frequencies, but instead one requires

the density of frequencies in any small frequency range.

C. GENERAL ASPECTS OF FREQUENCY SPECTRUM

Each branch of frequencies (16) of the characteristic Eq. (15) is a relation between f, φ_1, and φ_2 which can be expressed graphically in (φ_1, φ_2) space (from (9) both φ_1 and φ_2 are limited to values between $-\pi$ and π). For various constant values of f one obtains a family of curves in this space. A particular schematic curve from the family is given in Fig. 3. The space in the square bounded by the lines $\varphi_1=\pi$, $\varphi_1=-\pi$, $\varphi_2=\pi$, and $\varphi_2=-\pi$ is divided into at least two parts by each curve of the family. At any point of the set

$$S=\{(2\pi a_1/N),\ (2\pi a_2/N)\};$$

in this space one finds a frequency which lies on one of the curves of constant f. If the curve

$$f=f_1=F(\varphi_1,\ \varphi_2)=\text{constant} \tag{17}$$

passes through s_1 points of the set S, there are s_1 normal modes with frequency $f_1\nu_L$.

The curve (17) separates the points of the set S into two sub-sets, one of which, S_A, corresponds to those frequencies less than $f_1\nu_L$ and the other, S_B, to those with frequencies greater than $f_1\nu_L$. From (15) we find that in both branches the point (0, 0) corresponds to the frequency $\nu=0$. Therefore, (0, 0) is always in the sub-set S_A, and S_A must be the set which lies interior to the curve (17).

The number of frequencies less than $\nu=f\nu_L$ in one branch is then given by the sum

$$N(f\nu_L)=\sum_{(\varphi_1,\ \varphi_2)\ \subset\ S_A}\sum 1, \tag{18}$$

where the summation extends over all points of S interior to the curve $f=F(\varphi_1, \varphi_2)=$constant. As the total number of points in the lattice increases indefinitely, the points of the set S in (φ_1, φ_2) space become increasingly denser, and in the limit, (18) can be written as

$$\lim_{N\to\infty} N_{\pm}(f\nu_L)/N^2=(1/4\pi^2)\iint_{F_{\pm}(\varphi_1,\ \varphi_2)\le f} d\varphi_1 d\varphi_2. \tag{19}$$

The fraction of frequencies less than $\nu=f\nu_L$ in one

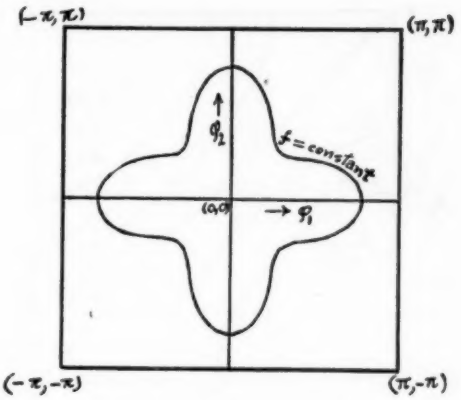

FIG. 3. Typical curve of constant frequency.

frequency branch is the fraction of the area in (φ_1, φ_2) space interior to the curve $F_{\pm}(\varphi_1, \varphi_2)=f$. The subscript "+" will be used to denote the branch f_+, and "−" the branch f_-.

The determination of the statistical mechanical properties of an atomic lattice depends on a knowledge of the frequency distribution function $g(\nu)$, which is defined so that $g(\nu)d\nu$ is the fraction of frequencies between ν and $\nu+d\nu$. $g_{\pm}(\nu)d\nu$ for one branch is related to the fraction of frequencies less than ν in that branch by the equation

$$g_{\pm}(\nu)=\lim_{N\to\infty}\frac{\partial}{\partial\nu}\left\{\frac{N_{\pm}(f\nu_L)}{N^2}\right\}$$

$$=\frac{1}{4\pi^2\nu_L}\frac{\partial}{\partial f}\iint_{F_{\pm}(\varphi_1,\ \varphi_2)\le f} d\varphi_1 d\varphi_2. \tag{20}$$

Since for the combination of both branches, the number of frequencies less than f is

$$N(f\nu_L)=N_+(f\nu_L)+N_-(f\nu_L),$$

the fraction of all frequencies less than f is

$$N(f\nu_L)/2N^2=\tfrac{1}{2}\{N_+(f\nu_L)/N^2+N_-(f\nu_L)/N^2\}.$$

Therefore, the complete frequency spectrum is given by

$$g(f\nu_L)=\lim_{N\to\infty}\frac{\partial}{\partial\nu}\left\{\frac{N(f\nu_L)}{2N^2}\right\}$$

$$=\tfrac{1}{2}\{g_+(f\nu_L)+g_-(f\nu_L)\}. \tag{20a}$$

Blackman's numerical method of approximating the frequency spectrum is based on (19) and (20).

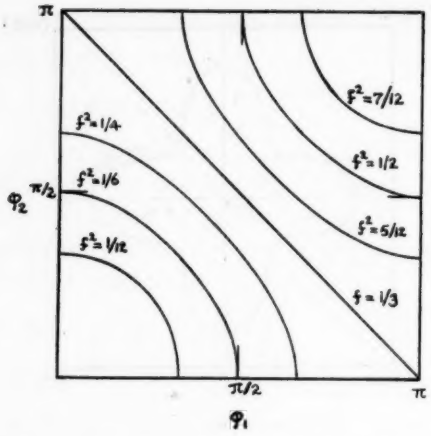

FIG. 4. Curves of constant frequency in f_- branch, $\tau=\frac{1}{3}$.

D. FREQUENCY SPECTRUM WHEN $\tau=\frac{1}{3}$

We shall first derive an expression for the frequency spectrum when the lattice parameters are such as to make $\tau=\frac{1}{3}$. This initial choice of τ is made because it leads to a simplification of the characteristic equation and an easily obtainable closed expression for the frequency distribution function, $g(\nu)$. This value of τ corresponds to a lattice with elastic isotropy.

In this case the characteristic equation factors immediately into two branches of frequencies:

$$f_+^2=\tfrac{1}{6}\{2(1-c_1c_2)+2-c_1-c_2\},$$
$$f_-^2=\tfrac{1}{6}(2-c_1-c_2).$$

The largest frequency of the f_+ branch, $f_+(\text{max.})$ occurs in the first quadrant of (φ_1, φ_2) space at $(\varphi_1, \varphi_2)=(\pi, 0)$ or $(0, \pi)$ and that of the f_- branch at (π, π), thus:

$$f_+^2(\text{max.})=1, \quad f_-^2(\text{max.})=\tfrac{2}{3}.$$

We shall now show that the frequency distribution of each branch can be expressed in closed form as complete elliptic integrals of the first kind.

Since each quadrant in (φ_1, φ_2) space contributes equally to the integrals in (19) and (20), we replace (19) by

$$\lim_{N\to\infty} N_\pm(f\nu_L)/N^2=\pi^{-2}\iint_{F_\pm(\varphi_1,\varphi_2)\le f} d\varphi_1 d\varphi_2, \quad (19a)$$

and (20) by

$$g_\pm(\nu)=(1/\pi^2\nu_L)(\partial/\partial f)\iint_{F_\pm(\varphi_1,\varphi_2)\le f} d\varphi_1 d\varphi_2, \quad (19b)$$

where the integrations extend over only that part of the *first* quadrant where $F_\pm(\varphi_1, \varphi_2)\le f$.

1. f_- Branch

Curves of constant f are plotted in (φ_1, φ_2) space in Fig. (4). Analytically these curves have the equation

$$\varphi_2=\cos^{-1}(2-\cos\varphi_1-6f^2). \quad (21)$$

When $f^2\le\frac{1}{3}$, the intersection points of the curves with the φ_1 and φ_2 axes are, respectively,

$$\varphi_1=\cos^{-1}(1-6f^2), \quad (21a)$$

$$\varphi_2=\cos^{-1}(1-6f^2). \quad (21b)$$

Then, according to (19a) the fraction of frequencies between 0 and $f\nu_L$, when $f^2\le\frac{1}{3}$, is

$$\mathbf{F}_-(f)=\lim_{N\to\infty} N_-(f\nu_L)/N^2$$
$$=\pi^{-2}\int_0^{\cos^{-1}(1-6f^2)}\int_0^{\cos^{-1}(2-\cos\varphi_1-6f^2)} d\varphi_1 d\varphi_2,$$
$$=\pi^{-2}\int_0^{\cos^{-1}(1-6f^2)}\cos^{-1}(2-\cos\varphi_1-6f^2)d\varphi_1,$$

and from (19b)

$$\nu_L g_-(f\nu_L)=12f\pi^{-2}\int_0^{\cos^{-1}(1-6f^2)} \times[1-(2-\cos\varphi_1-6f^2)^2]^{-\frac{1}{2}}d\varphi. \quad (22)$$

Letting

$$y-3f^2+1=\cos\varphi_1$$

we transform this integral into

$$\nu_L g_-(f\nu_L)=(12f/\pi^2)\int_{-3f^2}^{3f^2}\{[y^2-(3f^2)^2] \times[y^2-(2-3f^2)^2]\}^{-\frac{1}{2}}dy$$
$$=(24f/\pi^2)\int_0^{3f^2}\{[y^2-(3f^2)^2] \times[y^2-(2-3f^2)^2]\}^{-\frac{1}{2}}dy;$$

and letting $y=3f^2x$, we express $\nu_L g_-(f\nu_L)$ in the form of the complete elliptic integral of the first kind:

$$\nu_L g_-(f\nu_L)=\frac{24f}{(2-3f^2)\pi^2} \times\int_0^1\frac{dx}{[(1-x^2)(1-k^2x^2)]^{\frac{1}{2}}}, \quad (23)$$

where

$$k=3f^2/(2-3f^2). \tag{23a}$$

In the usual notation of elliptic integrals[9] the integral component of (23) is denoted by $K(k)$. Therefore,

$$\nu_L g_-(f\nu_L) = [24f/(2-3f^2)\pi^2]K[3f^2/(2-3f^2)]. \tag{24}$$

When $f^2>\frac{1}{3}$, the curve (21) intersects the lines $\varphi_1=\pi$ and $\varphi_2=\pi$ before it intersects the φ_1 and φ_2 axes; therefore, (22) is no longer valid. Since the points of intersection of (21) with $\varphi_1=\pi$ and $\varphi_2=\pi$ are, respectively,

$$\varphi_1=\cos^{-1}(3-6f^2), \quad \varphi_2=\cos^{-1}(3-6f^2),$$

when $f^2>\frac{1}{3}$:

$$\mathrm{F}_-(f)=\lim_{N\to\infty}\{N_-(f\nu_L)/N^2\}=\frac{1}{\pi^2}$$

$$\times\left\{\pi^2-\int_{\cos^{-1}(3-6f^2)}^{\pi}d\varphi_1\int_{\cos^{-1}(2-\cos\varphi_1-6f^2)}^{\pi}d\varphi_2\right\}$$

$$=\pi^{-2}\left\{\pi\cos^{-1}(3-6f^2)\right.$$

$$\left.+\int_{\cos^{-1}(3-6f^2)}^{\pi}\cos^{-1}(2-\cos\varphi_1-6f^2)d\varphi_1\right\},$$

and

$$\nu_L g_-(f\nu_L)=12f\pi^{-2}\int_{\cos^{-1}(3-6f^2)}^{\pi}$$

$$[1-(2-\cos\varphi-6f^2)^2]^{-\frac{1}{2}}d\varphi.$$

Letting $x=(2-3f^2)[\cos\varphi_1+3f^2-1]$, the integral reduces to

$$\nu_L g_-(f\nu_L)=(24f/3f^2\pi^2)$$

$$\times\int_0^1[(1-x^2)(1-k^2x^2)]^{-\frac{1}{2}}dx,$$

where $k=(2-3f^2)/3f^2$. Thus, when $f^2>\frac{1}{3}$,

$$\nu_L g_-(f\nu_L)=(8/f\pi^2)K((2-3f^2)/3f^2). \tag{24a}$$

2. f_+ Branch

Curves of constant f are plotted in (φ_1, φ_2) space in Fig. 5. Analytically, they are described by

$$\varphi_2=\cos^{-1}\{(4-6f^2-\cos\varphi_1)/(2\cos\varphi_1+1)\}. \tag{25}$$

In each of the three ranges

i. $0\le f^2\le\frac{2}{3}$,
ii. $\frac{2}{3}<f^2\le\frac{3}{4}$,
iii. $\frac{3}{4}<f^2\le 1$,

this curve has a different qualitative behavior (Fig. 5). Therefore an individual treatment is required for each range.

Range i. $0\le f^2\le\frac{2}{3}$. In this range the curves $f^2=$constant intersect the φ_1 and φ_2 axes at, respectively,

$$\varphi_1=\cos^{-1}(1-2f^2), \quad \varphi_2=\cos^{-1}(1-2f^2).$$

Thus,

$$F_+(f)=\lim_{N\to\infty}\{N_+(f\nu_L)/N^2\}$$

$$=\pi^{-2}\int_0^{\cos^{-1}(1-2f^2)}d\varphi_1\int_0^{\varphi_2(\varphi_1)}d\varphi_2,$$

where

$$\varphi_2(\varphi_1)=\cos^{-1}[(4-6f^2-c_1)/(2c_1+1)].$$

The integration with respect to φ_2 can be performed immediately:

$$F_+(f)=\pi^{-2}\int_0^{\cos^{-1}(1-2f^2)}$$

$$\times\cos^{-1}[(4-6f^2-\cos\varphi_1)/(2\cos\varphi_1+1)]d\varphi_1,$$

and

$$\nu_L g_+(f\nu_L)=12f\pi^{-2}\int_0^{\cos^{-1}(1-2f^2)}$$

$$\times[(2\cos\varphi+1)^2-(4-6f^2-\cos\varphi)^2]^{-\frac{1}{2}}d\varphi.$$

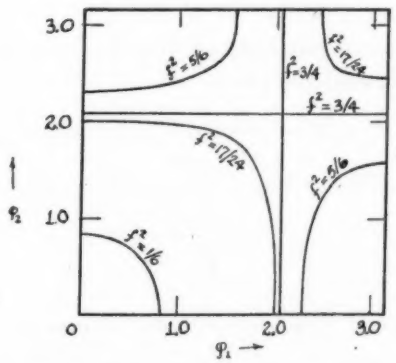

FIG. 5. Curves of constant frequency in f_+ branch, $r=\frac{1}{3}$.

[9] Whittaker and Watson, *Modern Analysis* (Cambridge University Press, London, 1935), Fourth Ed., p. 498.

Letting $u=\cos\varphi$ this reduces to

$$\nu_L g_+(f\nu_L)=(12f\pi^{-2})\int_{1-2f^2}^{1}\times[(1-u^2)(u+5-6f^2)(u-1+2f^2)]^{-\frac{1}{2}}du.$$

The transformation of this integral to the standare elliptic integral form is somewhat more complicated than in the f_- branch, so we shall refer to an integral table.[10] The zeros of the denominator appear in the order

$$1>(1-2f^2)>-1>6f^2-1.$$

Therefore, formula (551) of Pierce's tables applies, and

$$\nu_L g_+(f\nu_L)=\frac{4f}{\pi^2[1-(4/3)f^2]^{\frac{1}{2}}}K\left(f\left[\frac{2-3f^2}{3-4f^2}\right]^{\frac{1}{2}}\right). \tag{26}$$

Range ii. $\frac{2}{3}<f^2\leq\frac{3}{4}$. In this range of f values two regions of the square in Fig. 5 contribute to $N_+(f\nu_L)$. The first, as in range i, is in the neighborhood of the origin, and the fraction of roots in this range is

$$\lim_{N\to\infty}[N_+^{(1)}(f\nu_L)/N^2]=\pi^{-2}\int_0^{\cos^{-1}(1-2f^2)}\times\cos^{-1}\left(\frac{4-6f^2-\cos\varphi_1}{2\cos\varphi_1+1}\right)d\varphi_1. \tag{27a}$$

The other contribution comes from the region between the curve

$$\cos\varphi_2=(4-6f^2-\cos\varphi_1)/(2\cos\varphi_1+1),$$

and the corner at (π,π). For convenience let us transform the point (π,π) into the origin by the transformation

$$\vartheta_1=\pi-\varphi_1,\quad \vartheta_2=\pi-\varphi_2.$$

Then we are required to find the area between the origin and the curve

$$\cos\vartheta_2=(4-6f^2+\cos\vartheta_1)/(2\cos\vartheta_1-1).$$

When $\vartheta_2=0$, we have $\vartheta_1=\cos^{-1}(5-6f^2)$, so that

$$\lim N_+^{(2)}(f\nu_L)/N^2=\pi^{-2}\int_0^{\cos^{-1}(5-6f^2)}\times\cos^{-1}[(4-6f^2+\cos\vartheta_1)/(2\cos\vartheta_1-1)]d\vartheta_1.$$

[10] B. O. Pierce, *A Short Table of Integrals* (Ginn and Company, New York, 1929), Third Ed., p. 66.

The contribution to the frequency spectrum of the first region (after making the transformation $u=\cos\vartheta$) is

$$\nu_L g_+^{(1)}(f\nu_L)=12f\pi^{-2}3^{-\frac{1}{2}}\times\int_{1-2f^2}^{1}\{(1-u)(u+1)[u-(6f^2-5)]\times[u-(1-2f^2)]\}^{-\frac{1}{2}}du,$$

and that of the second region is

$$\nu_L g_+^{(2)}(f\nu_L)=12f\pi^{-2}3^{-\frac{1}{2}}\times\int_{5-6f^2}^{1}\{(1-u)(1+u)[u-(2f^2-1)]\times[u-(5-6f^2)]\}^{-\frac{1}{2}}du.$$

Both of these integrals are of the type (551) in Pierce's tables and have the value

$$\frac{4f}{\pi^2(1-f^2)}K\left(\frac{f}{1-f^2}(f^2-\tfrac{2}{3})^{\frac{1}{2}}\right).$$

Thus, when $\frac{2}{3}<f^2\leq\frac{3}{4}$

$$\nu_L g_+(f\nu_L)=\nu_L\{g_+^{(1)}(f\nu_L)+g_+^{(2)}(f\nu_L)\}=[8f/\pi^2(1-f^2)]K[(f/1-f^2)(f^2-\tfrac{2}{3})^{\frac{1}{2}}]. \tag{28}$$

Range iii. $\frac{3}{4}<f^2\leq 1$. In this range the fraction of frequencies less than $f\nu_L$ is $(1/\pi^2)$ (area of C) or, $(1/\pi^2)(\pi^2-A-B)$. Since $A=B$, it is also $(\pi^2-2A)/\pi^2$. If we introduce the new variables $\vartheta_1=\pi-\varphi_1$, and $\vartheta_2=\varphi_2$, the region B is transformed to the neighborhood of the origin and is bounded by the curve

$$\cos\vartheta_2=(4-6f^2+\cos\vartheta_1)/(1-2\cos\vartheta_1).$$

Thus

$$\lim_{N\to\infty}N_+(f\nu_L)/N^2=\pi^{-2}\{\pi^2-2\int_0^{\cos^{-1}(2f^2-1)}\times\cos^{-1}(4-6f^2+\cos\vartheta_1/1-2\cos\vartheta_1)d\vartheta_1\},$$

and

$$\nu_L g_+(f\nu_L)=24f\pi^{-2}3^{-\frac{1}{2}}\int_0^{\cos^{-1}(2f^2-1)}\times[(5-6f^2-\cos\vartheta)(2f^2-1-\cos\vartheta)]^{-\frac{1}{2}}d\vartheta.$$

Letting $u=\cos\vartheta$, this becomes

$$\nu_L g_+(f\nu_L) = 24f\pi^{-2}3^{-\frac{1}{2}}\int_{2f^2-1}^{1}[(1-u^2)(u-5+6f^2)\times(u-2f^2+1)]^{-\frac{1}{2}}du$$
$$= 8\pi^{-2}(f^2-\tfrac{2}{3})^{-\frac{1}{2}}K([1-f^2/f][f^2-\tfrac{2}{3}]^{-\frac{1}{2}}). \quad (29)$$

3. Discussion of Results

Let us first summarize the results of the calculations made in the last two sections. The frequency spectrum of the "−" branch is, according to (24),

$$\nu_L g_-(f\nu_L) = \begin{cases} [24f\pi^{-2}/(2-3f^2)]K(3f^2/(2-3f^2)) & \text{if } f^2\leq\tfrac{1}{3}, \quad (30a) \\ (8\pi^{-2}/f)K((2-3f^2)/3f^2) & \text{if } \tfrac{1}{3}<f^2\leq\tfrac{2}{3}, \quad (30b) \\ 0 \quad \text{if } f^2>\tfrac{2}{3}. \end{cases}$$

Using the theory of transformation of elliptic integrals, one can show that the expressions given above are equivalent to

$$\nu_L g_-(f\nu_L) = (12f/\pi^2)K(3f[\tfrac{2}{3}-f^2]^{\frac{1}{2}}) \quad f^2\leq\tfrac{2}{3}. \quad (30c)$$

This expression could have been derived from (22) by making the substitution $u=\cos\varphi$ and employing formula (554) in Pierce's tables. In the positive branch, according to (26), (28), and (29)

$$\nu_L g_+(f\nu_L) = \begin{cases} \dfrac{4f}{\pi^2[1-(4/3)f^2]^{\frac{1}{2}}}K\left(f\left[\dfrac{2-3f^2}{3-4f^2}\right]^{\frac{1}{2}}\right) & \text{if } 0\leq f^2\leq\tfrac{2}{3}, \quad (26) \\ \dfrac{8f}{\pi^2(1-f^2)}K\left(\dfrac{f}{1-f^2}[f^2-\tfrac{2}{3}]^{\frac{1}{2}}\right) & \text{if } \tfrac{2}{3}<f^2\leq\tfrac{3}{4}, \quad (28) \\ \dfrac{8}{\pi^2(f^2-\frac{2}{3})^{\frac{1}{2}}}K\left(\dfrac{1-f^2}{f}[f^2-\tfrac{2}{3}]^{-\frac{1}{2}}\right) & \text{if } \tfrac{3}{4}<f^2\leq 1. \quad (29) \end{cases}$$

Two asymptotic formulae for the complete elliptic integral $K(k)$ are useful in interpreting these expressions. The series

$$K(k) = \frac{\pi}{2}\left[1+(\tfrac{1}{2})^2k^2+\left(\frac{1\cdot3}{2\cdot4}\right)^2k^4+\left(\frac{1\cdot3\cdot5}{2\cdot4\cdot6}\right)^2k^6+\cdots\right] \quad (31)$$

converges if $k^2<1$. Of course it is most useful when k is very small. As $k\to1$,

$$K(k)\sim\log[4/(1-k^2)^{\frac{1}{2}}]. \quad (32)$$

By applying (31) to (30c)

$$\nu_L g_-(f\nu_L) = \frac{6f}{\pi}\left\{1+\tfrac{3}{4}f^2(2-3f^2)+\frac{81}{64}f^4(2-3f^2)^2+\cdots\right\}. \quad (33)$$

At each extreme of the frequency range $f\to0$ or $f^2\to\frac{2}{3}$

$$\nu_L g_-(f\nu_L)\sim 6f/\pi, \quad (33a)$$

a result in agreement with the Debye continuum theory of a two-dimensional lattice. The Debye theory yields a linear dependence of $g(f\nu_L)$ on f over the entire frequency range. Our spectrum is at variance with that of Debye for frequencies in the neighborhood of $(\nu/\nu_L)^2=f^2=\frac{1}{3}$, for here we can apply (32) to (30c) and obtain

$$\nu_L g_-(f\nu_L)\sim 12f\pi^{-2}\log[4/(1-3f^2)]. \quad (34)$$

Thus, as $f^2\to\frac{1}{3}$, $\nu_L g_-(f\nu_L)\to\infty$. The entire f_- branch is plotted in Fig. 6.

The low frequency behavior of the f_+ branch is obtained by applying (31) to (26):

$$\nu_L g_+(f\nu_L) = \frac{2f}{\pi[1-(4/3)f^2]^{\frac{1}{2}}}\left\{1+\frac{f^2}{4}\left(\frac{2-3f^2}{3-4f^2}\right)+\frac{9f^4}{64}\left(\frac{2-3f^2}{3-4f^2}\right)^2+\cdots\right\}. \quad (35)$$

As $f\to0$,

$$\nu_L g_+(f\nu_L)\sim 2f/\pi. \quad (36)$$

As $f^2\to\frac{3}{4}$ both $f(f^2-\frac{2}{3})^{\frac{1}{2}}/(1-f^2)$ and its reciprocal approach unity. Therefore, $\nu_L g_+(f\nu_L)$ has an infinity at $f^2=\frac{3}{4}$, and in the neighborhood of this point

$$\nu_L g_+(f\nu_L)\sim\frac{8f}{\pi^2(1-f^2)}\log\left\{\frac{4(1-f^2)}{[1-(4/3)f^2]^{\frac{1}{2}}}\right\} \quad \text{if } f^2<\tfrac{3}{4}, \quad (37a)$$
$$\to-\frac{\sqrt{3}}{2\pi^2}\log[1-(4/3)f^2]$$

$$\nu_L g_+(f\nu_L) \sim \frac{8}{\pi^2(f^2-\frac{2}{3})^{\frac{1}{2}}} \log\left\{4f\left(\frac{3f^2-2}{4f^2-3}\right)^{\frac{1}{2}}\right\}$$

if $f^2>\frac{3}{4}$. (37b)

$$\rightarrow -\frac{8\sqrt{3}}{\pi^2}\log[(4/3)f^2-1]$$

The complete f_+ branch of the spectrum is plotted in Fig. 7, and in Fig. 1 the entire spectrum

$$g(\nu)=\tfrac{1}{2}\{g_+(f\nu_L)+g_-(f\nu_L)\}$$

is plotted.

Qualitatively it is not surprising that singularities occur at the points $\nu=(\frac{1}{3})^{\frac{1}{2}}\nu_L$ and $\nu=(\frac{3}{4})^{\frac{1}{2}}\nu_L$.

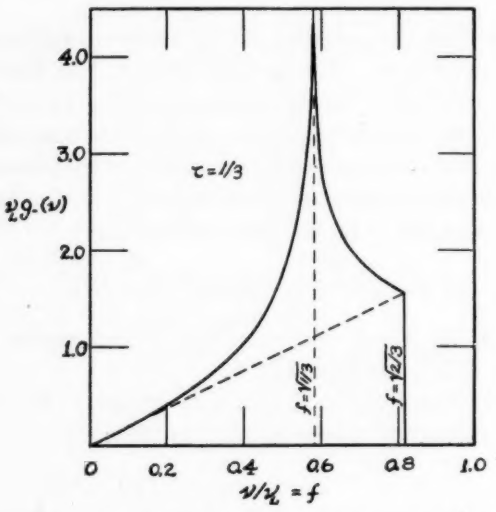

FIG. 6. Density of normal modes in f_- branch when $\tau=\frac{1}{3}$.

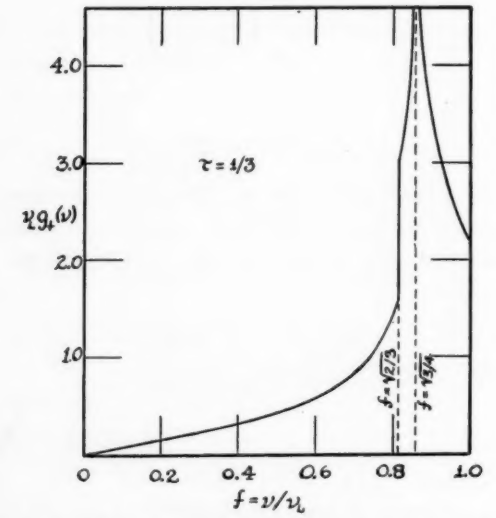

FIG. 7. Density of normal modes in f_+ branch when $\tau=\frac{1}{3}$.

The periodicity of (φ_1, φ_2) space demands that curves of constant frequency cut the square boundary normally except at the corners of the square. If $(\nu/\nu_L)^2<\frac{1}{3}$ these curves in the f_- branch are normal to the lines $\varphi_1=0$ and $\varphi_2=0$, while, if $(\nu/\nu_L)^2>\frac{1}{3}$ they are normal to $\varphi_1=\pi$ and $\varphi_2=\pi$. At the singular point $(\nu/\nu_L)^2=\frac{1}{3}$ they are normal to neither pair. In the f_+ branch the curves of constant frequency have two branches in the neighborhood of $(\nu/\nu_L)^2=\frac{3}{4}$. When $(\nu/\nu_L)^2<\frac{3}{4}$ one branch is normal to the lines $\varphi_1=0$ and $\varphi_2=0$, while the other branch is normal to $\varphi_1=\pi$ and $\varphi_2=\pi$. When $(\nu/\nu_L)^2>\frac{3}{4}$ one branch is normal to $\varphi_1=0$ and $\varphi_2=\pi$, the other to $\varphi_1=\pi$ and $\varphi_2=0$. At the singular point $(\nu/\nu_L)^2=\frac{3}{4}$ the two branches intersect.

E. GENERAL CASE $\tau<\frac{1}{2}$

In this section we shall study the general character of the frequency spectrum when $\tau<\frac{1}{2}$. When $\tau>\frac{1}{2}$ the effect of interactions of next-nearest neighbors exceeds that of nearest neighbors. Since this range of τ requires the evaluation of a different set of integrals (although of the same type) than those corresponding to $\tau<\frac{1}{2}$, and since it is physically of less interest than cases with $\tau<\frac{1}{2}$, we shall not discuss it here.

As in the special case $\tau=\frac{1}{3}$ there are two branches of the frequency spectrum, each corresponding to a branch of the characteristic Eq. (15). The largest frequency of the f_+ branch, $f_+(\text{max.})$ occurs in the first quadrant of (φ_1, φ_2) space at $(\varphi_1, \varphi_2)=(\pi, 0)$ or $(0, \pi)$ and that of the f_- branch at (π, π), thus,

$$f_+^2(\text{max.})=1, \tag{38a}$$

$$f_-^2(\text{max.})=1-\tau. \tag{38b}$$

Equations (19a) and (19b) remain valid in the range of τ of interest in this section. Each branch of the spectrum will be discussed separately.

1. f_- Branch

In order to analyze the frequency spectrum it is necessary to know the behavior of the curves of constant f in that part of (φ_1, φ_2) space bounded by the φ_1 and φ_2 axes and the lines $\varphi_1=\pi$ and $\varphi_2=\pi$. The points of intersection of these curves with the lines $\varphi_1=0$, $\varphi_2=0$, $\varphi_1=\pi$, $\varphi_2=\pi$, and $\varphi_1=\varphi_2$ will be especially useful in

describing this behavior. Of course all knowledge of the curves $f_-^2=$constant must be derived from the characteristic Eq. (16). Their symmetry with respect to the line $\varphi_1=\varphi_2$ is implied by the c_1, c_2 symmetry of (16). Three functions of f_- will appear frequently in our analysis:

$$q=2f_-^2/\tau, \quad p=2f_-^2/(1-\tau), \qquad (39)$$
$$r=(2f_-^2-1)/(2\tau-1).$$

The φ_1 and φ_2 intercepts of $f_-^2=$constant are at

$$\varphi_1=\cos^{-1}(1-q) \quad \text{and} \quad \varphi_2=\cos^{-1}(1-q). \qquad (40)$$

If $f_-^2>\tau$, the intercepts are outside the square of interest. In this case the intersection of the $f_-^2=$constant curves with the lines $\varphi_1=\pi$ and $\varphi_2=\pi$ are at the points

$$(\pi, \cos^{-1}r) \quad \text{and} \quad (\cos^{-1}r, \pi). \qquad (41)$$

The intersection with the line $\varphi_1=\varphi_2$ occurs at the point

$$(\cos^{-1}[1-p], \cos^{-1}[1-p]). \qquad (42)$$

Since, when $\tau\leq\frac{1}{2}$, $q>p$ we have

$$\cos^{-1}(1-q)>\cos^{-1}(1-p). \qquad (43)$$

That is, the intercept with the φ_1 axis occurs at a larger value of φ_1 than does the projection on this axis of the point (42). It is also easy to show that the intersection of $f_-^2=$constant with the line $\varphi_2=\pi$ occurs at a smaller value of φ_1 than does the intersection with the line $\varphi_1=\varphi_2$. On the basis of the above observations we have sketched schematically in Figs. 8–9 curves of constant f for the two possible cases, $f_-^2<\tau$ and $f_-^2>\tau$. The cross-hatched fractions of the square correspond to frequencies less than f_-.

Equation (19a) can be applied to the general f_- branch of the frequency spectrum. Instead of determining the entire area of the region in (φ_1, φ_2) space corresponding to frequencies less than f_-, we shall double (remembering the φ_1, φ_2 symmetry) that area in the triangle formed by the points $(0, 0)$, $(0, \pi)$, and (π, π). Thus, when $f^2<\tau$

$$\lim_{N\to\infty} N_-(f\nu_L)/N^2=\pi^{-2}\{\cos^{-1}(1-p)\}^2 + 2\pi^{-2}\int_{\cos^{-1}(1-p)}^{\cos^{-1}(1-q)} \cos^{-1}c_2 d\varphi_1,$$

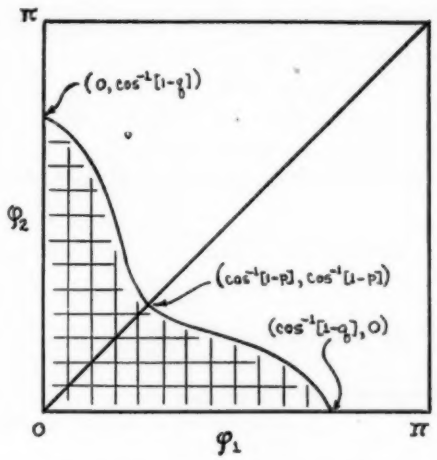

FIG. 8. Schematic diagram of curve of constant frequency in f_- branch when $\nu/\nu_L<\tau^{\frac{1}{2}}$.

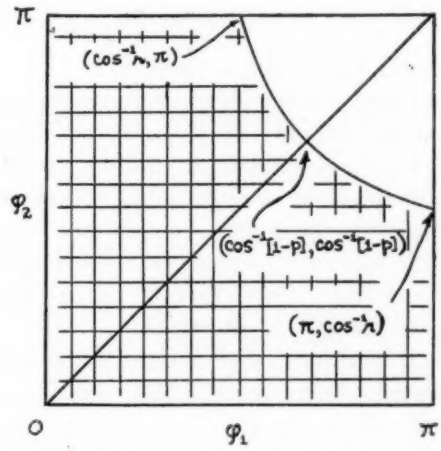

FIG. 9. Schematic diagram of curve of constant frequency in f_- branch when $\nu/\nu_L>\tau^{\frac{1}{2}}$.

and from (19b) and (39)

$$\nu_L g_-(f\nu_L)=-2\pi^{-2}\int_{\cos^{-1}(1-p)}^{\cos^{-1}(1-q)} \frac{(\partial c_2/\partial f)}{(1-c_2^2)^{\frac{1}{2}}} d\varphi_1. \qquad (44a)$$

Similarly, when $f^2>\tau$

$$\nu_L g_-(f\nu_L)=-2\pi^{-2}\int_{\cos^{-1}(1-p)}^{\pi} \frac{(\partial c_2/\partial f)}{(1-c_2^2)^{\frac{1}{2}}} d\varphi_1. \qquad (44b)$$

First, let us treat the case $f^2\leq\tau$. Making the substitution $x=\cos\varphi_1$, (44a) becomes

$$\nu_L g_-(f\nu_L)=-\frac{2}{\pi^2}\int_{1-q}^{1-p} \frac{(\partial c_2/\partial f)dx}{[(1-x^2)(1-c_2^2)]^{\frac{1}{2}}}. \qquad (45)$$

Some special properties of $c_2(c_1)=c_2(x)$ are re-

quired for our analysis. These are a direct consequence of the characteristic equation. When

$$c_1=\cos\varphi_1=x=1-q, \tag{46a}$$

we have

$$c_2(1-q)=1, \tag{46b}$$

$$a_1=(\partial c_2/\partial x)_{x=1-q}=\tau(\tau-1)/[2f^2(3\tau-1)-(4\tau^2+\tau-1)], \tag{46c}$$

$$a_2=(\partial^2 c_2/\partial x^2)_{x=1-q}=\frac{2\tau^2(3\tau-1)[2f^4(1-3\tau+4\tau^2)-f^2(8\tau^3+\tau^2-2\tau+1)+2\tau^3(\tau+1)]}{f^2[2f^2(3\tau-1)-(4\tau^2+\tau-1)]^3}. \tag{46d}$$

Thus, in the neighborhood of $x=1-q$

$$c_2(x)=1+a_1(x-1+q)+\tfrac{1}{2}a_2(x-1+q)^2+\cdots, \tag{47a}$$

and

$$\partial c_2/\partial f=(4fa_1/\tau)+(x-1+q)[(4fa_2/\tau)+\partial a_1/\partial f]+\cdots. \tag{47b}$$

Also, if $x=1-p$, then $c_2=1-p$.

These results enable us to study the nature of the integrand of (45). If $f^2\neq\tau$, in the interval $(1-q)\leq x\leq(1-p)$ it has an infinity at $(1-q)$ because of the term $(1-c_1)^{\frac{1}{2}}$ in the denominator. This infinity is not strong enough to cause the integral to diverge. However, as $f^2\to\tau$ we see that $(1-q)\to-1$ and $[(1+x)(1-c_2)]^{\frac{1}{2}}\to(-a_1)^{\frac{1}{2}}(1+x)$, causing the integral to diverge.

When f^2 is near τ, most of the contribution to the integral comes from values of x in the neighborhood of $(1-q)$. Therefore, by substituting (47a) into (45) we should be able to obtain a good approximation to $g_-(f\nu_L)$, provided that f^2 is not too much smaller than τ. Upon introduction of (47a), the integrand of (45) becomes:

$$\frac{\partial c_2/\partial f}{[(1-x^2)(1-c_2^2)]^{\frac{1}{2}}}=\frac{(4fa_1/\tau)+0[x-(1-q)]}{\{(-2a_1q)(1+x)[x-(1-q)]\}^{\frac{1}{2}}}. \tag{48}$$

Thus, letting $y=x-(1-q)$, we find

$$\nu_L g_-(f\nu_L)\sim-\frac{8fa_1}{\pi^2\tau(-2qa_1)^{\frac{1}{2}}}\times\int_0^{q-p}\frac{dy}{[y(y-(2-q))]^{\frac{1}{2}}};$$

or, as $f^2\to\tau$

$$\nu_L g_-(f\nu_L)\sim-\frac{8fa_1}{\pi^2\tau(-2qa_1)^{\frac{1}{2}}}\times\log\left\{\frac{2[(q-p)(2-p)]^{\frac{1}{2}}+2(1-p)}{(2-q)}\right\}. \tag{49a}$$

When f^2 is in the very near neighborhood of τ, $q\to2$, $a_1\to\tau/(2\tau-1)$, $(2-p)\to2(1-2\tau)/(1-\tau)$, and $-\log(2-q)\to\infty$; therefore,

$$\nu_L g_-(f\nu_L)\sim-4\pi^{-2}(1-2\tau)^{-\frac{1}{2}}\log(1-\tau^{-1}f^2). \tag{49b}$$

This frequency spectrum has a logarithmic infinity at $f^2=\tau$ in agreement with (34) in the special case $\tau=\frac{1}{3}$.

As $f\to0$, (45) is still applicable, but p and q both approach zero; therefore, for small values of f the integrand of (45) can be approximated by (since $x\simeq1$ in the entire range of integration)

$$\frac{\partial c_2/\partial f}{[(1-x^2)(1-c_2^2)]^{\frac{1}{2}}}=\frac{(4fa_1/\tau)+0(x-(1-q))}{2[(1-x)(-a_1)(x-(1-q))]^{\frac{1}{2}}}.$$

The substitution $y=1-x$ transforms (45) into

$$\nu_L g_-(f\nu_L)\sim\frac{1}{\pi^2}\int_q^p\frac{(4fa_1/\tau)dy}{(-a_1)^{\frac{1}{2}}[y(q-y)]^{\frac{1}{2}}}=\frac{8f(-a_1)^{\frac{1}{2}}}{\tau\pi^2}\left\{\frac{\pi}{2}-\sin^{-1}(\tau/1-\tau)^{\frac{1}{2}}\right\}. \tag{50}$$

Since, as $f^2\to0$, $a_1\to-\tau(\tau-1)/(4\tau^2+\tau-1)$

$$\nu_L g_-(f\nu_L)\sim\frac{8f}{\pi^2}\left(\frac{1-\tau}{\tau[1-\tau-4\tau^2]}\right)^{\frac{1}{2}}\times\left\{\frac{\pi}{2}-\sin^{-1}\left(\frac{\tau}{1-\tau}\right)^{\frac{1}{2}}\right\}. \tag{51}$$

This formula simplifies considerably in two

special cases of interest:

(a) if $\tau=\frac{1}{3}$, $\nu_L g_-(f\nu_L)\sim 6f/\pi$ which agrees with (33a), (52)

(b) as $\tau\to 0$, $\nu_L g_-(f\nu_L)\sim 4f/\pi\tau^{\frac{1}{2}}$.

When $f^2>\tau$ the frequency distribution is given by (44b). After the substitution $x=\cos\varphi_1$, it becomes

$$\nu_L g_-(f\nu_L)=-2\pi^{-2}\int_1^{1-p}\frac{(\partial c_2/\partial f)dx}{[(1-x^2)(1-c_2^2)]^{\frac{1}{2}}}. \quad (53)$$

By expanding all the functions of x in this integral about the point $x=-1$, and using the methods discussed above, one can show that as $f^2\to\tau$ $(f^2>\tau)$:

$$\nu_L g_-(f\nu_L)\sim -\frac{4f}{\pi^2[\tau(1-2\tau)]^{\frac{1}{2}}}\log(f^2\tau^{-1}-1). \quad (54)$$

Thus, the frequency spectrum has a logarithmic infinity as τ is approached from either side by f^2.

An asymptotic expression for $\nu_L g_-(f\nu_L)$ can be obtained as $f^2\to(1-\tau)$ from (44b). Here $(1-p)\to-1$; therefore, over the entire range of integration of (44b), $x\simeq -1$. Expanding all function in (44b) about this point, we have

$$\nu_L g_-(f\nu_L)\sim\frac{8f}{\pi^2(1-2\tau)[2(1-r)]^{\frac{1}{2}}}$$

$$\times\begin{cases}(-b_1)^{-\frac{1}{2}}[\frac{1}{2}\pi-\sin^{-1}(1+2\mu)] & \text{if } b_1<0, \quad (55)\\ (-b_1)^{-\frac{1}{2}}\log\{1+2\mu+2[\mu(1+\mu)]^{\frac{1}{2}}\} & \text{if } b_1>0, \quad (56)\end{cases}$$

where

$$\mu=b_1(2-p)/(1+r) \quad (57)$$

and

$$b_1=\tau[r(3\tau-1)-2\tau]/(1-2\tau)(1-\tau).$$

At the end of the "−" branch of the spectrum where $f^2=1-\tau$ (we write $\mu_0=\tau(1-5\tau)/(1-\tau)^2$)

$$\nu_L g_-(f\nu_L)=(4/\pi^2)$$

$$\times\begin{cases}[\mu_0(2\tau-1)]^{-\frac{1}{2}}[\frac{1}{2}\pi-\sin^{-1}(1-2\mu_0)] & \text{if } \tau>\frac{1}{5}, \quad (58a)\\ 2/(1-2\tau)^{\frac{1}{2}} \quad \text{if } \tau=\frac{1}{5}, & (58b)\\ [\mu_0(1-2\tau)]^{-\frac{1}{2}}\log\{1+2\mu_0+2[\mu_0(1+\mu_0)]^{\frac{1}{2}}\} & \text{if } \tau<\frac{1}{5}. \quad (59)\end{cases}$$

Note that if $\tau=\frac{1}{3}$, $\nu_L g_-(f\nu_L)=6(\frac{2}{3})^{\frac{1}{2}}/\pi$ which agrees with (33a).

The qualitative character of this branch of the frequency spectrum can be summarized in the following properties: (a) it is linear in the range of law frequencies; (b) a logarithmic infinity exists at $\nu=\tau^{\frac{1}{2}}\nu_L$; (c) there are no normal modes with frequencies greater than $\nu=(1-\tau)^{\frac{1}{2}}\nu_L$.

2. f_+ Branch

As in the analysis of the f_- branch we must have a description of the curves of constant f in (φ_1, φ_2) space. Three functions of f that will be important in the discussion of these curves in this branch are

$$\alpha_1=\{-(1-\tau)+[(1+3\tau)^2-16\tau f_+^2]^{\frac{1}{2}}\}/4\tau, \quad (60a)$$

$$\alpha_2=\{-(1-\tau)-[(1+3\tau)^2-16\tau f_+^2]^{\frac{1}{2}}\}/4\tau, \quad (60b)$$

and

$$s=[(2f^2-1)-(1-\tau)]/\tau. \quad (60c)$$

The φ_1 and φ_2 intercepts of the curves of constant f are at

$$\varphi_1=\cos^{-1}(1-2f_+^2) \text{ and } \varphi_2=\cos^{-1}(1-2f_+^2). \quad (61)$$

These points are on the boundary of the square of interest in (φ_1, φ_2) space for all values of f. The intersections of $f_+^2=$constant with the lines $\varphi_1=\pi$ and $\varphi_2=\pi$ are at the points

$$(\pi, \cos^{-1}s) \quad \text{and} \quad (\cos^{-1}s, \pi). \quad (62)$$

Whenever $f_+^2>(1-\tau)$ these intersections exist.

The points of intersection of $f_+^2=$constant with the line $\varphi_1=\varphi_2$ occur at the roots $c_2=c_1=\cos\varphi_1$ of the characteristic equation

$$g(c_1)=2\tau c_1^2+(1-\tau)c_1+[2f_+^2-(1+\tau)]=0. \quad (63)$$

These roots are $c_1=\alpha_1$ and $c_2=\alpha_2$. For given values of f_+ and τ the number of intersections is equal to the number of real roots of (62) which are between -1 and $+1$. A necessary and sufficient condition for the existence of one intersection is that $g(1)$ be of opposite sign from $g(-1)$. Since

$$g(1)=2f_+^2>0, \quad \text{and} \quad g(-1)=2[f_+^2-(1-\tau)],$$

the signs are opposite when $f_+^2<(1-\tau)$, and there is one intersection. This root is at $c_1=\alpha_1$. If $f^2>(1-\tau)$ there are *either two roots* between -1 and 1, *or none* in that interval. Clearly there are none if the discriminant of (63) is

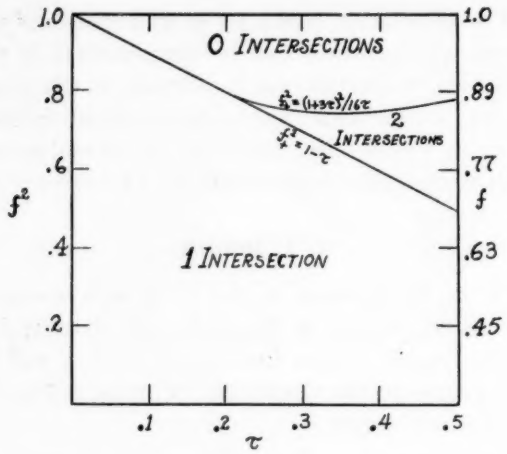

FIG. 10. Regions of constant number of roots of characteristic Eq. (63).

negative, that is, if

$$(1-\tau)^2-8\tau[2f_+^2-(1+\tau)]<0,$$

or

$$f_+^2>(1+3\tau)^2/16\tau.$$

Now, the sum of the two roots is

$$\alpha_1+\alpha_2=-(1-\tau)/2\tau.$$

Thus, if

(a) $f_+^2<(1+3\tau)^2/16\tau$,
(b) $\alpha_1+\alpha_2=-(1-\tau)/2\tau<-2$,
(c) $f_+^2>(1-\tau)$,

then at least one root must be smaller than -1. From above either both roots are in the interval bounded by -1 and $+1$, or neither are. Therefore, if $\tau<\frac{1}{5}$ both roots are outside the interval. If $0>\alpha_1+\alpha_2=-(1-\tau)/2\tau>-2$, which is the case when $\frac{1}{5}<\tau<1$, at least one root and, therefore, both must lie in the interval -1 to 1. The distribution of roots of (63) as obtained in these arguments is summarized in Fig. 10 where curves are plotted in f,τ space to separate regions corresponding to the various root distributions of (63). Thus, for any pair of values of f and τ one can determine the number of intersections of the $f=$constant curve with the line $\varphi_1=\varphi_2$.

On the basis of (61), (62), and Fig. 10 we have schematically represented in Figs. 11–13 the curves of constant f corresponding to the various regions in Fig. 10. When $f^2<(1-\tau)$ these curves have only one branch independent of τ. The shaded region corresponds to those points in (φ_1, φ_2) space which yield frequencies of normal modes less than $f\nu_L$. If $f^2>(1-\tau)$ the shape of the $f=$constant curves depends on whether or not $\tau<\frac{1}{5}$. When $\tau<\frac{1}{5}$ there are no intersections of $f=$constant with the line $\varphi_1=\varphi_2$, so the curve of constant f has the appearance of Fig. 13. When $\tau>\frac{1}{5}$ there are either two or no intersections with the line $\varphi_1=\varphi_2$ depending on whether

$$1-\tau<f_+^2<(1+3\tau)^2/16\tau,$$

or

$$f_+^2>(1+3\tau)^2/16\tau.$$

The first case is shown in Fig. 12 and the second in Fig. 13.

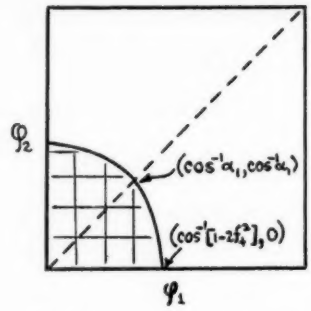

FIG. 11. Typical curve of constant frequency when $f^2<1-\tau$.

Each topologically different type of $f=$constant curve requires a different integral representation of $\nu_L g_+(f\nu_L)$. Therefore, we treat separately each of the following combinations:

(a) $\tau<\frac{1}{5}$ and $f^2<(1-\tau)$,
(b) $\tau<\frac{1}{5}$ and $f^2>(1-\tau)$,
(c) $\tau>\frac{1}{5}$ and $f^2<(1-\tau)$,
(d) $\tau>\frac{1}{5}$ and $(1-\tau)<f^2<(1+3\tau)^2/16\tau$,
(e) $\tau>\frac{1}{5}$ and $f^2\leq(1+3\tau)^2/16\tau$.

We shall now derive an integral representation for $\nu_L g_+(f\nu_L)$ corresponding to each of the above cases.

(a) and (c). In these cases

$$\lim_{N\to\infty} N_+(f\nu_L)/N^2=\frac{2}{\pi^2}\left\{\frac{\pi^2}{2}-(\pi-\cos^{-1}\alpha_1)^2-\int_0^{\cos^{-1}\alpha_1}(\pi-\cos^{-1}c_2)d\varphi_1\right\}$$

and from (19b) (letting $x=\cos\varphi_1$),

$$\nu_L g_+(f\nu_L)=-\frac{2}{\pi^2}\int_{\alpha_1}^{1}\frac{(\partial c_2/\partial f)dx}{[(1-x^2)(1-c_2^2)]^{\frac{1}{2}}}. \quad (64)$$

(b) and (e). Here

$$\lim_{N\to\infty} N_+(f\nu_L)/N^2 = \frac{2}{\pi^2}\left\{\frac{\pi^2}{2} - \int_{\cos^{-1}(1-2f^2)}^{\pi} (\cos^{-1}c_2)d\varphi_1\right\}$$

and (letting $x=\cos\varphi_1$)

$$\nu_L g_+(f\nu_L) = \frac{2}{\pi^2}\int_{-1}^{1-2f^2} \frac{(\partial c_2/\partial f)dx}{[(1-x^2)(1-c_2^2)]^{\frac{1}{2}}}. \quad (65)$$

(d). Two areas contribute normal modes with frequencies less than $f\nu_L$. The first is in the neighborhood of the origin, and for it

$$\lim_{N\to\infty} N_+^{(1)}(f\nu_L)/N^2 = 2\pi^{-2}\left\{\tfrac{1}{2}\pi^2 - \tfrac{1}{2}(\pi-\cos^{-1}\alpha_1)^2 - \int_0^{\cos^{-1}\alpha_1} [\pi-\cos^{-1}c_2]d\varphi_1\right\}.$$

The second is in the neighborhood of (π, π) and for it

$$\lim_{N\to\infty} N_+^{(2)}(f\nu_L)/N^2 = 2\pi^{-2}\left\{\tfrac{1}{2}\pi^2 - \tfrac{1}{2}(\cos^{-1}\alpha_1)^2 - \int_{\cos^{-1}\alpha_1}^{\pi} (\cos^{-1}c_2)d\varphi_1\right\}.$$

Thus,

$$\nu_L g_+^{(1)}(f\nu_L) = +\frac{2}{\pi^2}\int_{\alpha_1}^{1} \frac{(\partial c_2/\partial f)dx}{[(1-x^2)(1-c_2^2)]^{\frac{1}{2}}}, \quad (66a)$$

and

$$\nu_L g_+^{(2)}(f\nu_L) = \left|\frac{2}{\pi^2}\int_{-1}^{\alpha_2} \frac{(\partial c_2/\partial f)dx}{[(1-x^2)(1-c_2^2)]^{\frac{1}{2}}}\right|, \quad (66b)$$

where

$$g_+(f\nu_L) = g_+^{(1)}(f\nu_L) + g_+^{(2)}(f\nu_L). \quad (66c)$$

The absolute value sign is included on (66b) because $\nu_L g_+^{(2)}(f\nu_L)$ represents the rate of increase of area of region near (π, π) of f increases; this rate is always positive even though in the mechanics of integration one might obtain a negative value for the integral.

Let us now use Eqs. 64–66 to determine the qualitative character of the f_+ branch of the frequency spectrum, and to find its qualitative behavior in the neighborhood of its infinity and at each end of the frequency interval. We shall treat the two sets of τ, $\tau<\frac{1}{8}$ and $\tau>\frac{1}{8}$, separately.

i. $\tau<\frac{1}{8}$. We study first that portion of the frequency spectrum with $1-\tau<f^2<1$. In this range (65) is applicable. At the end of the interval, as $f^2\to1$, x in the entire range of integration $-1<x<1-2f^2$ is very close to -1. If all functions of x in (65) are expanded about $x=-1$

$$\nu_L g_+(f\nu_L) \sim \frac{16f\sin^{-1}(\gamma\tau)^{\frac{1}{2}}}{\pi^2[2\tau(1+s)\gamma\tau]^{\frac{1}{2}}}, \quad (67)$$

where

$$\gamma\tau = 1-(2+\tau)(1-f^2)(1-\tau)^{-1}$$

and (68)

$$s = 1-2\tau^{-1}(1-f^2).$$

As $f^2\to1$, we see that $\gamma\tau\to1$ and $1+s\to2$, so that in the limit, $\nu_L g_+(\nu_L) = 4/\pi\tau^{\frac{1}{2}}$. It is to be noted that this analysis is also valid when $\tau>\frac{1}{8}$. In particular when $\tau=\frac{1}{3}$ we obtain $\nu_L g_+(\nu_L) = 4(3^{\frac{1}{2}})/\pi$ which is in agreement with (27).

At the other end of the interval, as $f^2\to(1-\tau)+0$, the range of integration of (65) extends from $x=-1$ to $x=1$. Since at this frequency $c_2(-1)=-1$ we see that the integrand behaves as $(1+x)^{-1}$ as $x\to-1$, and the main contribution to the integral comes from values of x near -1.

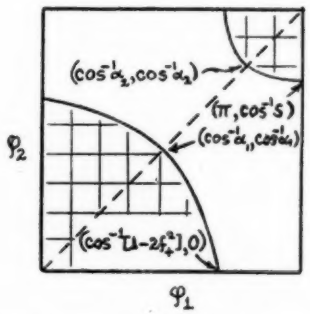

FIG. 12. Typical curve of constant frequency when $\tau>\frac{1}{8}$ and $1-\tau<f^2<(1+3\tau)^2/16\tau$.

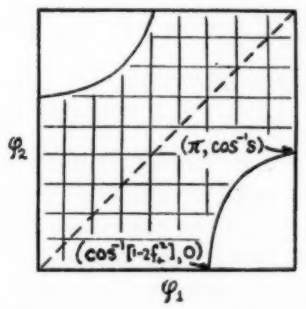

FIG. 13. Typical curve of constant frequency when $\tau<\frac{1}{8}$ and $f^2>(1-\tau)$ or $\tau>\frac{1}{8}$ and $f^2>(1+3\tau)^2/16\tau$.

Thus, as $f^2 \to (1-\tau)+0$ one obtains

$$\nu_L g_+(f\nu_L) \sim [4f/\pi^2\tau\gamma^{\frac{1}{2}}] \times \log\{\tau(8\tau\gamma+1)/2[f^2-(1-\tau)]\}, \quad (69)$$

so that $\nu_L g_+(f\nu_L)$ has a logarithmic infinity at $f^2=1-\tau$, provided $\tau<\frac{1}{5}$.

Now let us consider the low frequency part of the f_+ spectrum, that is, the region in which $f^2<(1-\tau)$. It is in this region that (64) is valid. At the beginning of the interval, as $f^2\to 0$, $\alpha_1\to 1$ and the range of integration $\alpha_1<x<1$ is limited to values of x very close to unity. As $x\to 1$,

$$c_2(x) = (1-2f^2) - e_1(x-1) + 0(x-1)^2,$$
$$\partial c_2/\partial f = -4f + 0(x-1),$$

where

$$e_1 = \tau(1-\tau)^{-1}[(3\tau+1) - 2f^2(1-\tau)].$$

e_1 is positive when f^2 is near or equal to zero. Substituting this expression for $c_2(x)$ into (64) we have

$$\nu_L g_+(f\nu_L) = 8f\pi^{-2}\int_{\alpha_1}^{1} \frac{dx[1+0(1-x)]}{\{4(1-f^2)(1-x)[2f^2-e_1(1-x)]\}^{\frac{1}{2}}}.$$

Letting $y=1-x$

$$\nu_L g_+(f\nu_L) \sim -\frac{4f}{\pi^2\{(1-f^2)e_1\}^{\frac{1}{2}}} \times \int_{1-\alpha_1}^{0} \frac{dy}{y[(2f^2/e_1)-y]}$$
$$= \frac{8f}{\pi^2\{e_1(1-f^2)\}^{\frac{1}{2}}} \sin^{-1}\left\{\frac{(1-\alpha_1)e_1}{2f^2}\right\}^{\frac{1}{2}}. \quad (70a)$$

For sufficiently small f,

$$e_1(1-\alpha_1)/2f^2 \sim \tau/(1-\tau), \quad e_1 \sim \tau(3\tau+1)/(1-\tau).$$

Therefore, as $f\to 0$

$$\nu_L g_+(f\nu_L) \sim [8f/\pi^2\{\tau(3\tau+1)/(1-\tau)\}] \times \sin^{-1}\{\tau/(1-\tau)\}^{\frac{1}{2}}. \quad (70b)$$

It is to be noted that the analysis necessary to obtain (70) is valid for values of $\tau<\frac{1}{5}$ and those $>\frac{1}{5}$. Therefore, (70) is correct in both of these cases. When $\tau=\frac{1}{3}$ (70b) reduces to $\nu_L g_+(f\nu_L) \sim 2f/\pi$, which is in agreement with (36), one can show that as $f^2\to(1-\tau)$ from the low frequency side, $\nu_L g_+(f\nu_L)\to\infty$. The analysis of the asymptotic manner of approach is somewhat more difficult than that given for the high frequency side and will not be given here.

ii. $\tau>\frac{1}{5}$. In the neighborhood of $f^2=0$ and $f^2=1$ the expressions for $g_+(f\nu_L)$, derived when $\tau<\frac{1}{5}$ are still valid for the integral representations (64) and (65), are valid in both cases. Therefore, as $f\to 0$

$$\nu_L g_+(f\nu_L) \sim [8f(1-\tau)/\pi^2\tau(3\tau+1)] \times \sin^{-1}[\tau/(1-\tau)]^{\frac{1}{2}},$$

and as $f^2\to 1$ (68) is still valid and in the limit

$$\nu_L g_+(f\nu_L) \to 4/\pi\tau^{\frac{1}{2}}.$$

The infinity in this branch of the frequency sprectrum now appears at $\nu/\nu_L=(1+3\tau)/4\tau^{\frac{1}{2}}$ instead of at $(1-\tau)^{\frac{1}{2}}$.

To prove our last statement we must show that if

$$f^2 = (1+3\tau)^2/16\tau \quad (71)$$

then $\nu_L g_+(f\nu_L)$ becomes infinite. In the special case $\tau=\frac{1}{3}$ this is true, for then (71) becomes identical with the result (37) of Section D. In general, from (60), when $f^2=(1+3\tau)^2/16\tau$, $\alpha_1=\alpha_2=-(1-\tau)/4\tau$. Therefore, the density of frequencies is given by the sum of the two integrals (66):

$$\nu_L g_+^{(1)}(f\nu_L) = \frac{2}{\pi^2}\int_{-(1-\tau)/4\tau}^{1} \frac{(\partial c_2/\partial f)dx}{[(1-x^2)(1-c_2^2)]^{\frac{1}{2}}},$$

$$\nu_L g_+^{(2)}(f\nu_L) = \left|\frac{2}{\pi^2}\int_{-1}^{-(1-\tau)/4\tau} \frac{(\partial c_2/\partial f)dx}{[(1-x^2)(1-c_2^2)]^{\frac{1}{2}}}\right|.$$

From the results of the Appendix it will be clear that both of these integrals diverge. If the characteristic Eq. (15) is written as

$$ac_2^2 + bc_2 + c = 0, \quad (72)$$

then

$$c_2 = [-b+(b^2-4ac)^{\frac{1}{2}}]/2a,$$

$$\partial c_2/\partial f = -\frac{\partial b/\partial f}{2a} + \frac{b(\partial b/\partial f) - 2a(\partial c/\partial f)}{a(b^2-4ac)^{\frac{1}{2}}}.$$

When $f^2=(1+3\tau)^2/16\tau$ the terms a, b, c, $\partial b/\partial f$ and $\partial c/\partial f$ are given by Eqs. (A-1)–(A-6) of the Appendix if the constant which appears there

represents $\lambda=-1+[(1+3\tau)^2/8\tau]$. Also,

$$b^2-4ac=[(1-\tau)^2/(16\tau)^2]\{4x\tau+(1-\tau)\}^2\times\{(4x\tau)^2+8(1-\tau)(4x\tau)+4(1-2\tau+13\tau^2)\}.$$

As $x\to-(1-\tau)/4\tau$

$a\to(3\tau-1)(1+\tau)/4$,

$b\to(3\tau-1)(1-\tau^2)/8\tau$,

$c\to(3\tau-1)(1+\tau)(1-\tau)^2/64\tau^2$,

$\partial b/\partial f\to 2f(1-\tau)$; $\partial c/\partial f\to 8\tau f$,

$b^2-4ac\sim 3(5\tau-1)(1+3\tau)(1-\tau)^2[4x\tau+(1-\tau)]^2/(16\tau)^2$,

$c_2\to -b/2a\to-(1-\tau)/4\tau$.

Therefore, the integrands of (66a) and (66b) become, in the neighborhood of $x=-(1-\tau)/4\tau$

$$\frac{\partial c_2/\partial f}{[(1-x^2)(1-c_2^2)]^{\frac{1}{2}}}=-\frac{48\tau[(1+3\tau)\tau/3(5\tau-1)]^{\frac{1}{2}}}{(1-\tau)[4x\tau+(1-\tau)]}\times[1+0(4x\tau+1-\tau)],$$

and both integrals diverge because of the pole at $x=-(1-\tau)/4\tau$.

The author wishes to thank Mr. H. Markovitz for checking many of the derivations in this work.

APPENDIX

Location of a Pole of $\partial c_2/\partial f$

The characteristic Eq. (15) can be written in the form (71)

$$ac_2^2+bc_2+c=0,$$

where

$$a=\tau(1-\tau)x+\tau^2, \quad \text{(A-1)}$$

$$b=\tau(1-\tau)x^2+[(1-\tau)^2+2\tau\lambda]x+\lambda(1-\tau), \quad \text{(A-2)}$$

$$c=\lambda^2-\tau^2+x\lambda(1-\tau)+\tau^2x^2, \quad \text{(A-3)}$$

$$\lambda=2f^2-1. \quad \text{(A-4)}$$

Since, in the f_+ branch,

$$c_2=-b/2a+(b^2-4ac)^{\frac{1}{2}}/2a, \quad \text{(A-5)}$$

we have

$$\partial c_2/\partial f=-(2f/a)[1-\tau+2\tau x]+[b(\partial b/\partial f)-2a(\partial c/\partial f)]a^{-1}(b^2-4ac)^{-\frac{1}{2}}, \quad \text{(A-6)}$$

where

$$\partial b/\partial f=4f[(1-\tau)+2\tau x], \quad \partial c/\partial f=4f[2\lambda+x(1-\tau)].$$

Thus, $\partial c_2/\partial f$ has a simple pole if b^2-4ac (as a function of x) has two equal roots; that is, if the quartic equation

$$b^2-4ac=\tau^2(1-\tau)^2x^4+2x^3(1-\tau)[(1-2\tau-\tau^2)+2\tau\lambda]\tau+x^2[(1-\tau)^4-4\tau^4+2\tau(1-\tau)^2\lambda+4\tau^2\lambda^2]+2(1-\tau)x[2\tau^3+\lambda(1-2\tau-\tau^2)]+4\tau^4+\lambda^2(1-3\tau)(1+\tau)=0 \quad \text{(A-7)}$$

has a double root. A necessary and sufficient condition for the existence of at least two equal roots in the quartic

$$x^4+Bx^3+Cx^2+Dx+E=0$$

is that the coefficients be related in such a manner as to cause the vanishing of the discriminent

$$\Delta=-4p^3-27q^2,$$

where

$$p=BD-4E+\frac{1}{3}C^2, \quad q=-B^2E+\frac{1}{3}BCD+\frac{8}{3}CE-D^2-\frac{2}{27}C^3.$$

We shall now show that $\Delta=0$ if $f^2=(1+3\tau)^2/16\tau$. From (A-4) this is equivalent to

$$\lambda+1=(1+3\tau)^2/8\tau.$$

In this case, if (A-6) is put into the form (A-7)

$$B=5(1-\tau)/2\tau,$$
$$C=3(7-14\tau+23\tau^2)/16\tau^2,$$
$$D=(1-\tau)(1-2\tau+7\tau^2)/4\tau^3,$$
$$E=(1-\tau)^2(1-2\tau+13\tau^2)/64\tau^4.$$

Therefore,

$$p=-3(1-5\tau)^2(1+3\tau)^2/(16)^2\tau^4,$$
$$q=2(1+3\tau)^3(1-5\tau)^3/(16\tau)^3.$$

Clearly with this value of p and q, $\Delta=0$ and (b^2-4ac) has a double root. The discriminant may vanish at other values of f, but those probably correspond to roots x, which are outside the range of integration of (66). If they were physically significant there would be more than one infinity in the positive branch of the frequency spectrum, which does not seem to be the case for those values of τ which have been studied in detail.

It can be verified by direct substitution that b^2-4ac has its double root at

$$x=-(1-\tau)/4\tau,$$

when $f^2=(1+3\tau)^2/16\tau$; in fact, in this case

$$b^2-4ac=[(1-\tau)^2/(16\tau)^2]\{4x\tau+(1-\tau)\}^2\{(4x\tau)^2+8(1-\tau)4x\tau+4(1-2\tau+13\tau^2)\}.$$

THE JOURNAL OF CHEMICAL PHYSICS VOLUME 15, NUMBER 8 AUGUST, 1947

The Application of Ultrasonic Waves to the Study of Electrolytic Solutions

I. A Modification of Debye's Equation for the Determination of the Masses of Electrolytic Ions by means of Ultrasonic Waves[1]

JOHN BUGOSH, ERNEST YEAGER, AND FRANK HOVORKA
Departments of Chemistry and Physics, Western Reserve University, Cleveland, Ohio

(Received April 28, 1947)

Debye's equation for the alternating potential which should accompany the passage of ultrasonic waves through an electrolytic solution is modified and extended by the addition of terms representing corrections for relaxation forces, electrophoretic effects, thermal diffusion, and the pressure gradient associated with the material wave.

I

WHILE a knowledge of the effective masses and hydration numbers of electrolytic ions is of importance to solution theory, no method, as yet, has offered reliable values.[2] In 1933, P. Debye proposed a method[3] which would indicate the masses of solvated electrolytic ions directly. The method consists of introducing ultrasonic waves into an electrolytic solution and measuring differences in potential within the solution arising from the dynamical reactions of the ions to the material wave. Differences in the accelerations imparted to the cations and anions because of their different masses and frictional coefficients should produce periodic excesses of either cations or anions at a given point in the solution and hence periodic variations in potential.

In the original paper, Debye derived an equation for the magnitude of the effect, which he indicated could only be considered as an approximation, since interionic attraction had been neglected. S. Oka[4] extended Debye's equation, allowing for the electrophoretic and relaxation effects. In 1938, however, J. J. Hermans[5] showed that Oka's correction terms amounted to only a few parts of one percent while other, more important factors were missing in Debye's original equation. Hermans pointed out that Debye's equation has the disadvantage that when the densities of the ions are the same as that of the solvent, the expression for the potential is not zero. To remedy the situation, Hermans suggested the inclusion of terms accounting for the pressure gradient resulting from the ultrasonic wave as well as the effect of diffusion.

In the present paper, it is the purpose of the authors to derive an equation based on the original proposal of Debye and incorporating the suggestions of Oka and Hermans. Several of the approximations involved in the development of Debye's equation have been modified.

II

At any instant the sum of the forces acting on an ion in solution must be equal to the product of its mass and acceleration:

$$e_jX-\rho_j(v_j-v_0)-e_j\left\{\frac{|e_1e_2|q\kappa X}{(3DkT)[1+\sqrt{q}(1+i\omega\Theta)^{\frac{1}{2}}]}\right\}$$

$$-\frac{e_jX\kappa\rho_j}{6\pi\eta_0}-\frac{kT}{n_j}\frac{\partial n_j}{\partial x}+V_js_0\frac{dv_0}{dt}=m_j\frac{dv_j}{dt}. \quad (1)$$

The first term[6] of this expression represents the force associated with an electrical component X on an ion of the jth sort with the electrical

[1] A portion of the thesis submitted by E. Yeager and J. Bugosh in partial fulfillment of the requirements for the degree of Master of Science in Chemistry at Western Reserve University, August 1946.

[2] A comprehensive survey (up to 1946) and critical analysis of methods for determining hydration values as well as a compilation of results is included in the thesis (footnote 1). The last published survey of such methods can be found in Z. Elektrochem. **28**, 161 (1922) and Kolloid-Zeits. **35**, 264 (1924) by R. Fricke.

[3] P. Debye, J. Chem. Phys. **1**, 13 (1933).

[4] S. Oka, Proc. Phys.-Math. Soc., Japan **13**, 413 (1933).

[5] J. J. Hermans, Phil. Mag. (7) **25**, 426 (1938); (7) **26**, 674 (1938).

[6] Throughout this mathematical development only the component (x) in the direction of propagation of the ultrasonic wave will be considered.

charge e_j. Multiplication of the frictional coefficient ρ_j by the differences between the velocity of the ions, v_j, and that of the solvent, v_0, gives the second term. The third term is the usual expression for the relaxation force where Θ is the relaxation time, ω the angular frequency of the oscillating electric field, k the Boltzmann constant, D the dielectric constant of the solvent, T the absolute temperature, and the quantity q is defined for the case in which only two sorts of ions are present by:

$$q=[e_1/\rho_1-e_2/\rho_2][(e_1-e_2)(1/\rho_1+1/\rho_2]^{-1}.$$

The fourth term represents the contribution of the electrophoretic force where η_0 is the viscosity of the solvent, and κ is the characteristic quantity of the Debye-Hückel theory, i.e., $1/\kappa$ is the thickness of the ionic atmosphere in centimeters. The diffusion force is represented by the fifth term where n_j is the number of ions of sort j per cubic centimeter of solution. The sixth term is the force associated with the pressure gradient where V_j is the volume of an ion of the jth sort, s_0 is the density of the solvent, and dv_0/dt is the acceleration of the solvent.

For the purpose of manipulation, Eq. (1) can be expressed in the form

$$e_jX(1-\kappa C_j)-\rho_j(v_j-v_0)-\frac{kT}{n_j}\frac{\partial n_j}{\partial x}+V_js_0\frac{dv_0}{dt}=m_j\frac{dv_j}{dt}, \quad (2)$$

where

$$C_j=\frac{q|e_1e_2|}{[3DkT][1+\sqrt{q}(1+i\omega\Theta)^{\frac{1}{2}}]}+\frac{\rho_j}{6\pi\eta_0}. \quad (3)$$

In order to solve these equations we note that we have j equations and $2j+1$ variables, namely, $n_1, n_2, \cdots n_j$; $v_1, v_2, \cdots v_j$; and the electrical field strength X. From the equation expressing the conservation of ions, we obtain j equations

$$\frac{\partial n_j}{\partial t}+\frac{\partial(n_jv_j)}{\partial x}=0. \quad (4)$$

From Poisson's relation we have the remaining equation

$$\partial X/\partial x=4\pi/D\sum_j n_je_j, \quad (5)$$

where $\partial X/\partial x$ represents the rate of change of the field strength component X with respect to distance.

Making the usual assumptions concerning periodic phenomena, we have

$$v_0=a_0\exp i(\omega t-\sigma x), \quad (6)$$

$$v_j=a_j\exp i(\omega t-\sigma x), \quad (7)$$

and

$$X=A\exp i(\omega t-\sigma x). \quad (8)$$

If g is the velocity of the sound wave in the solution, Λ its wave-length, and σ a constant, then

$$\sigma=\omega/g=2\pi/\Lambda. \quad (9)$$

Assuming further that the quantity n_j can be considered as made up of two parts, we obtain

$$n_j=\bar{n}_j+\nu_j, \quad \text{where } \nu_j\ll\bar{n}_j. \quad (10)$$

Then $\bar{n}_j$ will be a constant equal to the equilibrium value and will be subject to the neutrality restriction,

$$\sum_j \bar{n}_je_j=0. \quad (11)$$

The quantity ν_j will represent the periodic variations from the equilibrium value produced by the ultrasonic wave, so that

$$\nu_j=\alpha_j\exp i(\omega t-\sigma x). \quad (12)$$

Substituting the expressions (6), (7), (8), (10), (11), and (12) into Eqs. (2) and simplifying, we have

$$e_jA(1-\kappa C_j)-\rho_j(a_j-a_0)+\frac{kTi\sigma\alpha_j}{\bar{n}_j+\alpha_j\exp i(\omega t-\sigma x)}+iV_js_0a_0[\omega-a_0\sigma\exp i(\omega t-\sigma x)]=im_ja_j[\omega-a_j\sigma\exp i(\omega t-\sigma x)]. \quad (13)$$

Similarly, applying the same substitutions to Eqs. (5) and (4), we have

$$A=-(4\pi/Di\sigma)\sum_j e_j\alpha_j, \quad (14)$$

and

$$\alpha_j=\frac{\bar{n}_ja_j\sigma}{\omega-2\sigma a_j\exp i(\omega t-\sigma x)}, \quad (15)$$

since $\partial\bar{n}_j/\partial t=0$. Substituting the expressions for

α_j and A into Eq. (13) and simplifying, we obtain

$$a_j\rho_j+im_ja_j\omega-im_ja_j^2\sigma\exp i(\omega t-\sigma x)-\frac{kTi\sigma^2a_j}{\omega-\sigma a_j\exp i(\omega t-\sigma x)}$$

$$-\frac{e_ji4\pi}{D}\left[\sum_i\frac{e_i\bar{n}_ia_j}{\omega-2\sigma a_j\exp i(\omega t-\sigma x)}\right][1-\kappa C_j]-iV_js_0a_0[\omega-a_0\sigma\exp i(\omega t-\sigma x)]=\rho_ja_0. \quad (16)$$

If each term of Eq. (16) is multiplied by $\bar{n}_je_j/\rho_j$ and the j equations summed,

$$\sum_j\bar{n}_je_ja_j+i\omega\sum_j\bar{n}_je_jm_ja_j/\rho_j-i\sigma\exp i(\omega t-\sigma x)\sum_j\bar{n}_je_jm_ja_j^2/\rho_j$$

$$-kTi\sigma^2\left[\sum_i\frac{\bar{n}_je_j}{\rho_j}\left(\frac{a_j}{\omega-\sigma a_j\exp i(\omega t-\sigma x)}\right)\right]-is_0a_0[\omega-a_0\sigma\exp i(\omega t-\sigma x)]\sum_j\frac{\bar{n}_je_jV_j}{\rho_j}$$

$$-\frac{i4\pi}{D}\left[\sum_i\frac{\bar{n}_je_j^2}{\rho_j}(1-\kappa C_j)\right]\sum_i\frac{\bar{n}_je_ja_j}{\omega-2\sigma a_j\exp i(\omega t-\sigma x)}=a_0\sum_j\bar{n}_je_j=0. \quad (17)$$

To obtain a first order approximation we shall make the substitution,

$$a_j=a_0+\beta_j, \quad \text{where} \quad |\beta_j|\ll a_0 \quad (18)$$

in Eq. (17). If we apply the neutrality restriction (11) and consider the terms β_j^2, $\omega m_j\beta_j/\rho_j$, $\sigma\beta_j\exp i(\omega t-\sigma x)$, insignificant compared with $\omega-\sigma a_0\exp i(\omega t-\sigma x)$; and $\sigma a_0\exp i(\omega t-\sigma x)$ insignificant compared with ω; and

$$-kTi\sigma^2\left\{\sum_i\frac{\bar{n}_je_j}{\rho_j}\left[\frac{\beta_j}{\omega-\sigma a_0\exp i(\omega t-\sigma x)-\sigma\beta_j\exp i(\omega t-\sigma x)}\right]\right\}$$

insignificant compared with

$$-kTi\sigma^2\left\{\sum_i\frac{\bar{n}_je_j}{\rho_j}\left[\frac{a_0}{\omega-\sigma a_0\exp i(\omega t-\sigma x)-\sigma\beta_j\exp i(\omega t-\sigma x)}\right]\right\},^{7}$$

Eq. (17) becomes

$$\sum_j\bar{n}_je_j\beta_j=[ia_0^2\sigma\exp i(\omega t-\sigma x)\sum_j\bar{n}_je_jm_j/\rho_j-i\omega a_0\sum_j\bar{n}_je_jm_j/\rho_j$$

$$+(kTi\sigma^2a_0/\omega)\sum_j\bar{n}_je_j/\rho_j+i\omega s_0a_0\sum_j\bar{n}_je_jV_j/\rho_j][1-(i4\pi/\omega D)\sum_j\bar{n}_je_j^2/\rho_j(1-\kappa C_j)]^{-1}. \quad (19)$$

Combining Eqs. (11), (14), (15), and (18) and applying the above approximations, we obtain

$$A=(4\pi i/\omega D)\sum_j\bar{n}_je_j\beta_j. \quad (20)$$

By combining Eqs. (19) and (20),

$$A=\frac{4\pi a_0}{\omega D}\left\{\frac{\omega\sum_j\bar{n}_je_jm_j/\rho_j-(kT\sigma^2/\omega)\sum_j\bar{n}_je_j/\rho_j-\omega s_0\sum_j\bar{n}_je_jV_j/\rho_j}{1-(4\pi i/\omega D)[\sum_j\bar{n}_je_j^2/\rho_j(1-\kappa C_j)]}\right\}. \quad (21)$$

By Eq. (8)

$$X=A\exp i(\omega t-\sigma x)=-\partial\Phi/\partial x. \quad (22)$$

[7] These approximations can be verified by numerical calculations.

Substituting the expression for A into Eq. (22) and integrating, we obtain

$$\Phi=\frac{ga_0 4\pi}{\omega D}\left\{\frac{\sum_j \bar{n}_j e_j m_j/\rho_j-(kT\sigma^2/\omega^2)\sum_j \bar{n}_j e_j/\rho_j-s_0\sum_j \bar{n}_j e_j V_j/\rho_j}{i+(4\pi/\omega D)[\sum_j \bar{n}_j e_j^2/\rho_j(1-\kappa C_j)]}\right\}, \tag{23}$$

since $\sigma=\omega/g$. The constant of integration which would correspond to the normal electrode potential has been neglected since we are only interested in the effect of the ultrasonic waves.

If we multiply the expressions for $(1-\kappa C_j)$ obtained from Eq. (3) by $\bar{n}_j e_j^2/\rho_j$, and sum the resulting j equations,

$$\sum_j \frac{\bar{n}_j e_j^2}{\rho_j}(1-\kappa C_j)=\sum_j \frac{\bar{n}_j e_j^2}{\rho_j}-\frac{\kappa|e_1 e_2|}{3DkT}\left[\frac{q}{1+\sqrt{q(1+i\omega\Theta)}}\right]\sum_j \frac{\bar{n}_j e_j^2}{\rho_j}-\kappa\sum_j \frac{\bar{n}_j e_j^2}{6\pi\eta_0}. \tag{24}$$

The right side of Eq. (24) can be expressed in terms of measurable quantities if we realize that

$$\sum_j \bar{n}_j e_j^2/\rho_j=\lambda_\infty,$$

$$\kappa\sum_j \frac{\bar{n}_j e_j^2}{6\pi\eta_0}=\lambda_{II},$$

and

$$\frac{\kappa|e_1 e_2|}{3DkT}\left[\frac{q}{1+\sqrt{q(1+i\omega\Theta)}}\right]\sum_j \frac{\bar{n}_j e_j^2}{\rho_j}=\lambda_{I\omega}-\frac{i\omega}{4\pi}(D_\omega-D),$$

where λ_∞ is the specific conductance at infinite dilution, λ_ω the specific conductance at the angular frequency ω, $\lambda_{I\omega}$ the part of the specific conductance depending on the relaxation forces of the ionic atmosphere, λ_{II} the part of the specific conductance depending on the electrophoretic forces, and D_ω the dielectric constant of the solution at the angular frequency ω[8]. Remembering that $\lambda_\omega=\lambda_\infty-\lambda_{I\omega}-\lambda_{II}$, we can rewrite Eq. (24) as

$$\sum_j \bar{n}_j e_j^2/\rho_j(1-\kappa C_j)=\lambda_\omega+(i\omega/4\pi)(D_\omega-D). \tag{25}$$

If Eqs. (23) and (25) are combined,

$$\Phi=\frac{4\pi g a_0}{\omega D}\left[\frac{\sum_j \bar{n}_j e_j m_j/\rho_j-(kT\sigma^2/\omega^2)\sum_j \bar{n}_j e_j/\rho_j-s_0\sum_j \bar{n}_j e_j V_j/\rho_j}{4\pi\lambda_\omega/\omega D+iD_\omega/D}\right]\exp i(\omega t-\sigma x). \tag{26}$$

If we denote the amplitude of the alternating component of the potential by Φ_0, then

$$\Phi=\Phi_0\exp i(\omega t-\sigma x-\Delta), \tag{27}$$

where Δ represents the phase angle by which the alternating component lags behind the material wave. When Eq. (26) is written in the same form as Eq. (27),

$$\Delta=\arctan\frac{\omega D_\omega}{4\pi\lambda_\omega}, \tag{28}$$

[8] For the dependence of conductivity upon frequency, see H. Falkenhagen, *Electrolytes*, Trans. by R. P. Bell (Oxford University Press, Oxford, 1934), pp. 182–192.

and

$$\Phi_0=\frac{ga_0 4\pi}{\omega D}\left\{\frac{\sum_i \frac{\bar{n}_j e_j m_j}{\rho_j}-\frac{kT\sigma^2}{\omega^2}\sum_i \frac{\bar{n}_j e_j}{\rho_j}-s_0\sum_i \frac{\bar{n}_j e_j V_j}{\rho_j}}{\left[\left(\frac{D_\omega}{D}\right)^2+\left(\frac{4\pi}{\omega D}\lambda_\omega\right)^2\right]^{\frac{1}{2}}}\right\}. \tag{29}$$

Equation (29) may be put in a more practical form if we consider a solution containing n molecules of solute per cubic centimeter, every one of which splits into p_j $(j=1, 2)$ different ions of valence z_j $(j=1, 2)$. We may then write

$$\bar{n}_j=p_j\bar{n}, \quad e_j=z_j\epsilon, \quad \text{and also} \quad m_j=M_j m_H,$$

where ϵ is the magnitude of the electronic charge, M_j the gram-ionic weight, and m_H the mass of the hydrogen atom.[9] Applying these substitutions to Eq. (29) and multiplying the numerator by λ_∞ and the denominator by its equal, $\sum \bar{n}_j e_j^2/\rho_j$ we obtain

$$\Phi_0=\frac{4\pi g a_0\lambda_\infty}{\omega D\epsilon}\left\{\frac{m_H\sum_i \frac{p_j z_j M_j}{\rho_j}-\frac{kT}{g^2}\sum_i \frac{p_j z_j}{\rho_j}-s_0\sum_i \frac{p_j z_j V_j}{\rho_j}}{\left[\sum_i \frac{p_j z_j^2}{\rho_j}\right]\left[\left(\frac{D_\omega}{D}\right)^2+\left(\frac{4\pi}{\omega D}\lambda_\omega\right)^2\right]^{\frac{1}{2}}}\right\}. \tag{30}$$

The corresponding equation derived by Debye is

$$\Phi_0=\frac{4\pi g a_0\lambda_\infty}{\omega D\epsilon}\left\{\frac{m_H\sum_i \frac{p_j z_j M_j}{\rho_j}}{\left[\sum_i \frac{p_j z_j^2}{\rho_j}\right]\left[1+\left(\frac{4\pi}{\omega D}\lambda_\infty\right)^2\right]^{\frac{1}{2}}}\right\}.$$

Equation (30) is identical with that of Debye if the following approximations are made:

$$D_\omega/D=1; \quad \lambda_\omega=\lambda_\infty;$$

$$kT/g^2\sum_j p_j z_j/\rho_j=0;$$

$$s_0\sum_j p_j z_j V_j/\rho_j=0.$$

The first two of these approximations are equivalent to neglecting the electrophoretic and relaxation forces, while the third and fourth are equivalent to neglecting the corrections for diffusion and the pressure gradient, respectively.

In order to show that the equation as developed satisfied the requirement, previously stated, that no alternating component exists when the density of the solvent is equal to the density of the ions, Eq. (30) may be written

$$\Phi_0=c\left(\frac{c'+m_H\sum_j p_j z_j M_j/\rho_j-m_H s_0\sum_j p_j z_j M_j/\rho_j d_j}{\sum_j p_j z_j^2/\rho_j}\right), \tag{31}$$

[9] The choice of the hydrogen atom is made here to facilitate a comparison with the equation of Debye. To be exact, m_H should be replaced by the mass of the oxygen atom divided by sixteen.

where d_j is the density of an ion of the jth sort, and c and c' are defined by

$$c=\frac{4\pi g a_0 \lambda_\infty}{\epsilon\omega D[(D_\omega/D)^2+(4\pi\lambda_\omega/\omega D)^2]^{\frac{1}{2}}},$$

$$c'=-kT/g^2\sum_j p_j z_j/\rho_j.$$

If we apply Eq. (31) to a uni-univalent salt represented by

$$AB\rightleftharpoons A^+ + B^-,$$

then

$$\Phi_0=c\left[\frac{c'+\left(\frac{1}{\rho_A}-\frac{s_0}{\rho_A d_A}\right)m_H M_A-\left(\frac{1}{\rho_B}-\frac{s_0}{\rho_B d_B}\right)m_H M_B}{1/\rho_A+1/\rho_B}\right].$$

When $s_0=d_B$, Φ_0 will depend only upon the mass of ion A; when $s_0=d_A$, Φ_0 will depend only upon the mass of ion B; when $s_0=d_A=d_B$, Φ_0 is no longer a function of the masses of the solvated ions and we have the equation

$$\Phi_0=-\frac{ckT}{g^2}\left(\frac{\rho_B-\rho_A}{\rho_B+\rho_A}\right).$$

Thus, the potential differs from zero only by a term representing the small correction for diffusion.

In view of the optimism expressed by other workers[10–13] both at the time of the original proposal as well as for several years later, it seems strange that no one has successfully detected the effect in the case of electrolytic solutions.[14] Debye recently restated his belief in the existence of the effect.[15] In 1933 Debye expressed the opinion that the measurement of the effect should be comparatively simple. Other investigators,[16] as well as the authors, have reached the conclusion that this was an understatement. While the measurement of an alternating component whose magnitude is approximately one microvolt is simple in itself, the features of this experiment make it difficult. Whether the ultrasonic waves are produced by means of a piezoquartz crystal or magnetostriction, the electrodes employed in detecting the effect must come comparatively close to lead wires of the ultrasonic generator carrying radio-frequency current, and unless extreme precautions with respect to shielding are exercised, direct coupling between the detection apparatus and the radio-frequency generator will result.

Apparatus has been developed by the authors for the detection of this effect. Experimental work is in progress and will be published in the near future.

The authors wish to acknowledge the valuable assistance of Professor M. G. Boyce of the Mathematics Department at Western Reserve University and Mr. Charles Fletcher of the Physics Department at Western Reserve University in critically examining this paper.

[10] H. Falkenhagen, *Electrolytes* (Oxford University Press, 1933), p. 170.

[11] N. A. McKenna, *Theoretical Electrochemistry* (D. Van Nostrand Company, New York, 1938), p. 350.

[12] R. P. Bell, Ann. Rep. Prog. Chem. **31**, 67 (1934).

[13] J. Baborovsky, Collection Czechoslov. Chem. Commun. **10**, 557 (1938).

[14] Although this effect has not been found for electrolytes, the effect has been observed in the case of colloidal solutions. A. Rutgers, Physica **5**, 46 (1938); Nature **157** [3977], 74 (1946).

[15] In personal correspondence (November 1945).

[16] A. Rutgers, Physica **5**, 46 (1938); Nature **157** [3977], 74 (1946).

Absorption Spectrum of Borazole in the Vacuum Ultraviolet

J. R. PLATT
Physics Department, University of Chicago, Chicago, Illinois

H. B. KLEVENS* AND G. W. SCHAEFFER
Chemistry Department, University of Chicago, Chicago, Illinois

The absorption spectra of triborine-triamine or borazole, $B_3N_3H_6$, has been studied with a fluorite vacuum spectrograph in the region 2250–1700A in *n*-heptane solution. The compound was prepared by the reaction between diborane and ammonia.

Four diffuse bands are found, starting at 1995A, with spacing about 900 cm^{-1}. These seem analogous to the 2000A bands of benzene, but the intensity is about 10 times smaller. A strong continuum, like the 1800A benzene peak, has its maximum at 1720A or below. No bands like the benzene 2600A group were found, though they would have been seen if their intensities had been only 1/20th that of the latter.

The spectrum of a boron hydride, B_5H_9, has also been obtained but shows only a featureless continuum in this wave-length region.

INTRODUCTION

THE absorption spectra of triborine-triamine or borazole, $B_3N_3H_6$, and of a boron hydride, B_5H_9, have been studied in the region 2250–1700A. The compounds were studied in *n*-heptane solution in an 0.13-mm cell.

The borazole spectrum is much like that of benzene. This similarity is reasonable from the resemblances between the electronic structures in the two compounds. Borazole, which is isoelectronic with benzene, exhibits properties so similar to that compound that it has frequently been called "inorganic benzene." On the basis of chemical properties,[1,2] electron diffraction,[3] isomer number,[4] and infra-red and Raman spectra,[5] the compound has been demonstrated to have a ring structure analogous to benzene. Resonance between structure I and the two equivalent structures of type II is probably adequate to describe the molecule.[1] The contribution of structures II is evident from the decrease in the B−N bond distance which is 1.44A for borazole compared with 1.62A for the simple B−N bond as observed in trimethylaminoborine.[6]

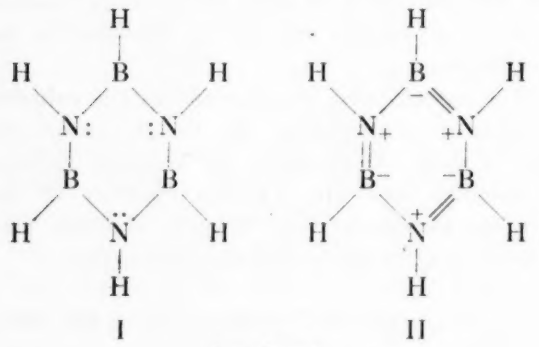

I (two forms) II

APPARATUS AND TECHNIQUE

The Cario-Schmitt-Ott fluorite vacuum spectrograph used in the present work was kindly loaned to us by the University of Michigan. Absolute intensities were measured by methods like those described earlier.[7] However, the sector-rotor used before for photometric calibration was not available, and the calibration was performed by use of timed exposures, the correction for reciprocity failure being obtained with the help of calibrated screens. Below 1800A, where the light source is relatively weak, it was necessary to make a correction for scattering in the spectrograph, and the absolute values are less reliable in this region. The correction was estimated by extrapolation from measurements of the scattered background light below 1700A

* Present address: Research Laboratories, the Firestone Tire & Rubber Company, Akron, Ohio.

[1] E. Wiberg and A. Bloz, Berichte **73**, 209 (1940).
[2] A. Stock and E. Pohland, Berichte **59**, 2215 (1926).
[3] S. H. Bauer, J. Am. Chem. Soc. **60**, 524 (1938).
[4] H. I. Schlesinger, L. Horwitz, and A. R. Burg, J. Am. Chem. Soc. **58**, 409 (1936).
[5] B. L. Crawford, Jr. and J. T. Edsall, J. Chem. Phys. **7**, 223 (1939).
[6] S. H. Bauer, J. Am. Chem. Soc. **59**, 1804 (1937).
[7] J. R. Platt, I. Rusoff, and H. B. Klevens, J. Chem. Phys. **11**, 535 (1943).

where the *n*-heptane solutions are known to be completely opaque.

Extinctions computed from different plates are consistent to ±20 percent, and the mean values given here are believed to be accurate to the same figure. Particular pains were taken to get higher accuracy in measuring the intensity fluctuations in the diffuse vibrational structure in the borazole. Positions of maxima and minima could be estimated visually to 2 or 3A on these bands.

BORAZOLE

Preparation[8]

Borazole, $B_3N_3H_6$, was prepared by the reaction between diborane and ammonia using a modification of the procedure given by Schlesinger, Ritter, and Burg.[9] Ammonia, about 2 liters, is carefully condensed in a uniform film on the wall of a 1-liter reaction tube which is provided with a side-arm break-off tip and attached to a vacuum apparatus. Diborane, exactly one mole for each two moles of ammonia taken, is condensed on to the ammonia film by means of liquid nitrogen. The reaction tube is allowed to warm slowly to −112°C, and it is allowed to stand at this temperature until the total pressure is less than 0.5 mm. The tube is then evacuated for several minutes, sealed from the vacuum apparatus, and immediately placed in a furnace at 300°C for 30 minutes. The reaction tube is reattached to the vacuum apparatus by means of a tube-opener, cooled with liquid nitrogen, opened, and the hydrogen removed. The tube is heated to 60°C, and the volatile material is transferred to the vacuum apparatus for purification. The product is purified by fractional condensation through −80°C, −112°C, and −196°C baths. Pure borazole (vapor tension[1] at 0°C, 85.4 mm; observed, 85.3 mm) is trapped at −112°C. The yield is 35 to 40 percent based on the diborane taken.

The heptane solutions were prepared in the vacuum apparatus. The borazole was measured as the gas (568 cc at 28°C and 138 mm pressure) and the *n*-heptane as the liquid (10.23 cc). The measured amounts of the two substances were distilled into a tube, sealed from the apparatus, and stored in the sealed tube until just before use.

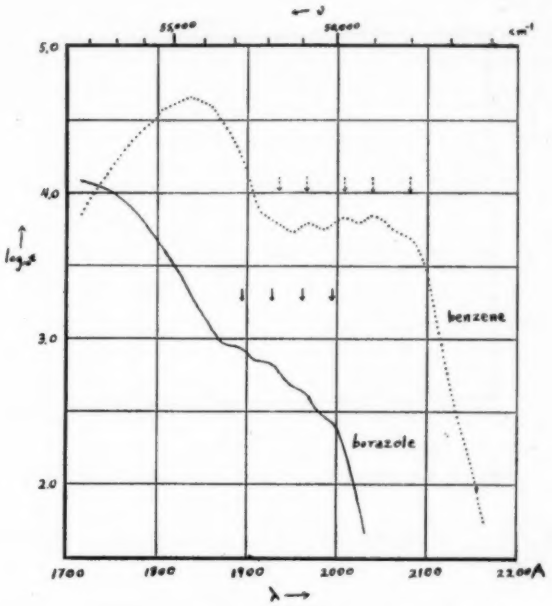

FIG. 1. Absorption spectrum of borazole ($B_3N_3H_6$) and benzene in *n*-heptane solution.

Spectrum

The absorption spectrum of the borazole in *n*-heptane solution is shown in Fig. 1, together with the spectrum of benzene in *n*-heptane solution for comparison. The benzene curve is taken from another paper.[10] The positions of the maxima in the 2000A region, as estimated visually, are indicated by arrows on the graph. In borazole, these maxima are as follows:

1995A	50,100 cm^{-1}
1962	50,950
1928	51,850
1895	52,750

The spacing in this series is about 900 cm^{-1}. Within the accuracy of measurement this may be taken to agree with either of the totally symmetric frequencies, 851 and 938 cm^{-1}, already

[8] The experimental methods used in the chemical part of this work are described in the publications of Schlesinger and co-workers, Chem. Rev. **31**, 1 (1942) and of Stock, *The Hydrides of Silicon and Boron* (Cornell University Press, Ithaca, New York, 1933).

[9] H. I. Schlesinger, D. M. Ritter, and A. B. Burg, J. Am. Chem. Soc. **60**, 1296 (1938).

[10] J. R. Platt and H. B. Klevens, Paper presented at Symposium on Color and Electronic Spectra of Complex Molecules, Division of Physical and Inorganic Chemistry of the American Chemical Society meeting at Evanston, Illinois, December 30–31, 1946 (to be published in Chem. Rev.).

known in the ground state.[5] In benzene, also, the excited states show little change in the breathing frequency.

At shorter wave-lengths, the absorption curve of borazole rises to intensities characteristic only

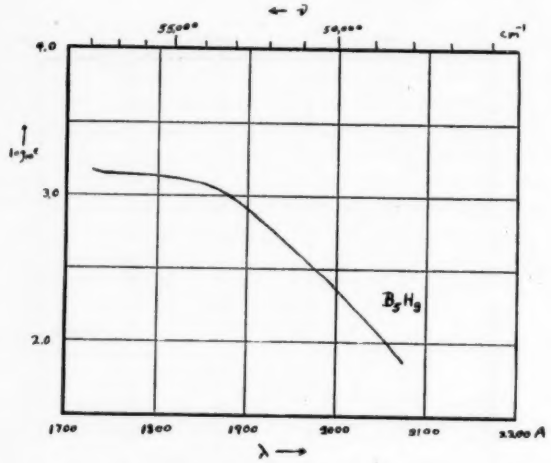

FIG. 2. Spectrum of B_3H_9 in *n*-heptane solution.

of $N \rightarrow V$ transitions.[11] The peak must lie below 1720A.

DISCUSSION

If we assume complete sharing of the free electron pair on each nitrogen by a boron and nitrogen atom together, the electronic structure of borazole becomes identical with that of benzene. One would expect, therefore, the upper levels of the borazole to correspond with those of benzene and the same characteristic bands to be present in both spectra.[12]

The striking similarity of the spectra is seen in Fig. 1. It appears that the diffuse series in borazole starting at 1995A may be identified with the diffuse benzene $^1A_{1g} \rightarrow {}^1B_{1u}$ series starting at 2080A.[13] The strong continuum in borazole rising to a peak at 1720A or below must then correspond to the $^1A_{1g} \rightarrow {}^1E_{1u}$ benzene peak at 1830A (also called the $N \rightarrow V$ transition).

Against these identifications is the low intensity of the 1995 borazole bands and the failure to find bands like the 2600A benzene group, even though the highest borazole concentration used was twenty times as strong as that necessary for detecting these bands in benzene.

Nevertheless, three aspects of the spectrum favor this assignment. First, there is the smallness of the frequency shifts between the borazole and benzene spectra if we adopt this assignment —only 2000 cm^{-1} shift for the 1995A group, and perhaps 4000 or 5000 cm^{-1} for the $N \rightarrow V$ peak; any other correspondence between the bands would involve much larger wave-length shifts. Second, there is the similarity in appearance between the 1995A and 2080A groups. The diffuse 1995A group is only slightly more diffuse than the 2080A group and does not look anything like the sharp, strongly shaded bands of the 2600A benzene group, nor like the almost structureless $N \rightarrow V$ peak. Third, there is the very great absorption intensity of borazole at 1720A, with a molar extinction, ϵ, of over 10,000/mole-cm, which is stronger than has been

[11] The notation $N \rightarrow V$ for certain transitions in olefins and ring compounds is attributable to Mulliken. See Mulliken and Rieke, Rep. Prog. Phys. (Phys. Soc. Lond., 1941) **8**, 231.

[12] Professor R. S. Mulliken has shown that a detailed theoretical analysis supports this conclusion. We are indebted to him for the following statement which he has prepared for inclusion here:

"In benzene, the absorption regions λ2600, λ2000, and λ1800 are believed to correspond to transitions from a $^1A_{1g}$ normal state having electron configuration $\cdots(1a_{2u})^2(1e_{1g})^4$, to the three respective states $^1B_{2u}$, $^1B_{1u}$, and $^1E_{1u}$ of the excited electron configuration $\cdots(1a_{2u})^2(1e_{1g})^3 1e_{2u}$. The symbols are group theory symbols of the usual type for over-all electronic states (capital letters) or for outer-electron molecular orbitals (small letters), and appropriate to the symmetry group of benzene (D_{6h}). The transitions $^1A_{1g} \rightarrow {}^1B_{2u}$ and $^1A_{1g} \rightarrow {}^1B_{1u}$ are forbidden according to the electronic selection rules for symmetry D_{6h}, while $^1A_{1g} \rightarrow {}^1E_{1u}$ is strongly allowed for radiation with electric vector vibrating in the plane of the molecule.

"The symmetry of borazole, assuming a planar arrangement of maximum symmetry, is D_{3h}. Although this symmetry is lower than that of benzene, nevertheless it can be shown that a one-to-one correspondence and a close resemblance between the electron configurations and over-all states of borazole and benzene are to be expected. Using symbols appropriate to D_{3h} symmetry, the normal state should be a $^1A_1'$ state of configuration $\cdots(1a_2'')^2(1e'')^4$, and there should be low excited states $^1A_2'$, $^1A_1'$, and $^1E'$, all of electron configuration $\cdots(1a_2'')^2(1e'')^3 2e''$. (Here, as in benzene, there should also, of course, be corresponding triplet states.) Further, the transitions from the $^1A_1'$ to the $^1A_2'$ and $^1A_1'$ excited states are forbidden by the electronic selection rules, while that to the $^1E'$ state is strongly allowed for radiation with dipole moment vibrating in the molecular plane, in complete analogy to benzene.

"The analogy extends even further. In benzene, the occurrence of the 'forbidden' transitions $^1A_{1g} \rightarrow {}^1B_{2u}$ and $^1A_{1g} \rightarrow {}^1B_{1u}$ is explained mainly by coupling (of the upper or lower) electronic state with a degenerate vibration of class E_{2g} (the same for both transitions). In close analogy, the occurrence of $^1A_1' \rightarrow {}^1A_2'$ and $^1A_1' \rightarrow {}^1A_1'$ in borazole would be expected through coupling with a degenerate vibration of class E' (the same for both transitions)."

[13] M. Goeppert-Mayer and A. L. Sklar, J. Chem. Phys. **6**, 645 (1938).

observed in this region in solution for any but $N \rightarrow V$ transitions.

These similarities then lend further support to the postulated ring structure and electronic structure of borazole.

But then the problem arises of explaining the relative weakness of the 1995A group in borazole and the absence of any group near 2600A. However, since in benzene these are forbidden transitions deriving their strength from interaction with the allowed $N \rightarrow V$ transition through electronic-vibrational coupling,[12,13] it may be that the interaction constant for the 1995A transition is simply smaller in borazole by a factor of 10 or more. Perhaps this constant is relatively smaller still for the bands corresponding to the 2600A group, and as a result they have not been found simply because high enough concentrations or vapor pressures have not yet been used.

The relation between benzene and borazole is like that between graphite and boron nitride crystals. It is well known that the BN is built up of hexagonal "borazole" units (with hydrogens omitted) as graphite is built of "benzene" units.

The physical characteristics of graphite, with its infinite lattice of conjugated double bonds, are closely duplicated in boron nitride. The only great change is one of color—from black to white. This may be related to the changes found here in going from benzene to borazole—a shift of the spectrum to shorter wave-lengths and a great relative weakening of the long wave-length bands. The electrical characteristics of BN, such as its semiconductivity and photo-conductivity in the ultraviolet, deserve to be investigated for the light they may throw on these relationships.

A BORON HYDRIDE

We have also obtained the spectrum of one of the boron hydrides, B_5H_9, in *n*-heptane solution in the same wave-length region. Dr. A. E. Finholt kindly made up the sample for us in the solution. The observed spectrum is shown in Fig. 2. It is a featureless continuum, increasing in intensity to a molar extinction of over 1500 per mole-cm below 1740A. There is too little structure to make possible any conclusions for or against current theories of the B_5H_9 molecule.[14] Vapor measurements at shorter wave-lengths are indicated to be necessary.

We wish to thank our colleagues in the Physics and Chemistry Departments, and in particular Professor R. S. Mulliken, for helpful discussions on the interpretation of these spectra.

[14] K. S. Pitzer, J. Am. Chem. Soc. **67**, 1126 (1945).

THE JOURNAL OF CHEMICAL PHYSICS VOLUME 15, NUMBER 8 AUGUST, 1947

The Thermodynamic Properties of Water Substance 0° to 150°C

PART VI *

FREDERICK G. KEYES
Department of Chemistry, Massachusetts Institute of Technology, Cambridge, Massachusetts

(Received April 7, 1947)

Commitments regarding additional research on the properties of water in the region below 200°C made on the occasion of the Third International Conference on Steam Tables in 1934 have been largely completed. Correlation of all new data using James A. Beattie's determinations of the relation of the International temperature scale of 1927 to the thermodynamic scale discloses a high degree of thermodynamic consistency from 0° to 150°C between thermal data, vapor pressures, and equation of state information. The proposed vapor pressures over the temperature range are probably accurate to ±0.002°C. New measurements of vapor pressure over the range are, however, desirable but the ultimate in refinements of temperature control and pressure accuracy should be sought if the indicated discrepancies are to be resolved. Tables of vapor pressure, pressure-temperature derivatives, essential temperature-scale magnitudes, enthalpies, and entropies are given. An equation of state for steam is reported from 0° to 460°C, valid for low pressures and based on the ensemble of volume data and enthalpy pressure coefficients available.

FOLLOWING the publication of tables of the thermodynamic properties of steam in 1936,[1] additional research was undertaken at M.I.T. to obtain experimental confirmation[1a] of the properties of the gaseous phase of water estimated in part by extrapolation in the region below 200°C, a region which had proved virtually impossible of precise exploration by the volume-measuring methods used in the temperature range from 460° to 200°C. The formulation of the volume properties of the gaseous phase in the latter region led to an equation of state $v = F(pT)$,[2] which was used to compute derived properties in the low pressure saturated and super-heated region; justification was secured from the agreement of computed specific volumes between 100 and 200°C with the measurements by Knoblauch, Linde, and Klebe,[3] Joule-Thomson computed coefficients with the measurements of Davis and Kleinschmidt,[4] and other deductions following from thermodynamic relationships.

The additional investigation of steam properties referred to above and begun in 1932[5] soon proved to be of considerable technical difficulty, but a final report was published in 1938.[6] It dealt with the direct determination by a continuous-flow method of the enthalpy variation of steam with pressure from 38° to 125°C. In the same apparatus measurements were also made of the heat capacity in such a way as to lead to C_p^0 values which could be compared with those computed from spectroscopic observations. From the pressure variation of the enthalpy at con-

* Parts I–V have appeared as follows: Part I. Frederick G. Keyes, "Methods and procedures used in the Massachusetts Institute of Technology program of investigation of the pressures and volumes of water to 460°C," Proc. Am. Acad. **68**, 505 (November, 1933); Part II. Leighton B. Smith, Frederick G. Keyes, and Harold T. Gerry, "The vapor pressure of water," *ibid.* **69**, No. 3, 137 (January, 1934); Part III. Leighton B. Smith and Frederick G. Keyes, "Volumes of unit mass of liquid water and their correlation as a function of pressure and temperature," *ibid.* **69**, No. 7, 285 (April, 1934); Part IV. Frederick G. Keyes, Leighton B. Smith, and Harold T. Gerry, "The specific volume of steam in the saturated and superheated condition together with derived values of the enthalpy, entropy, heat capacity and Joule Thomson coefficients," *ibid.* **70**, No. 8, 319 (February, 1936); Part V. Samuel C. Collins and Frederick G. Keyes, "The heat capacity and pressure variation of the enthalpy for steam from 38° to 125°C," *ibid.* **72**, No. 8, 283 (April, 1938).

[1] J. H. Keenan and F. G. Keyes, *Thermodynamic Properties of Steam* (John Wiley and Sons, Inc., New York, 1936).

[1a] See Mech. Eng. **57**, 710 (1935) for the report on the Third International Conference on Steam Tables. There will be found in this reference the commitments made by the several participating national groups with respect to further research. The contributions by the group at M.I.T. have been partially fulfilled and would have been completed but for the war. An important part of the fulfilled commitment is used in the present paper.

[2] F. G. Keyes, L. B. Smith, and H. T. Gerry, Proc. Am. Acad. Arts and Sci. **70**, 319 (1936).

[3] O. Knoblauch, R. Linde, and H. Klebe, Mitteilung über Forschungsarbeiten auf dem Gebeite des Ingenieurwesens (Julius Springer, Berlin, 1905), Heft 21.

[4] R. V. Kleinschmidt, Mech. Eng. **48**, 155 (1926); H. N. Davis and J. H. Keenan, World Eng. Conf. Reports, Tokyo (1929).

[5] F. G. Keyes and S. C. Collins, Nat. Acad. Sci. **18**, 328 (1932).

[6] S. C. Collins and F. G. Keyes, Proc. Am. Acad. Arts and Sci. **72**, 283 (1938).

stant temperature, important new information bearing on the equation of state was secured confirmatory of the general accuracy of the extrapolations below 200°C referred to earlier.

Another investigation of importance for low pressure properties of water was published by Moser and Zmaczynski[7] in 1939. In this investigation new and highly precise data for the vapor pressure of water from 73.5° to 128.6°C were obtained—very welcome information since no new data had appeared for the region below 100°C since the work of Holborn and Henning (1908) and Scheel and Heuse (1910).[8] Since precision and reproducibility in thermometry have improved notably since 1920, the new low vapor-pressure measurements assist greatly in resolving a difficulty which will be apparent in what follows.

Finally, a highly important series of measurements from 0° to 100°C of the vaporization quantity $vTdp/dT$, or γ, and also the heat capacity of the liquid phase were published in 1939 by Osborne, Stimson, and Ginnings.[9] The new heat measurements are remarkably precise and provide additional information needed to apply the test of thermodynamic consistency to the ensemble of available data.

In addition to the new steam data now available, portions of the extensive thermometric investigations which James A. Beattie and his collaborators have carried out have been published and can be used to fill a gap in our knowledge of the relation of the international temperature scale to the thermodynamic scale. A considerable part of these extraordinarily precise investigations bear on platinum resistance thermometry, gas thermometry, and the position of fixed points in the range zero to the normal boiling point of sulfur. A new fixed point, the N.B.P. of mercury, has been determined[10] and its use shown to be necessary for reproducing the thermodynamic scale by means of the platinum resistance thermometer from 0° to 444.7°C.

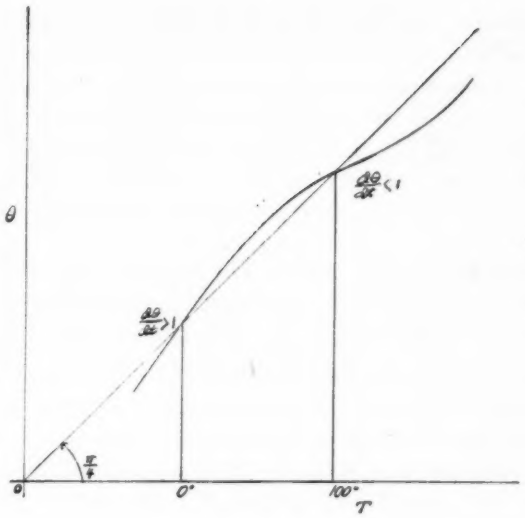

FIG. 1.

The thermometric measurements of more immediate usefulness for the purpose of the present paper have not yet appeared in detail,[10a] namely the results of the comparisons of the indications of the platinum resistance thermometers conforming to the specifications of the international scale (Θ scale) of 1927[11] and the nitrogen gas thermometer at 0, 25, 50, 75, 100, 150, 200, 250, 300, 400°C and the N.B.P. of sulphur. The thermodynamic temperatures (T scale) at these points were determined by extrapolation to zero pressure of the gas-thermometer readings at ice-point pressures 0.6, 0.45, and 0.333 meters of mercury, and also by utilizing virial coefficients for nitrogen.[12] I am grateful to Professor Beattie for his generosity in placing his values of $(T-\Theta)$ at my disposal. The use of the latter values in the present paper will illustrate the fundamental importance of a knowledge of the relation of the thermodynamic or T scale to the scale in common use, Θ scale, when applying the test of thermodynamic consistency.

There are two aspects presented in the use of the quantity $(T-\Theta)$. These are, first, the direct use in transferring a quantity, for example a measured pressure, from the Θ scale to the ther-

[7] H. Moser and A. Zmaczynski, Phys. Zeits. **40**, 221 (1939).

[8] L. Holborn, K. Scheel, and F. Henning, *Wärmetabellen* (Friedrich Vieweg und Sohn, Braunschweig, Germany, 1919).

[9] N. S. Osborne, H. F. Stimson, and D. C. Ginnings J. Research Nat. Bur. Stand. **23**, 197 (1939).

[10] J. A. Beattie, "The thermodynamic temperature of the ice point," in *Temperature* (Reinhold Publishing Company, New York, 1941), p. 74.

[10a] Edwin Blaisdell and Joseph Kaye, "Location of the normal sulphur and mercury boiling points on the thermodynamic temperature scale," in *Temperature* (Reinhold Publishing Company, New York, 1941), p. 127.

[11] G. K. Burgess, J. Research Nat. Bur. Stand. **1**, 635 (1927).

[12] F. G. Keyes, "Gas thermometer scale, *Temperature* (Reinhold Publishing Company, New York, 1941), p. 45.

TABLE I. v_g cc per gram.

t°C	1936 Steam Tables	Goff and Gratch	Percent difference S.T.-G.G.	1934 tolerance cc
40	19546.2	19546.0	+0.0010	±19.0
60	7679.3	7679.9	−0.0078	± 7.7
100	1673.07	1673.13	−0.0036	± 1.7

modynamic or T scale. The second, and often the more important case relates to considerations involving derivatives, $dp/dT=(dp/d\Theta)(d\Theta/dT)$, for example, in thermodynamic equations. The essential features of the situation may be made clear by reference to the diagram, Fig. 1.

The line at $\pi/4$ in the Θ, T diagram defines a set of points for which $\Theta=T$; $d\Theta/dT\gtrless1$. The curve passing through the fixed points 0 and 100°C is drawn representative of the course of the experimentally determined points for the relation of the international to the thermodynamic scale as determined by Beattie. It will be noted that at some point between 0 and 100°C the course will be parallel to the $\pi/4$ line, or $d\Theta/dT=1$ although $T\neq\Theta$. The ratio $d\Theta/dT$ is clearly almost, if not exactly, unity at 50°C. The following type of situation often arises. A quantity is measured at 100°C, for example $\gamma=(L+v_fTdp/dT)=v_gTdp/dT$, where L is the heat of evaporation, v_f the specific volume of the saturated liquid, v_g that of the saturated vapor, T the thermodynamic temperature, and p the pressure, which is to be compared with the calculated value of γ. The value of v_g may be assumed given by the equation of state, Eq. (8), namely 1673.27 cc per g, while the value of dp/dT from Table III is 27.122 mm, or 0.0356868 atmos. Accordingly, v_gTdp/dT becomes 2257.38 i.j. (international joules). But $d\Theta/dT$ from Table III is 0.999653 and $v_g\Theta dp/d\Theta=2258.16$ i.j. The mean observed value (17 observations) from the 1939 published report of Osborne, Stimson, and Ginnings[9] is 2257.32 i.j. It is therefore clear that thermodynamic correlation of vapor pressure data and volume data with calorimetric data without a knowledge of $d\Theta/dT$ would be impossible, even at a fixed point, for data accurate to better than a part in 3000. At 50°C the $d\Theta/dT$ is sufficiently close to unity for every practical purpose. However, Θ differs from T by about 0.01°C; a quantity too small, of course, to be practically significant for some purposes.

The present paper will contain the results of a thermodynamic correlation of the available experimental data on the vapor pressure, the pressure-temperature derivatives, the volumes, heats of evaporation, and enthalpies. The result desired is a set of values of these properties at round temperatures accompanied by an estimate of their accuracy for the temperature range 0° to 150°C. The investigation will provide additional values of steam properties in the range regarded with some uncertainty by the delegates of Great Britain, the United States, Germany, and Czechoslovakia participating in the Third International Conference on Steam Tables held in Washington, New York, and Boston during September 1934.[1a] The skeleton table of properties, Table I of the reference, will have the prospect of being assigned tolerances considerably smaller at such time as a new conference may convene. A brief statement regarding the author's conception of the meaning attached to the concept of tolerances follows. In making the statement, however, it will be understood that what is expressed comprises personal impressions of a former delegate to the Steam Tables Conference. The statement has no official status whatever.

By way of brief review of research on water, the American Society of Mechanical Engineers sponsored a series of investigations of its properties in the early 1920's. The A.S.M.E. Steam Tables Committee, under the able chairmanship of George A. Orrok, very soon solicited the collaboration of British, German, and Czechoslovak colleagues, which resulted in a coordinated research program of international scope. During the three conferences, London 1929, Berlin 1930, U.S.A. 1934, the results of the investigations in progress were reviewed and the work of the conferees culminated in Table I, with assigned tolerances by the end of the 1934 conference.[1a] The tolerances set are *not*, however, definitive estimates of the accuracy* of the quantities to which they are attached. The primary purpose of setting tolerances was to narrow the range of values

* The connotation attaching to the term "accuracy" used here is that of the relation of an observed magnitude to the "true" value. The term "precision" is taken to mean the reproducibility of observations. An observer may secure precise results which are quite inaccurate.

which would be acceptable in an "international" table of properties. This is a matter of great convenience because prior to the first tables of properties of steam formulated by J. H. Keenan in 1930, the range and accuracy of the fundamental data was too restricted in both accuracy and extent for modern turbine design and test requirements. A table within the tolerances set is known to be of sufficient accuracy for practical purposes, and has the great merit of bringing the interpretation of tests and specifications into a uniform state for ready evaluation. An illustration of the meaning of a tolerance would be the value of the vapor pressure of water at 0°C. Since this is a fixed point on the temperature scale, the temperature assignment is unassailable. The pressures observed at different times by different investigators indicates that the precision may be expressed by the number 4.580 mm±0.001 with a maximum spread of 0.0036 mm. The tolerance assigned, however, is ±0.0044 mm. Another example: the volume of the vapor at 100°C and 1-atmos. pressure is given as 1673.2 ccg^{-1}±1.7 cc, but there is convincing evidence that the accuracy of the number is two or perhaps threefold less than the tolerance assigned.

It will be clear from the foregoing examples of the meaning of the term "tolerance" that it would be misleading to conclude, as has been done recently,[13] that Table I and Table II[1] of the saturation properties below 100°C are inaccurate. Thus the authors state "uncertainties of at least ±0.04 percent at 104°F, ±0.08 percent at 140°F, and ±0.10 percent at 212°F must be assigned to the steam table values of v_g." The values preferred by Goff and Gratch appear in Table I below, along with similar values from Table I of the Steam Tables.[1]

The actual volumes listed by Goff and Gratch at 40°C and 60°C are given for pressures on the thermodynamic scale. They have been changed to correspond to pressures on the international scale used for the Steam Tables.

THE VAPORIZATION MEASUREMENTS

The measurements of γ or $v_g T dp/dT$ in the range 0 to 100°C made by Osborne, Stimson, and Ginnings[9] were carried out in a third, especially constructed, apparatus after 155 measurements[14] at eight temperatures had been made in the first calorimeter in the range from 100° to 270°C, and 214 measurements in a second apparatus at 19 temperatures in the range 100 to 374° (critical temperature 374.13°C). The measurements in the range 0 to 100°C represent a high point in the science and art of heat measurements. They are listed in Table II, the first column of which lists temperatures in degrees C on the international scale. The second column lists the values of $(T-\Theta)$ from Beattie's lower temperature comparisons of the thermodynamic and international scales. The third and succeeding columns give the values of the arithmetic means of the γ-measurements, the average of the sum of the deviations from the average value of γ at each temperature, the square root of the average value of the sum of the squares of the deviations from the arithmetic average values of γ, or the standard deviation s.[15] The sixth column gives values of γ calculated with the empirical equa-

TABLE II. The first column lists centigrade temperatures on the international, Θ-scale, followed by the difference between the international and thermodynamic scales. The third column lists observed mean values of the vaporization quantity $\gamma = v_g T dp/dT$, designated γ_{obs} for water. The fourth and fifth columns contain the average deviation from the means of γ_{obs} and the standard deviation, $s = [\Sigma(x_i - \bar{x})^2/n]^{\frac{1}{2}}$. The smoothed values, or γ_{sm}, are followed by the ratios $(RT/pv)_s$ at saturation.

1	2	3	4		5	6	7	8
t_Θ	$(T-\Theta)$	γ_{obs}	Dev. from weighted mean		s	γ_{sm} Eq. (2)	$(RT/pv)_s$ Eq. (8)	$\gamma_{sm} \times (RT/pv)_s$
0		2500.72	0.124	(5)†	0.137	2500.51	1.00053	2501.78
1	−0.0004	2497.92	0.285	(15)	0.321			
5	−0.0011	2488.34	0.089	(11)	0.100	2488.63	1.00064	2490.25
10	−0.0041	2476.73	0.263	(14)	0.281	2476.80	1.00081	2478.80
15	−0.0060	2464.81	0.262	(6)	0.376	2465.00	1.00100	2467.34
20	−0.0075	2453.36	0.312	(10)	0.382	2453.21	1.00123	2456.15
25	−0.0087	2441.31	0.418	(13)	0.504	2441.41	1.00152	2444.96
30	−0.0097	2429.43	0.335	(11)	0.384	2429.59	1.00184	2433.87
40	−0.0109	2405.87	0.173	(10)	0.206	2405.84	1.00266	2412.01
50	−0.0110	2381.84	0.288	(11)	0.361	2381.88	1.00388	2390.66
60	−0.0098	2357.65	0.202	(8)	0.244	2357.68	1.00523	2369.83
70	−0.0078	2333.25	0.148	(6)	0.170	2333.19	1.00708	2349.60
80	−0.0055	2308.51	0.125	(11)	0.168	2308.40	1.00939	2330.01
90	−0.0028	2283.41	0.088	(4)	0.090	2283.27	1.01225	2311.14
100		2257.32	0.208	(17)	0.301	2257.75	1.01574	2293.28
110	+0.0035					2231.54*	1.01989	
120	+0.0072					2204.75*	1.02484	
130	+0.0115					2177.26*	1.03066	
140	+0.0160					2149.00*	1.03745	
150	+0.0211					2119.87*	1.04529	

† The numbers in parentheses are the numbers of determinations made at each temperature.
* The starred values are from Osborne, Stimson, and Ginnings' Table I, page 265 of reference 17.

[13] J. A. Goff and S. Gratch, "Low pressure properties of water −160° to 212°F." Am. Soc. Heating and Ventilating Eng. **18**, 125 (1946).

[14] N. S. Osborne, H. F. Stimson, J. Research Nat. Bur. Stand. **5**, 411 (1930).

[15] F. D. Rossini and W. E. Deming, "The assignment of uncertainties to the data of chemistry and physics," J. Wash. Acad. **29**, 416 (1939).

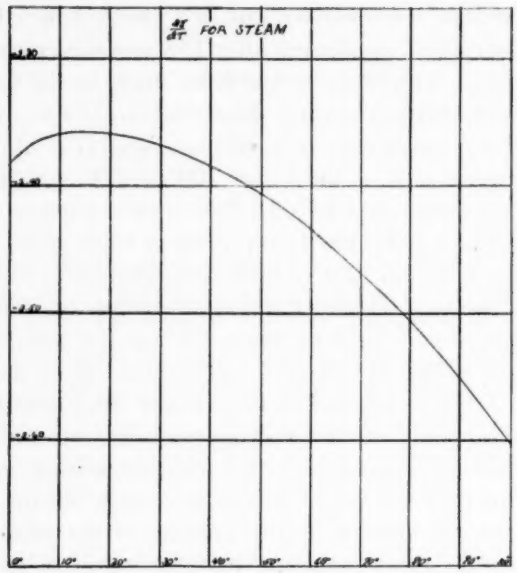

FIG. 2.

tion (2) obtained by integration of Eq. (1). The seventh column contains values of $(RT/pv)_s$ designating the ratio at the saturation values for the vapor computed from the Eq. (8). The last column contains the product of γ_{sm} and $(RT/pv)_s$.

$$d\gamma/dt = -2.3840 + .00325t - 1.186607\cdot 10^{-4}t^2 + 1.100284\cdot 10^{-6}t^3 - 4.53677\cdot 10^{-9}t^4; \quad (1)$$

$$\gamma_{sm} = 2500.51 - 2.3840t + 1.625\cdot 10^{-3}t^2 - 3.95554\cdot 10^{-5}t^3 + 2.7507\cdot 10^{-7}t^4 - 8.56354\cdot 10^{-10}t^5. \quad (2)^{**}$$

The value of γ at 100°C is especially interesting because values obtained from each of the three varieties of apparatus are available. The average measured value from the 1930 measurements is 2258.71 i.j. while 2257.79 i.j. was obtained in 1937, and 2257.32 i.j. in 1939. Relative to the value of the 1939 series we have a drop of 1.39 i.j. and 0.47 i.j. The value 2257.71 i.j. however is listed as preferred in Table I of the 1939 paper;[16] a value near that obtained by the authors by weighting "according to the number of observations and to give the observations of 1930–32 and those of 1937, respectively, one-fourth and one-half the weight of the observations" of the 1939 series. The difference between the 1937 mean value at 100°C and the 1939 value, namely 0.47, seems large. Some evidence indicating a preference for the 1939 value will appear later.

In the fourth steam paper of 1936[2] the discussion beginning on page 346 shows that the course of dL/dT, where L is the latent heat of evaporation, exhibits a maximum at about 15°C. An attempt was made at that time to compute the course of the derivative from the following equation:

$$dL/dT = C_{pg} - C_{pf} + [(\mu cp)_g - (\mu cp)_f]dp/dT, \quad (3)$$

where cp's are the constant pressure specific heats for the gas and liquid phases, and μ's are the Joule-Thomson coefficients. It was considered doubtful at the time that fully reliable values for differential quantities could be obtained for Eq. (3), and the quantitative aspect of the discussion was postponed. We may now compute the derivatives of $d\gamma/dt = d/dt(L+\beta)$, where $\beta = v_f T dp/dT$ and correlate the values empirically.[17] Figure 2 shows the course of $d\gamma/dt$ (Eq. (1)).

THE VAPOR PRESSURE EQUATION FOR WATER

An equation for $d\gamma/dt$, having the correct course with temperature, is suitable upon integration in forming an equation for γ_s to be used in the following equation of thermodynamics:

$$v_g T(dp/dT) = \gamma_{sm} = (pv/RT)_s \cdot RT^2(d\ln p/dT),$$

or

$$d\ln p/d\tau = -1/R\cdot\gamma_{sm}(RT/pv)_s = -\gamma_s/R, \quad (4)$$

where τ is the symbol for T^{-1} and $(RT/pv)_s$ differs from unity by the amount of the departure from the ideal gas laws.

The values of γ were measured on the international scale of temperature but since the rate of change of γ with temperature is of the order of 2.4 i.j. per degree, or approximately one part per 1000 of the value of γ, the maximum correction at 50° to express γ on the thermodynamic scale amounts to only 0.024; a quantity perhaps tenfold smaller than the possible error in γ.

** The coefficient of t^5 was altered slightly in the final adjustment.

[16] N. S. Osborne, H. F. Stimson, and D. C. Ginnings, J. Research Nat. Bur. Stand. **23**, 261 (1939).

[17] To obtain accurate derivatives of a function tabulated at equal intervals of the independent variable, use has been made for many years of a method based on a Lagrangian fourth-degree polynomial, worked out by George Rutledge, Phys. Rev. **40**, 262 (1932). The method is as reliable and rapid as it is little known.

The factor $(RT/pv)_s$, a measure of the departure of the saturated volumes from the ideal gas laws, may be regarded as expressed on the thermodynamic scale, provided accurate values can be obtained for the gas-law defect. The value of the ratio increases from 1.00053 at 0° to 1.01574 at 100°C, or to obtain the ratio to a part in 10,000 it is required that the departure from the ideal gas laws be known to one in 5 at 0°, and one in 160 at 100°C. The values of the ratio factor employed were obtained from Eq. (8) using for v_s the values given by Osborne, Stimson, and Ginnings.[18] However after obtaining the final values for the vapor pressure from Eq. (7), final values of $(RT/pv)_s$ were computed and these appear in Table II.

The 1936 equation of state led to a value of the ratio at 100°C 1.0159, the value 1.01574 results from a new equation of state, Eq. (8), obtained by considering all the available evidence. Goff and Gratch,[13] considering only the Collins and Keyes[6] $(\partial H/\partial p)_T$ data in the range 38.94 to 125°C,[13] tabulate values of p and v leading to 1.01583, while at zero degrees their values lead to 1.00048. The ratios deduced from the data of Osborne, Stimson, and Ginnings[16] are, respectively, 1.00056 and 1.01591, using the tabulated volume and pressure of Table II of the reference. The volume at 100°C was deduced, however, from the value of $\gamma = 2257.71$ i.j., whereas the value observed in the later series of 17 observations is 2257.32. Moreover the thermodynamic temperature-scale value of Tdp/dT was not employed because of lack of knowledge of $d\Theta/dT$. Using the value of the latter quantity from Beattie's work, namely 0.999653, $(RT/pv)_s$ at 100°C becomes 1.01573.[18]

The values of $\gamma(RT/pv)_s$ given in column 8 of Table II are formed by multiplying the smoothed γ_{sm} values of column 6 by the first approximation values of $(RT/pv)_s$, referred to above. The course of the $\gamma(RT/pv)_s$ values show no minimum or maximum although the curvature is greater in the region 0 to 30° than onward to 100°C. The equation representing the values follows:

$$\gamma_s = \gamma(RT/pv)_s = 2501.78 - 2.3124t + 1.36148 \cdot 10^{-3}t^2 + 8.609233 \cdot 10^{-6}t^3 + 2.56 \cdot 10^{-9}t^4. \quad (5)$$

Upon substituting the foregoing equation into the differential equation (4), and integrating, the

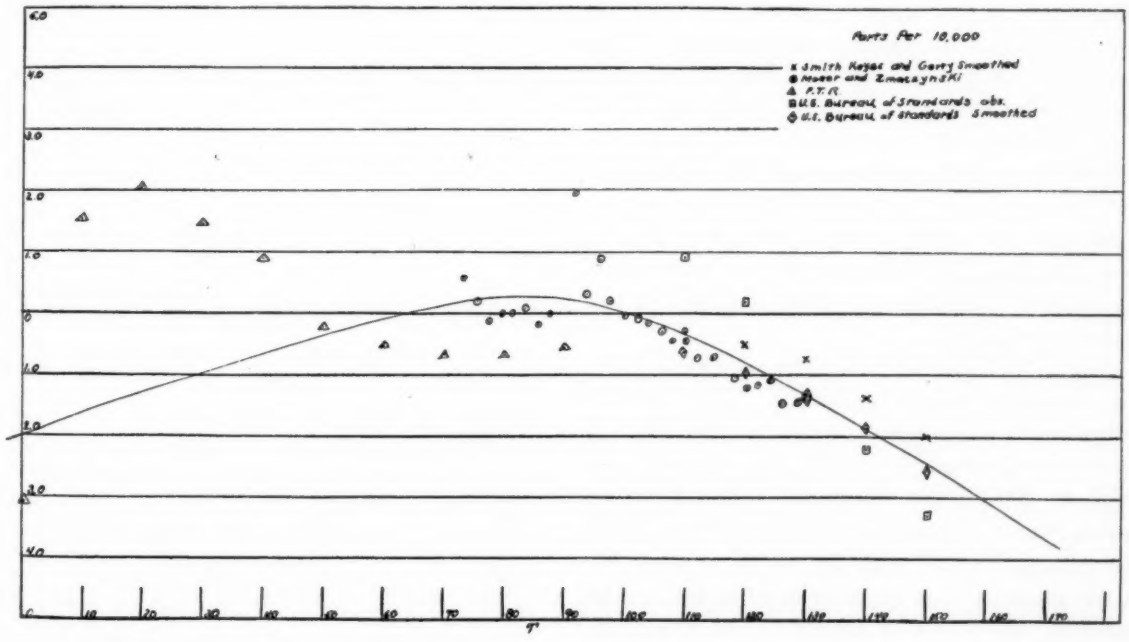
Parts Per 10,000
x Smith Keyes and Gerry Smoothed
● Moser and Zmaczynski
△ P.T.R.
⊡ U.S. Bureau of Standards obs.
◇ U.S. Bureau of Standards Smoothed
t°

FIG. 3.

[18] The value of v_g at 100°C given by Osborne, Stimson, and Ginnings in reference 16 is 1673.0. The above value of $d\Theta/dT$ needed to employ the thermodynamic equation for calculating v from γ leads to $v_g = 1673.3$ in agreement with the equation of state value.

following vapor-pressure equation is obtained where C_{100} is a constant determined for the pressure 1 atmos. at 100°C.

$$\log p^{mm} = -2892.3693\tau - 2.892736 \log T - 4.28022 \cdot 10^{-3} T + 2.73522 \cdot 10^{-6} T^2 + 8.03167 \cdot 10^{-10} T^3 + C_{100}, \quad (6)$$

$$C_{100} = +19.2462415.$$

The experimental values of the pressure given in the *Wärmetabellen*,[8] Table 44, 0 to 150°C, were changed to correspond to the thermodynamic scale using the values of $T-\Theta$ from column 2 of Table II. The latter values were also used to transfer the temperatures given by Moser and Zmaczynski[7] to the thermodynamic scale and likewise the temperatures given for the measurements from 110° to 150°C by Osborne, Stimson, Fioch, and Ginnings.[19] The pressure-temperature measurements of Smith, Keyes, and Gerry[20] were made from 150° to 374°C and the pressure values beginning at 100° and extending to 140°C from Table 44 of the *Wärmetabellen* were used in the correlation. The smoothed or correlation values in the latter temperature range were also transferred to the thermodynamic scale along with the smoothed values of Osborne, Stimson, Fioch, and Ginnings. The ensemble of pressure-temperature values were then used in Eq. (6) to compute values of the constant designated C_{obs}, and the differences from the value of the constant C_{100}, designated ΔC, listed. It will be evident that ΔC is equivalent to $\log p_{obs} - \log p^{100}$, where p^{100} signifies pressures computed at temperatures corresponding to pressures p_{obs}, but using always the constant of integration determined at 100°C and 1 atmos. given with Eq. (6).

A graph of the ΔC values *versus* temperature, Fig. 3, clearly indicates a trend. Three pressure values were given great weight in the final correlation of pressures, namely, the defined value $p=1$ at 100°C, the smoothed values from Osborne, Stimson, Fioch, and Ginnings[19] and Smith, Keyes, and Gerry[20] and the value at zero. The latter pressure was given special study by Dr. Osborne, the result of which he communicated to the writer in a letter of February 1934. The letter states: "Thiesen and Scheel in 1900 give the mean value 4.579 mm±.001 at 0°. By examining the observations . . . we find the rounded mean to be 4.5792, and the spread among the individual results to be 0.0036 mm. In 1909 Scheel and Heuse give a mean value of 4.5788 mm±0.0006 with a spread of 0.0030. But these two determinations are not the only ones available. A posthumous paper by K. Prytz was published in *Math. Fys. Meddaleisen Danske Vidensk. Selskab.* **2**, No. 2, 1 (1931), giving an account of a determination of the vapor pressure at the triple point. This temperature of +0.01°C is sufficiently close to the normal ice point to allow very reliable reduction to the same basis as the Physikalische Technische Reichsanstalt. He did not consider his work as final but he gives results of three measurements. When reduced to the zero point they give a mean of 4.5834 mm with a spread of 0.0014 mm. The mean of the three independent determinations giving them equal weight is 4.5804 mm±0.001."

The most recent observed values at 150°C listed below comprise those reported by Osborne, Stimson, Fioch, and Ginnings[19] and Smith, Keyes, and Gerry.[20]

O.S.F.G.

Silver container	3–25–32	4.6954 atmos.
	3–28–32	4.6961
	3–29–32	4.6955
	3–30–32	4.6978
	4– 1–32	4.6972
	7– 1–32	4.6942
	7– 7–32	4.6973
	7–21–32	4.6989
	8– 1–32	4.6959
	Mean	4.6969±0.00136
	Smoothed value	4.6977

S.K.G.

Container		
No. 2 machinery steel	7–15–29	4.705 atmos.
No. 2B 18/8 stainless steel	7–30–32	4.6966
No. 2B 18/8 stainless steel	8– 1–32	4.6968
Omitting No. 2 container value, mean		4.6967
	Smoothed value	4.6983

The measurement of steam properties in machinery steel even at 150°C was found to be unreliable because of the interaction of water leading to hydrogen evolution. The means of the

[19] N. S. Osborne, H. F. Stimson, E. F. Fioch, and D. C. Ginnings, J. Research Nat. Bur. Stand. **10**, 155 (1933).
[20] L. B. Smith, F. G. Keyes, and H. T. Gerry, Proc. Am. Acad. Arts and Sci. **69**, 137 (1934).

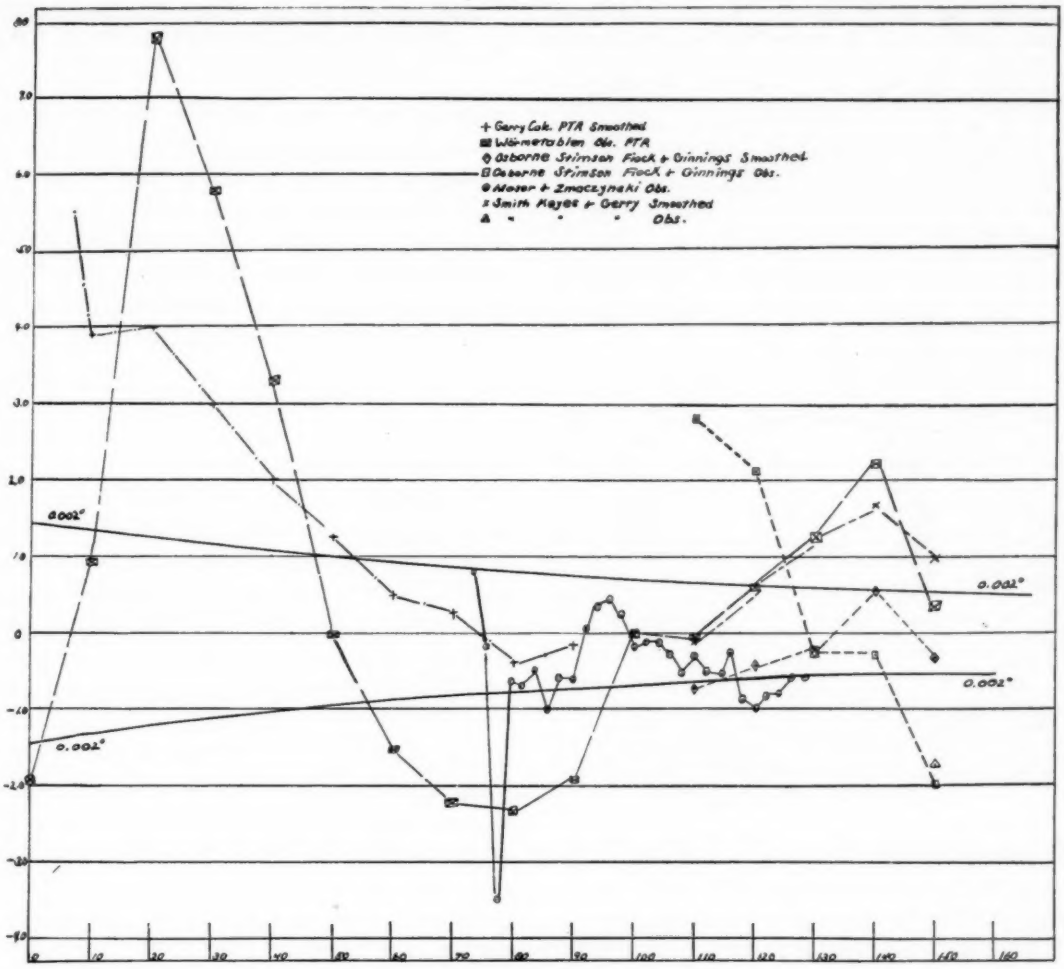

FIG. 4.

$$\text{Log}\, p^{mm} = -(28.92.3693/T) - 2.892736 \log T - 4.9369728 \cdot 10^{-3} T + 5.606905 \cdot 10^{-6} T^2 - 4.645869 \cdot 10^{-9} T^3 + 3.7874 \cdot 10^{-12} T^4 + 19.3011421$$

two independent values are in good agreement, the pressure difference corresponding to 0.0016°. However, the smoothed values given by Osborne, Stimson, Fioch, and Ginnings and Smith, Keyes, and Gerry, while in agreement to a part in 8000, differ in their mean from the mean of the observed pressures by a part in 3900. This difference may possibly be justified since the smoothing functions used by both groups of observers were arrived at only after many trials and would be expected to result in the "best" (least square) values employing all pressures to the critical temperatures.*** Acting on the assumption that the correlation value of the pressure at 150°C is the most accurate, the "correction" curve for the ΔC; t plot passes between the smoothed values. The result is that at 150°C t_T the calculated pressure, Eq. (5), is less than the mean of the smoothed value by a part in 12,000 while the agreement with the smoothed values of Osborne, Stimson, Fioch, and Ginnings and Smith, Keyes, and Gerry is satisfactory below 150°C.

The plot, Fig. 4, shows the deviations of the various values of pressure from the final vapor equation (7). It is clear that the observed points representing Moser and Zmaczynski, and those observed by Osborne, Stimson, Fioch, and Ginnings and Smith, Keyes, and Gerry at 150°C can

*** The reader may consult the deviation plots in the original papers (references 19 and 20) showing the departures over the range 100° to 374°C in parts per ten-thousand of the observed from the smoothed values.

TABLE III. "M and Z" refers to the smoothed values of pressure as given by H. Moser and A. Zmaczynski, while the "G and G" refers to the pressures listed by J. H. Goff and S. Gratch. The seventh column lists the smoothed values given by N. S. Osborne, H. F. Stimson, E. F. Fioch, and D. C. Ginnings in 1933. The pressures are expressed on the thermodynamic scale of temperatures from Beattie's $T-\Theta$ values. The eighth column of $d\Theta/dT$ values are deduced from J. A. Beattie's difference formula while the values of dp/dT result from the equation obtained by differentiating Eq. (7). Units of pressure are standard millimeters of Hg.

1	2	3	4	5	6	7	8	9
t_T	Vapor pressure Eq. (7)	Warme-täbellen values corr.*	Steam Table values corr.	M and Z corr.	G and G	O.S.F.G. corr.	$d\Theta/dT$	dp/dT
0	4.580	4.579	4.579		4.5812		1.000422	0.3328
10	9.203	9.212	9.213		9.205		1.000325	0.6167
20	17.529	17.543	17.539		17.531		1.000232	1.0852
30	31.824	31.842	31.833		31.825		1.000144	1.8268
40	55.338	55.356	55.341		55.335		1.000061	2.9504
50	92.558	92.56	92.558		92.555		0.999981	4.5931
60	149.469	149.45	149.452		149.457		0.999906	6.9177
70	233.808	233.76	233.78		233.788		0.999842	10.1121
80	355.310	355.23	355.26	355.282	355.278		0.999771	14.3873
90	525.924	525.82	525.89	525.915	525.891		0.999717	19.9746
100	760.00	(760.00)	760.00	760.00			0.999653	27.122[1]
110	1074.44		1074.51	1074.394		1074.43	0.999601	36.091
120	1488.79		1488.90	1488.691		1488.79	0.999553	47.152
130	2025.36		2025.60	2025.113		2025.33	0.999510	60.581
140	2709.24		2709.58			2709.16	0.999472	76.661
150	3568.34		3568.46			3568.05	0.999437	95.675

* The tabulated pressures marked "corr." have been transferred to the thermodynamic scale using column 2 of Table II and column 9 of Table III.

[1] At 100° the value of $dp/d\Theta$ obtained by J. A. Beattie and B. E. Blaisdell, Am. Acad. Arts and Sci. **71**, 361, (1937), from measurements of the variation of the steam point with pressure is 27.1313 mm per 1°C. Upon multiplication by $d\Theta/dT$, the value $dp/dT=27.122$ is obtained in agreement with that derived from Eq. (7)

be better represented as a separate ensemble by a straight line passing through 100° and between the latter's points. Sometimes coincidences in data are baffling and this is an example. For the present the pressures computed from Eq. (7) for the vapor pressure of water appear the most reasonable that can be proposed.

$$\log p^{mm} = -2892.3693\tau - 2.892736 \log T - 4.9369728\cdot 10^{-3}T + 5.606905\cdot 10^{-6}T^2 - 4.645869\cdot 10^{-9}T^3 + 3.7874\cdot 10^{-12}T^4 + 19.3011421. \quad (7)$$

Values of pressures computed from the equation are given in Table III. The derivatives dp/dT may be obtained by differentiating Eq. (7) and these values also appear in Table III. Both the pressures and the derivatives calculated correspond to values on the thermodynamic scale of temperature t_T°C. Finally, Table III contains observed pressures transferred to the thermodynamic scale which, in the case of Moser and Zmaczynski, have been taken from their own smoothed list of pressure values.

THE RELATION BETWEEN GAMMA-VALUES OBSERVED AND COMPUTED FROM THE VAPOR-PRESSURE EQUATION

Using the values of dp/dT computed from Eq. (7), we may form the quantity $RT^2(d\ln p/dT)$, the equivalent of γ_s which will be designated $\gamma_{s\ \mathrm{calc}}$. The values of $\gamma_{s\ \mathrm{calc}}$ are listed in Table IV in the second column while the succeeding columns contain in order, the value of γ_{calc}, obtained by dividing $\gamma_{s\ \mathrm{calc}}$ by $(RT/pv)_s$ given in the seventh column of Table II, and the values of $\gamma_{sm}-\gamma_{\mathrm{calc}}$.

It will be observed that γ_{calc} is larger than γ_{sm} and γ_{obs}, but that at 0°, 50°, and 100°C the agreement with the observed values compare very favorably. The differences are all of the same sign below 90°C which could be interpreted, assuming the measured pressures and the values of $(RT/pv)_s$ to be unassailable, to mean that the γ_{obs} values were affected with a constant error of about 0.3 i.j. However except for the recent measurements of Moser and Zmaczynski below 100°C there is complete lack of data obtained with modern thermometric technique. Indeed this is the weakness of all the older measurements because high purity platinum for thermometers and superior techniques of design and construction are scarcely more than twenty years old. Therefore, before any definitive conclusion can be drawn regarding the differences $\gamma_{sm}-\gamma_{\mathrm{calc}}$, new measurements of pressure should

TABLE IV. The value of γ_s calc. results from Eq. (7) and is the quantity $RT^2(d\ln p/dT)$. The third column results from dividing the quantities of the second column by corresponding $(RT/pv)_s$ ratios. The last column exhibits the difference between smoothed γ-values and the γ calc. values of column 3.

t_T	γ_s calc Eq. (7)	γ calc Eq. (7)	$(\gamma_{sm}-\gamma_{\mathrm{calc}})$
0	2501.89	2500.56	−0.05
10	2479.09	2477.08	−0.28
20	2456.57	2453.55	−0.34
30	2434.38	2429.91	−0.32
40	2412.57	2406.17	−0.33
50	2391.20	2381.95	−0.07
60	2370.32	2357.99	−0.31
70	2349.99	2333.48	−0.29
80	2330.27	2308.59	−0.19
90	2311.23	2283.26	+0.01
100	2292.94	2257.41	+0.34
110	2275.47	2231.09	+0.45
120	2258.88	2204.13	+0.62
130	2243.27	2176.54	+0.72
140	2228.71	2148.26	+0.74
150	2215.30	2119.32	+0.55

be available. It will be observed that the γ-differences correspond to very small pressure differences.

The course of $(\gamma_{sm}-\gamma_{calc})$ above 100° exhibits a change of sign and of magnitude which enhances the doubts expressed above in discussing the pressures at 150°C. Relative to the values of γ below 100°, those above 100° are, however, probably less accurate. Thus the average deviation for the twenty 1930 measurements at 150°C is 0.59, and s is 0.66.

Regarding the accuracy of the factor $(RT/pv)_s$ consider for example the number at 150°C where an error of one in 4000 would bring the γ-values into agreement. However, this implies an error of one in 180 in the effects of intermolecular force given by the equation of state. For all practical purposes of the moment the result is satisfying and an improved showing must await additional observations of vapor pressure from 0 to 150°C, consistently accurate to a part in 10,000 or better.****

THE ENTHALPY OF STEAM

Values of the enthalpy of steam below 100°C at the time of the 1936 edition of the Steam Tables[1] were obtained by extrapolation as regards the departure of water vapor from the ideal state. The enthalpy equation used was based, except for the gas-imperfection factors, on the values of C_p^0 for gas phase computed by A. R. Gordon[21] with the constant of integration determined from Osborne, Stimson, and Ginnings' value of the enthalpy reported at the Third International Conference on Steam, namely, 2675.35 i.j. The value 2675.33 i.j. is the most recent value listed by Osborne, Stimson, and Ginnings[22] and this value will be used as part of the basis to establish the enthalpy equation.

The equation of state of steam has been under revision during the last year in the form

Table V.

1 t_T	2 B_1 cc/g	3 B_2 cc/g	4 B_3 cc/g	5 $-F_1$	6 $-F_2$	7 $-F_3$	8 h_g Eq. 10	9 $h_g(ST)-h_g(10)$ parts per 10^4
				international joules				
0	−102.93	$-2.89\cdot10^5$	$-2.83\cdot10^7$	69.65	238.7		2500.64	+5.9
10	−84.34	$-1.52\cdot10^5$	$-1.20\cdot10^7$	54.62	78.3	65.14	2519.00	+5.9
20	−70.27	$-0.85\cdot10^5$	$-0.55\cdot10^7$	43.60	59.91	25.34	2537.26	+5.4
30	−59.42	$-4.98\cdot10^4$	$-0.27\cdot10^7$	35.42	32.38	11.87	2555.40	+4.4
40	−50.89	$-3.04\cdot10^4$	$-0.14\cdot10^7$	29.22	18.24	5.65	2573.38	+4.3
50	−44.08	$-1.93\cdot10^4$	$-7.28\cdot10^5$	24.44	10.95	2.55	2591.17	+3.7
60	−38.57	$-1.25\cdot10^4$	$-4.06\cdot10^5$	20.70	6.48	1.27	2608.71	+3.3
70	−34.04	$-0.85\cdot10^4$	$-2.37\cdot10^5$	17.72	4.12	0.676	2625.95	+3.2
80	−30.29	$-5.92\cdot10^3$	$-1.42\cdot10^5$	15.33	2.70	0.378	2642.80	+2.8
90	−27.14	$-4.21\cdot10^3$	$-0.88\cdot10^5$	13.38	1.81	0.216	2659.26	+2.1
100	−24.48	$-3.06\cdot10^3$	$-5.53\cdot10^4$	11.77	1.24	0.126	2675.20	+1.6
110	−22.20	$-2.27\cdot10^3$	$-3.57\cdot10^4$	10.43	0.864	0.077	2690.57	+1.5
120	−20.24	$-1.71\cdot10^3$	$-2.36\cdot10^4$	9.31	0.617	0.042	2705.31	+1.2
130	−18.54	$-1.31\cdot10^3$	$-1.69\cdot10^4$	8.36	0.447	0.031	2719.22	+1.3
140	−17.06	$-1.02\cdot10^3$	$-1.08\cdot10^4$	7.54	0.332	0.024	2732.15	+4.0
150	−15.75	$-0.81\cdot10^3$	$-0.75\cdot10^4$	6.85	0.249	0.010	2744.76	+1.5

The coefficients of the pressure series for the entropy equations, M_1, M_2, etc, follow from above B and F factors as follows, where τ signifies T^{-1}:

$M_1=B_1\tau-\tau F_1$ $\quad F_1=(\partial B_1\tau/\partial\tau)$

$M_2=1/2RB_2\tau^2-\tau F_2$ $\quad F_2=1/2R(\partial B_2\tau^2/\partial\tau)$

$M_3=1/3R^2B_3\tau^3-\tau F_3$ $\quad F_3=1/3R^2(\partial B_3\tau^3/\partial\tau)$

$p=\varphi(v, T)$. An equation sufficient for all purposes of this paper follows:

$$\log \mathbf{R}T/pv=\log\omega/v+\psi\omega/v^2, \qquad (8)$$

where $\omega=v-\beta$ and $\psi=\psi_0+\psi_1\rho$. For units of cc per gram of steam, standard atmospheres, the quantities are:

$$\mathbf{R}=R/M=4.55465\,;\ T=273.16+t\,;$$
$$\beta=2.061\,;\ \psi_0=1260.17\tau\cdot10^{7.4238\cdot10^4\tau^2}\,;\dagger$$
$$\psi_1=49.97(2.4+1286\tau)\tau\cdot\psi_0^3.$$

The Eq. (8) may be expanded into the following form sufficiently exact for many purposes:

$$pv=\mathbf{R}T(1+B_1(p/\mathbf{R}T)+B_2(p/\mathbf{R}T)^2+B_3(p/\mathbf{R}T)^3), \qquad (8a)$$

where the units are as before, and

$$B_1=(\beta-\psi_0)\,;\ B_2=(\beta\psi_0-\psi_1-1/2\psi_0^2),$$
$$B_3=(5/6\psi_0^3-\psi_0\psi_1+\beta\psi_1-5/2\psi_0^2\beta-\beta^3+3\beta^2\psi_0).$$

Table V gives the B coefficients and derivatives of these quantities.

The specific-heat equation at constant pressure for limiting pressure zero will be taken to be as follows:

$$C_p^0=1.4722+7.7726\cdot10^{-4}T+47.8418\tau\text{(i.j.)},\dagger\dagger \qquad (9)^{23}$$

**** The best accord in pressure measurements by independent observers is about a part in 10,000, namely, the case of the vapor pressure of CO_2 at zero degrees. The sensitivity of pressure measurements using the pressure balance with electric-contact means of detecting equilibrium can easily be made a part in 20,000. Consistent accuracy to this degree in vapor-pressure measurements will be needed to resolve fully such discrepancies as now exist in the above data.

[21] A. R. Gordon, J. Chem. Phys. **2**, 65 (1934).

[22] N. S. Osborne, H. F. Stimson, and D. C. Ginnings, J. Research Nat. Bur. Stand. **23**, 261 (1939).

† The quantities ψ_0 and ψ_1 are given for use with base 10 logs.

†† The factor by which international joules is to be multiplied to obtain absolute joules is 1.0002 in this paper.

[23] Equation 9 results from modifying Eq. 22 of reference 2 based on A. R. Gordon's work (reference 21) by making the correction for "centrifugal stretching" of the water molecule as calculated by E. B. Wilson, Jr.,

and

$$\int C_p^0 dT = 1.4722(T-T_0)+3.8863\cdot 10^{-4} \times (T^2-T_0^2)+110.16\log_{10} T/T_0. \quad (9a)$$

The constant of the enthalpy equation, h_0, has been evaluated from the known saturation values at 0° and 100°C in the following way. First using the observed value of γ at 0°, namely, 2500.72, the value of $v_f T dp/dT$ 0.01, and the F factors from Table V, we find $h_0(\gamma_{obs}\ 0°)$ 2501.14 i.j. Similarly from γ at 100°C, 2257.32 of 1939 and 2257.79 of 1937, we have the mean 2257.56. The quantity $v_f T dp/dT$ is 1.41 and combining $\int C_p^0 dT$ with the F factors we find $h_0(\gamma_{obs}\ 100°)$ 2501.06 i.j.

Second, taking the corresponding smoothed values of γ given in Table II we have h_0, (γ smoothed 0°) = 2500.93 i.j. and h_0, (γ smoothed 100°) = 2501.25 i.j. The mean of all four values is h_0 = 2501.09 i.j. per gram and we may write for the enthalpy of the vapor phase of water the equation following, subject to the convention that the enthalpy of the saturated liquid phase is zero at zero degrees centigrade.

$$h_g = 1801.55+1.4722T+3.8863\cdot 10^{-4}T^2 +110.16\log T+F_1 p+F_2 p^2+F_3 p^3, \quad (10)$$

where F_1, etc. designates the quantities, $(\partial B_1\tau/\partial\tau)$, $(1/2R)\cdot(\partial B_2\tau^2/\partial\tau)$, and $(1/3R^2)\cdot(\partial B_3\tau^3/\partial\tau)$.

The enthalpy values computed from Eq. (10) appear in column 8 of Table V, and in the same table column 9 gives the deviation from the values listed in the 1936 Steam Tables. The latter values, although within the 1934 international tolerances, are in every case larger.

The deviation of the enthalpies by Eq. 10 from the 1939 enthalpy assignments by Osborne, Stimson, and Ginnings are within the limits of error of the experimental error of the direct heat measurements from 0° to 100°C, namely, a part in 8000 at most. However above 100°C the Osborne, Stimson, and Ginnings values are higher, reaching a maximum of 4.7 parts per 10,000 at 150°C. The results of the γ-measurement series indicate a larger statistical s value relative to the series of 100°C and for lower temperatures, but that they can be in error by as much as a part in 2000 seems doubtful. Actually the agreement between the Osborne, Stimson, and Ginnings assignments and those of the Steam Table improves as higher temperature values are compared, and it may be that a small error in trend of the C_p^0 is responsible. A revision of the computation of the energy of the water molecule is due, among other items, because of an improved knowledge of the radiation constant C_2. A. R. Gordon used 1.4324 while R. T. Birge lists 1.4385 in 1941.

THE ENTROPY OF THE VAPOR

The entropy equation may be written as follows:

$$s = s_0+\int_{T_0}^{T} C_p^0 dT/T - R\ln p - \int_0^p (\partial v/\partial T - R/p)dp. \quad (11)$$

From Eq. (8a) the last term of the above relation may be evaluated in the form $M_1 p+M_2 p^2+M_3 p^3$, and the M coefficients obtained simply from the tabulations of Table V for B and F by use of the relationships at the foot of the table. The final equation follows where s_0 is obtained from the value of s "observed" at 0°C and 100°C, the convention being adopted that s for the saturated liquid is zero at 0°C.

$$s = -1.4988-1.06243\log p+3.38987\log T +7.7726\cdot 10^{-4}T-47.8418\tau +M_1 p+M_2 p^2+M_3 p^3\cdots. \quad (12)$$

The agreement of the entropy values computed from the foregoing equation with the tabulated values of the entries in Table I of the Steam Tables is 4.5 parts per 10,000 at 0°, 1.4 parts at 100°, and 0.6 parts at 150°C. The agreement with the assignments of Osborne, Stimson, and Ginnings is excellent, the greatest deviation amounting to 2.5 parts per 10,000 at 150°C.

J. Chem. Phys. **4**, 526 (1936); a calculation confirmed later by a recomputation [C. C. Stephenson and H. O. McMahon, J. Chem. Phys. **7**, 614 (1939)] of the rotational partition function from Dennison, Ginsburg, and Weber's data, Phys. Rev. **52**, 160, (1937). The relation 1 i.j. = 1.0002 ab.j. has been used.

Letters to the Editor

THIS section will accept reports of new work, provided these are terse and contain few figures, and especially few halftone cuts. The Editorial Board will not hold itself responsible for opinions expressed by the correspondents. Contributions to this section should not exceed 600 words in length and must reach the office of the Managing Editor not later than the 15th of the month preceding that of the issue in which the letter is to appear. No proof will be sent to the authors. The usual publication charge ($4.00 per page) will not be made and no reprints will be furnished free.

Isotopic Nitrogen Exchange between Nitrogen Pentoxide and Dioxide

RICHARD A. OGG, JR.
Department of Chemistry, Stanford University, Stanford University, California
June 17, 1947

THE mechanism proposed for the *chemically* complex decomposition of nitrogen pentoxide, i.e.,[1]

$$\begin{aligned} &N_2O_5 \rightarrow NO_3+NO_2 && k_1,\\ &NO_3+NO_2 \rightarrow N_2O_5 && k_2,\\ &NO_3+NO_2 \rightarrow NO_2+O_2+NO && k_3,\\ &NO+N_2O_5 \rightarrow 3NO_2 \quad \text{rapid,} && \\ &\text{with } k_3 \ll k_2, && \end{aligned}$$

leads to the expectation of a relatively rapid exchange reaction of nitrogen between nitrogen pentoxide and dioxide. This prediction has been tested by use of the positron active N^{13}. Inasmuch as the large decay constant (a half-life of some 9.9 minutes) necessitates a rapid procedure, the tests were performed with solutions in carbon tetrachloride. However, previous rate studies[2] suggest an identical mechanism for nitrogen pentoxide decomposition in the gas phase and in "inert" solvents.

A thin graphite disk was bombarded with a high speed deuteron beam to produce N^{13}, which remains trapped in the graphite. The disk was then burned in a current of dry oxygen, the products being condensed in a liquid-air cooled trap already containing anhydrous "carrier" nitrogen dioxide. The contents were then dissolved in dried carbon tetrachloride. Almost quantitative transfer of the nitrogen activity into nitrogen dioxide was achieved. Nitrogen pentoxide was prepared in an all-glass apparatus by ozonization of nitrogen dioxide, and was dissolved in cold carbon tetrachloride in a closed system. To minimize its decomposition, tests were made considerably below room temperature.

For exchange experiments, volumetrically measured samples of the respective oxide solutions were mixed, and after a brief measured period the mixture was shaken briskly with excess saturated aqueous barium hydroxide solution. After saturation with carbon dioxide the solution was filtered. To the filtrate were added successively equimolar amounts of sodium nitrite and silver nitrate solutions. The silver nitrite precipitate was filtered and washed, and its activity was determined with a Geiger counter. Large counting rates assured high accuracy.

In the otherwise identical blank experiments, the nitrogen pentoxide solution was first extracted with the aqueous barium hydroxide, and the nitrogen dioxide solution was then added. Separate tests showed exchange between aqueous nitrate and nitrite ions to be negligibly slow.

Inasmuch as the radioactivity was initially confined to the nitrogen dioxide, the proposed exchange would be manifest as a *decrease* in the activity of the silver nitrite precipitate (as compared with the simultaneous activity of that from the blank). The extent of approach toward exchange equilibrium was judged from this ratio and from the molar ratio of the respective oxides, based on chemical analyses of the original solutions.

These experiments have furnished unequivocal evidence of the expected exchange reaction. At 10°C the process is rapid but measureable as to rate—the half-life is of the order of two minutes for solutions some 10^{-1} and 5×10^{-2} molar, respectively, with respect to pentoxide and dioxide. For comparison, the half-life of the pentoxide decomposition[2] at this temperature is some sixty hours.

Acknowledgment is made of the courtesy of the Crocker Radiation Laboratory of the University of California and of the Department of Physics of Stanford University in providing the necessary exposures with the cyclotron, and of the experimental assistance rendered by Dr. M. Sienko and Dr. C. A. Alvarez-Tostado.

[1] R. A. Ogg, Jr., J. Chem. Phys. **15**, 337 (1947).
[2] For references and discussion see L. S. Kassel, *Kinetics of Homogeneous Gas Reactions* (Chemical Catalogue Company, New York, 1932).

On the Decomposition of Organic Compounds by Ionizing Radiations

WARREN M. GARRISON
Department of Chemistry, University of Wyoming, Laramie, Wyoming
June 13, 1947

SHEPPARD and Whitehead[1] found that the decomposition of palmitic acid by high energy deuterons produces H_2 and CO_2 as the major gaseous products, and pentadecane as the principal liquid product. In a recent article Burton[2] pointed out that a much greater diversity of products should be observed if the locus of excitation in the molecule corresponds to the point of initial ionization. He suggested that the vacant orbital may shift to a preferred position in the COOH end of the molecule; however, a mechanism was not postulated for interactions of the type suggested.

It is of interest to note that such a migration of a vacant orbital along a saturated hydrocarbon chain would be expected as a result of a form of resonance in the ion which has not heretofore been described. For example, in a saturated hydrocarbon chain the sigma-electrons forming the C−C bonds are in essentially the same energy state. If one of those electrons is removed, the vacant orbital could not be assigned to any particular C−C bond. The following structures, each containing a one-electron bond, would have

identical energy and steric configuration and would, therefore, be in resonance:[3]

$$-C{:}C{:}C{\cdot}C-$$
$$-C{:}C{\cdot}C{:}C-$$
$$-C{\cdot}C{:}C{:}C-$$

An increase in the chain length would increase the number of resonating forms.

As a result of this resonance, a terminal group containing a multiple bond, or an electron in a higher energy level, would be able to interact and supply an electron to the vacant orbital. As a result ionization produced along the chain could appear as a formal charge in the bond acting as an electron source.

This shifting of a "positive hole" as a result of the resonance described above makes the saturated chain an effective conductor, and is an interesting exception to the more general observation that resonance through a saturated chain is insignificant.

[1] C. W. Sheppard and W. L. Whitehead, Bull. Am. Assoc. Pet. Geol. **30**, 32 (1946).
[2] M. Burton, J. Phys. Coll. Chem. **51**, 611 (1947).
[3] G. E. K. Branch and M. Calvin, *The Theory of Organic Chemistry* (Prentice-Hall, Inc., New York, 1941).

The Structure of Diborane

W. C. Price
Ryerson Physical Laboratory, University of Chicago, Chicago, Illinois
July 10, 1947

A RE-EXAMINATION of the infra-red spectrum of diborane has revealed the following important features which rule out the ethane-type structure but agree very well with the interpretation of the electron-diffraction results in terms of a bridge model.[1]

(1) The rotational structures of the perpendicular bands around 2600 and 970 cm^{-1} have been resolved and shown to have well-marked alternation of intensities. This favors the bridge structure, for which the spin factor is 9:7, as against the ethane-type structure which requires that every third line be slightly accentuated as for example in the 12-μ band of ethane.[2]

(2) The analysis of the rotational structure using the symmetrical top approximation yields values for $C''-D''$ of 2.15 cm^{-1} for the 2600 band, and 2.05 cm^{-1} for the 970 band. The expected values for C'' and D'' calculated from the data based on the bridge-model interpretation of the electron-diffraction results are $C''=2.63$ cm^{-1} and $D''=0.58$ or 0.55 cm^{-1}, according to which of the larger moments of inertia is taken. This agreement is as good as can be expected while the values calculated using the data obtained by interpreting the electron-diffraction results in terms of the ethane-type structure[3] (*viz.* $C''=1.94$ and $D''=0.65$) are quite incompatible with the spectroscopic figures.

(3) Although we have not yet been able to resolve the parallel bands, the high resolving power of our Perkin-Elmer instrument (which is capable of resolving the rotational structure of the 4.2-μ carbon dioxide band) has given us much information about the envelopes of these bands. This has brought to light a striking correspondence of the bands of ethylene with those of diborane (bridge model) in which the CH_2 and terminal BH_2 groups undergo the same bending and stretching motions. Corresponding bands are listed in Table I.

TABLE I. Corresponding bands in diborane and ethylene.

Type	Ethylene	Diborane
$\nu_9 CH(b_{2u})$	3105.5	2620
$\nu_{11} CH(b_{3u})$	2989.5	2527
$\nu_{12} CH_2(b_{3u})$	1443.5	1175
$\nu_7(b_{1u})$	949.2	974

The type symbols are those used by Herzberg for ethylene.[4] While the structural features of these bands are remarkably similar, no such close similarity could be found with the band envelopes of ethane. The assignments confirm those made by Bell and Longuet-Higgins for a bridge-type model.[5]

The ultraviolet absorption spectrum of diborane has been examined at low pressures down to 1000A. The first strong absorption is a broad diffuse band appearing about 1350A at an equivalent thickness of 0.004 mm of the gas at N.T.P. It is followed by further diffuse absorption of similar strength below 1200A. This is compatible with an ionization potential between 11 and 12 electron volts, and shows that all the electrons are fairly tightly bound. At higher pressures the bands spread out to longer wave-lengths and presumably merge into the relatively weak bands reported by Blum and Herzberg.[6]

The above work forms part of a program sponsored by the Office of Naval Research. The author is indebted to Dr. George Schaeffer for preparing the sample of diborane and to Professor R. S. Mulliken for much helpful advice. Thanks are also due to Professor E. Teller, G. Herzberg, and H. I. Schlesinger for suggestions and discussions.

[1] S. H. Bauer, Chem. Rev. **31**, 43 (1942); H. C. Longuet-Higgins and R. P. Bell, J. Chem. Soc. 250 (1943); K. S. Pitzer, J. Am. Chem. Soc. **67**, 1126 (1945).
[2] R. G. Owens and E. F. Barker, J. Chem. Phys. **10**, 146 (1942).
[3] S. H. Bauer, J. Am. Chem. Soc. **59**, 1096 (1937).
[4] G. Herzberg, *Infrared and Raman Spectra* (D. Van Nostrand Company, Inc., New York, 1945), p. 107.
[5] R. P. Bell and H. C. Longuet-Higgins, Proc. Roy. Soc. **183A**, 357 (1945).
[6] E. Blum and G. Herzberg, J. Phys. Chem. **41**, 91 (1937).

On the Number of Independent Constituents and the Phase Rule

I. Prigogine and R. Defay
Faculté des Sciences et Faculté des Sciences appliquées, Université Libre de Bruxelles, Bruxelles, Belgique
June 27, 1947

IN a recent paper,[1] Stuart R. Brinkley, Jr. has given an analytical criterion for the determination of the number of independent constituents. However, this criterion is only valid in the very particular case in which all substances forming the system are in chemical equilibrium. Consider, for instance, the gaseous system H_2, O_2, H_2O, and H_2O_2. According to Brinkley's criterion the number of inde-

pendent constituents is two. This is only true when the equilibriums $H_2+\frac{1}{2}O_2 \rightleftarrows H_2O$ and $H_2+O_2 \rightleftarrows H_2O_2$ are established. But we can obviously apply phase rule even when one of the components H_2O or H_2O_2, or both of them, are in metastable equilibrium (in absence of the appropriate catalyst). In these cases Brinkley's criterion cannot be applied.

We think that it is preferable to use the general Jouguet's criterion[2] which gives in every case the number of independent constituents. Consider a system containing s constituents (independent or not) which undergo r reactions, in the field of temperature and pressure studied. Let us write these reactions in the form

$$\Sigma_\gamma \nu_{\gamma\rho} M_\gamma = 0, \quad (\gamma = 1 \cdots s;\ \rho = 1 \cdots r).$$

We have to consider the matrix $\|\nu_{\gamma\rho}\|$ formed by the stoechiometric coefficients. The number of *distinct* chemical reactions, r', is given by the rank of this matrix. Then, it can be shown quite easily that the number of independent constituents is given by

$$s' = s - r'.$$

So Jouguet's criterion permits a straightforward analytical calculus of the number of independent constituents.

[1] Stuart R. Brinkley, Jr., J. Chem. Phys. **14**, 563, 686 (1946).
[2] E. Jouguet, Notes de mécanique chimique, J. Ec. Polyt. (Paris), 2de série, 21eme cahier (1921); R. Defay, Bull. Acad. Roy. Belg. **17**, [5], 940 (1931); I. Prigogine and R. Defay, *Thermodynamique Chimique* (Ed. Desoer, Liège, Belgigue, 1946), Tome II, Chapt. XLI.

Errata: On the Behavior of Pure Substances Near the Critical Point

[J. Chem. Phys. **15**, 314 (1947)]
O. K. Rice
University of North Carolina, Chapel Hill, North Carolina

THE asterisk, page 318, Eq. (16), is not part of the symbol $\bar{s}_s$ but refers to the footnote at the bottom of the page. In Eqs. (19), (20), and (21) the asterisk *is* part of the mathematical symbol.

On page 323, in the mathematical expression two lines before Eq. (39) P should be p.

On page 325, second column, line 21, the statement "α will go to about -0.5×10^{-4}" should read "α/kT will go to about -0.5×10^{-4}."

On page 325 two lines were omitted after line 28 of the second column. The corrected portions of the sentences involved read: "the maximum value of tc_t occurs at $t=t_{max}=|kT_m/\alpha|$, or, at 0.1-atmos. compression, at $t=2\times10^4$. At this point $\gamma t^{\frac{1}{2}}/kT_m=2.5$ and $\gamma(tv/u)^{\frac{1}{2}}/kT_m$ might be about 3, indicating. . . ."

On page 326, the sixth line before Eq. (46), $c_t^{-1}-v_f'$ should be $c_t^{-1}+v_f'$.

On page 326, lines 3 and 7 after Eq. (46) the denominator of Eq. (45) is actually equal to the cube of the quantities given.

On page 331, second column, line 25, the word "derivation" should be "derivative."